Morphogenesis control by mechanical stress: Mechanism behind efficient plant growth

Dissertation

for the award of the degree

Doctor rerum naturalium

of the Georg-August-Universität Göttingen

within the doctoral program
Physics of Biological and Complex Systems
of the Göttingen Graduate School of Neurosciences, Biophysics, and Molecular Biosciences (GGNB)
of the Georg-August University School of Sciences (GAUSS)

submitted by
Jason Khadka
from Morang, Nepal
Göttingen 2019

Thesis advisory committee

Dr. Karen Alim
Biological Physics and Morphogenesis
Max Planck Institute for Dynamics and Self-Organization

Prof. Dr. Stefan Klumpp
Institute for the Dynamics of Complex Systems
Georg-August-Universität Göttingen

Dr. Florian Rehfeldt
Third Institute of Physics
Georg-August-Universität Göttingen

Examination board

Dr. Karen Alim (Referee)
Biological Physics and Morphogenesis
Max Planck Institute for Dynamics and Self-Organization

Prof. Dr. Stefan Klumpp (Co-referee)
Institute for the Dynamics of Complex Systems
Georg-August-Universität Göttingen

Dr. Florian Rehfeldt
Third Institute of Physics
Georg-August-Universität Göttingen

Dr. David Zwicker
Theory of Biological Fluids
Max Planck Institute for Dynamics and Self-Organization

Dr. Azam Gholami
Laboratory of Fluid Physics, Pattern Formation, and Biocomplexity
Max Planck Institute for Dynamics and Self-Organization

Prof. Dr. Annette Zippelius
Institute for Theoretical Physics
Georg-August-Universität Göttingen

Date of the oral examination: May 29th, 2019

An intelligent being {…} would find that nature, as it were, refuses his collaboration– she does all herself, doom the individual to inactivity, indeed to nilhilism.

ERWIN SCHRÖDINGER ■ WHAT IS LIFE?

Abstract

Morphogenesis of plants and animals often emerges from mechanical moulding and deformations. Yet, how precisely cells as individual mechanical entities can act to shape a tissue reliably and efficiently is still puzzling. In plants, the mechanics of cells within a tissue is particularly well defined as individual cell growth is essentially mechanical yielding of cell wall in response to internal turgor pressure. Most intriguingly, cell wall stiffness is controlled by biological signalling and is observed to respond to mechanical stresses building up within a tissue. What is the role of such a mechanical feedback during morphing in three dimensions? Here, we propose a three dimensional vertex model to investigate the mechanics in plants tissues. We employ the model to examine the onset of organogenesis at the shoot tip and the polarised growth of plant tissue that leads to the elongated shoot.

To investigate the mechanism of organ growth from the shoot apical meristem, a tissue at the tip of the plants, we simulate the bulging of young organs, called the primordia, on the surface of the tissue. We find that the primordia are initiated and their growth primarily governed by the ratio of growth rates of faster growing primordial cells to slower growing meristem cells surrounding them. By introducing the remodelling of cell walls with stresses through mechanical feedback, we observe, remarkably, that the outgrowth of the primordia is more efficient when the feedback is allowed to modify the cellular growth. Our quantitative analysis of simulation data shows that the feedback acts by not only modulating cell growth, by reorganising the walls, but also by changing the stress pattern within the tissue. The twofold mechanism by which feedback acts allows the self-amplification and propagation of growth and stress anisotropies on the tissue. We observe that it significantly alters the mechanical properties of boundary cells around the growing primordia.

These cells face increased anisotropic stresses and are restricted from growing. With our study, we see that this restructuring of tissue mechanics forms a stiff ring-like boundary around the primordia, which effectively squeezes out the organ. The experimental observations reported in literature on the growing plant tissues corroborate our findings. Thus, we show that the mechanical feedback on cellular growth enables plants to grow organs efficiently out of the meristem by reorganising the cellular growth rather than increasing the growth rates of primordial cells further.

The elongated body of plant is vital in positioning the growing organs to gather resources better. In the second part of the work, we investigate the transformation of the hemispherical apical surface of plant into the tall cylindrical body by simulating the elongation of the plant tissue. Through the various arrangements of growth on the tissue, we analyse the efficiency of mechanical development of plants in lengthening the shoot. We find that the confined growth on the peripheral regions as observed in the meristem of plants is the most efficient to generate elongation. The elongation from the peripheral growth is the highest regardless of the mechanical feedback and the application of cell division. With this, we deduce that the plants are adept at generating cylindrical body and optimally placing the organs.

In conclusion, we show that the three-dimensional mechanical modelling is a dependable method for exploring plant morphogenesis. We prove that plant cells read from the tissue-wide mechanical patterns to organise their growth and that the mechanical feedback guides efficient initiation of organs from the apical surface. With the analysis of spatial arrangement of growth, we also confirm that the growth pattern in the meristem is optimised to enhance the development of elongated body of plants.

Contents

PUBLICATION DECLARATION

Some of the text and figures in chapter 1, 2 and 3 are included in the following manuscript submitted for publication:

Jason Khadka, Jean-Daniel Julien and Karen Alim. submitted (2019)

The research in the manuscript was designed by Jason Khadka (J.K.), Jean-Daniel Julien (J-D.J.) and Karen Alim (K.A.). J.K. performed the research. J.K., J-D.J. and K.A. wrote the article.

1 Mechanics in morphogenesis

The creation of all multi-cellular organisms starts out with a single cell. The cell grows, differentiates and moulds itself to create the form of an organism. The growth at the scale of a cell is unpredictable and stochastic but the outcome at the organism scale is robust and reproducible. What leads to this ordering on higher scales, despite the apparent stochasticity on the cellular level, has been a mystery.

The quest to find an answer to this age old question has prompted numerous research works over the last century. In one of the most prominent publications, D'arcy Thompson studied the possible formation of organism through physical processes by looking at the resemblance to physical materials [1]. For example, the shape of *Hexactinellid sponges* could be partly explained by slow aggregation of particles in colloids. He also examined the impact of physical forces on the form of organisms, like stress on a cellular packing can create asymmetric shapes starting from symmetric cells (Fig. 1.1). In another seminal work, Alan Turing proposed the symmetry breaking and the formation of patterns in biology as an outcome of the reaction and diffusion of morphogens in the organism [2]. He explained that the patterning of tentacles in *Hydra*, phyllotaxis in plants and the gastrulation of a blastula could all be accounted by reaction and diffusion systems.

In these two works, the modern approach to the exploration of morphogenesis is beautifully captured. The biochemical processes that are vital in the forging of tissues and organs face physical forces, thus the physical investigation of tissue formation should be able to discern the mechanism behind the morphogenesis.

Recent works on the physical study of biological systems have been successful in describing nu-

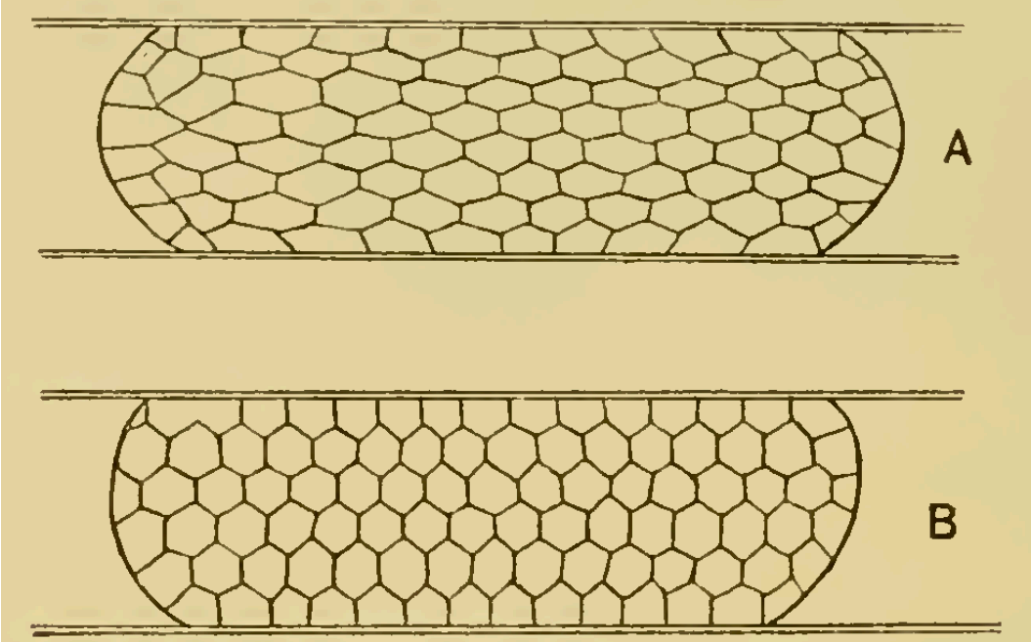

Figure 1.1: The bubbles in soap froth between two plates have homogenous hexagonal shapes as seen in B. When external stress is applied through the plates, the angles between the edges deform and the bubbles are elongated (shown in A). This resembles the shape of cells in columnar epithelium such as the intestine. *This is an illustration from page 322, chapter VII, of [1].* [1]

merous different systems across domains of life. The dynamics driven by adhesion and line tension among cells are able to explain the geometry of cellular packing and appendages formation in *Drosophila* [3, 4]. Fluid flow has been associated with formation of vasculature in animals and shaping of network in slime molds [5, 6]. The regulation of tissue properties by mechanics in plants are considered to be the determinant behind the tissue morphology [7].

These few examples provide a good indication on the significance of mechanics in moulding tissues and organs in organisms. Yet, the complete understanding on the interaction of mechanics and the individual entities involved in morphogenesis is still to be found. In the work presented here, we follow on the similar footsteps and concentrate on the mechanical shaping of tissues in plants. We investigate the effectiveness of mechanical sensing, intercellular interaction and mechanical responses from cells in morphing of plant tissues.

[1] Cambridge University Press. All rights reserved. Reproduced with permission of Cambridge University Press through PLSclear.

1.1 Growth of plant organs

All aerial organs in plants grow out from shoot apical meristem (SAM). It is found at the very tip of the shoot and it generates stem cells and lateral organs for plants through its lifetime (Fig. 1.2). The SAM is organised into three zones, the peripheral zone (PZ), central zone (CZ) and the rib zone (RZ) (Fig. 1.3). The central zone is the location for the stem cell niche of plants. The cells from central zone divide and provide cells to the peripheral zone to differentiate and form organs. The central zone is also characterised by lower mitotic activity as compared to the peripheral zone [8].

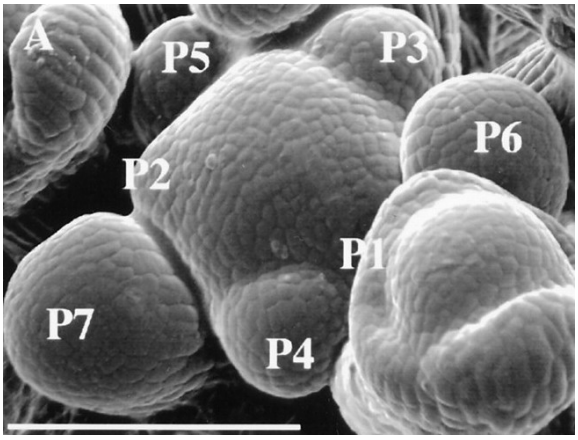

Figure 1.2: The scanning electron microscopy of shoot apical meristem (SAM). P1-P7 are the primordia labelled from younger to oldest. The scale bar shows $100\mu m$. *Adapted from [8].*[2]

The organs on SAM grow out initially as a small bulge, called the primordia (Fig. 1.2), on the tissue surface. The bulge is initiated by a group of cells in peripheral zone and rib zone. As the primordia grow into organ and out of the tissue, the cells are replaced by the dividing stem cells from central zone and thus the SAM sustains its growth throughout the life of plant [9].

As a mechanical entity, SAM can be considered as a hemispherical dome siting a top of a cylindrical shoot (Fig. 1.4). The epidermal cells (L1 in Fig. 1.3) in the SAM are much stiffer than the inner cells, thus it can be treated as a shell inflated by an inner pressure [10]. The indentation measurements on SAM have shown results consistent to the assumption with an estimated inner turgor pressure of $0.82 \pm 0.16MPa$ acting on the epidermal layer [11]. The stresses on the cells at the SAM can

[2]The image is derivative of a material that is a copyright of the American Society of Plant Biologists and is permitted to reprint: https://aspb.org/publications/aspb-journals/permission-to-reprint

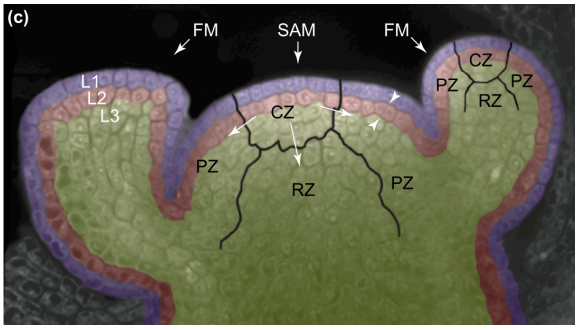

Figure 1.3: The confocal laser-scanning micrography image of SAM of Arabidopsis and the adjacent floral meristems. The meristem is divided into three layers, the epidermal (L1) and subepidermal layers (L2), and the internal layers (L3). The black outlines are the approximate boundaries between the peripheral zone (PZ), central zone (CZ) and the rib zone (RZ). Cells in PZ differentiate into lateral organs. Central zone provides cells to the peripheral zone and rib zone contributes to stem and lateral organ growth. The floral meristem emerge out of the meristem and have same organisation as the shoot apical meristem. They create flowers and stop growing after some production. *Reprinted from [9].* [3]

then be approximated by calculating the mechanics of a cylinder with hemispherical top inflated by a pressure [12]. At the very top of the dome shaped tissue stresses are isotropic, whereas at the cylindrical flanks, the circumferential stresses are higher than the radial stresses, see Fig. 1.4.

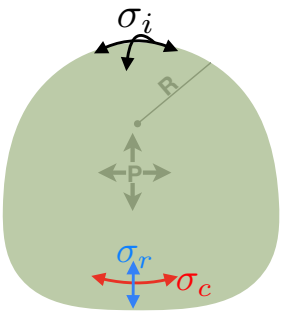

Figure 1.4: The shoot apical meristem can be imagined as a shell inflated by a pressure from underneath. The dome top of the SAM has isotropic stress denoted by $\sigma_i = \frac{PR}{2}$, where P is the inner turgor pressure and R is the radius of dome. On the cylindrical flanks, circumferential stress $\sigma_c = PR$ is larger than the radial stress $\sigma_r = \frac{PR}{2}$.

To understand the impact of such stresses on the growth of cells and the formation of tissue, we need to understand the mechanism behind cellular growth. In the next sections, we will dive into the biology and the accompanying mechanics responsible for cellular growth in plants.

[3] Copyright 2003, reprinted with permission from Elsevier.

1.1.1 Mechanics shaping plant cells

Plant cells are enclosed by rigid cell walls and the mechanics of these walls dictates the cell growth (Fig. 1.5). The growth largely results from uptake of water by cells and yielding of cell wall under growing turgor pressure [13, 14]. The pressure is isotropic within the cell, thus, any growth patterning relies on the anisotropic properties of the cell wall. Most strikingly, the growth of cells within a tissue is coupled mechanically through the shared walls. Expansion of one cell is communicated to all immediate neighbours through forces on cell walls and junctions. This mechanical coupling along with biochemical signalling have been suggested as possible organisers of growth in plant tissue [15–17].

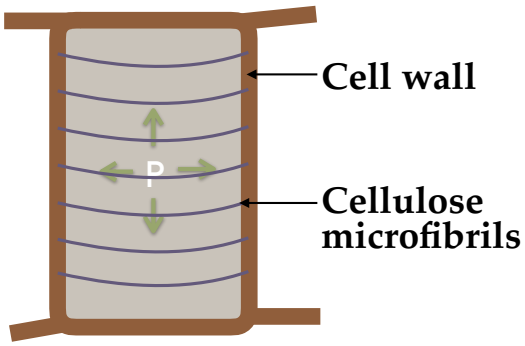

Figure 1.5: Plant cells are enclosed by cell walls, which are shared between the cells. The turgor pressure P from within the cell pushes on the walls but are bounded by the rigidity of the cell walls derived from the cellulose microfibrils present in them.

It has been long observed that cellulose microfibrils of the cell wall are oriented in transverse direction in elongating cells [18]. The microfibrils, which are bound together by hemicelluloses and are embedded in a matrix of pectin, are the major load bearing component of the cell wall [7]. The stiffness of the wall depends on the orientation of the fibers and is higher in the direction parallel to the orientation of the cellulose fibers [19]. The positioning and role of microfibrils have been described as like “hoops around a barrel” [18]. This is crucial in promoting anisotropic cellular growth from an isotropic pressure.

Cortical microtubules (CMTs), present in the cell cortex, are decisive in the deposition of new microfibrils on the cell wall as they mediate the movement of cellulose synthase complexes [20, 21]. The complexes move along the tracks lined up with CMTs and align the cellulose microfibrils along

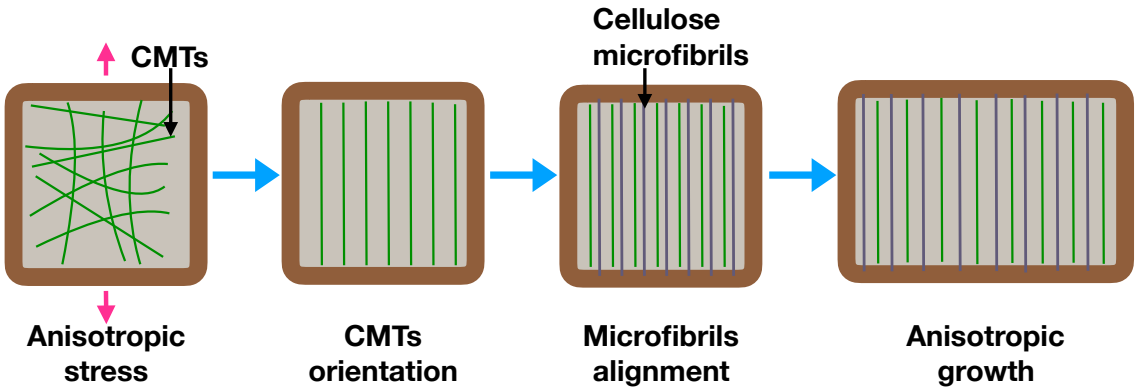

Figure 1.6: Anisotropic stress on cell (shown by pink arrow) orient the cortical microtubules (CMTs) in the direction of maximal stress. The cellulose microfibrils are paved in the same orientation as CMTs, like "hoops arround a barrel", resulting in stiffer wall in that direction. As a consequence, the cell grows orthogonal to the maximal stress towards the less rigid direction of the wall.

the directions of microtubules [22, 23]. The orientation of CMTs itself is strongly linked with mechanical stresses on the walls [10, 24–26]. The microtubules generally align towards the direction of maximal stress and arrange as "hoops" around the cell, which results in paving of cellulose microfibrils in the same direction [10, 20, 26, 27]. Therefore, stress patterns emerging during development are a putative key actor to organize growth and shapes of tissues in plants (Fig. 1.6).

1.1.2 Growth hormones involved in morphogenesis

Besides the elastic yielding and restructuring of cell wall under stress, the patterns of cellular growth in plants are driven by biochemical signaling [28]. A suggestion for biochemical activity in plant morphogenesis can be traced back to Ciesielski (in 1871), who wrote about "transmitted influence" in his study of gravitropism[4] in the roots [29]. The roots with tips cut off when extended horizontally did not show any effect of gravitropism. Further, it was observed that if the tips were cut off with some delay after extending the roots horizontally, the roots would bend like being acted on by gravitropism, even if the orientation was changed [30]. Similar "transmitting influence" was also observed in the investigation of phototropism [30]. Paál in 1919, with his research on coleoptile tips of *Coix*, came to the conclusion that in the tips, a "substance" or a "mixture" is

[4]It is the growth process of plants directed by gravity. Roots show positive gravitropism (towards the gravity) and stems show negative gravitropism (away from gravity).

produced that is distributed around and if this "substance" is accumulated on one side, the growth rate changes resulting in curvature on the tissue [31–33]. Kögl and Haagen-Smit are thought to be the first to isolate the growth hormones responsible for the "transmitting influence" and named them "auxin" from greek verb *auxein* meaning "to grow" [34, 35]. The development of techniques to collect growth hormones through diffusion in agar blocks later led to the isolation of 3-indoleacetic acid (IAA) from corn kernels [32, 36, 37]. With the systematic study of biochemicals in growth, it was soon realised that the IAA was an important member of the auxin group and that the auxin was central in plant morphogenesis [33].

The role of auxin is plentiful inside the plant biology. It is vital in cellular growth as it mediates cell wall loosening and elongation among other functions [38–41]. IAA specifically causes reduction in hemicellulose polysaccharides, increases pectin polymerisation and viscosity, resulting in reduced stiffness of cell wall [39, 40]. The organ formation in plants from shoot apical meristem is preceded by accumulation of auxin and consequent local promotion of cellular growth [16, 42–44]. Initial outgrowth of organs from the SAM, called the primordia (Fig. 1.2), have been observed to be surrounded by localised auxin efflux carrier PIN1 [15, 42, 44]. PIN1 proteins are asymetrically located on the cells and they carry the directional flow of auxin through the tissue into the primordia [45]. The dynamical gradient of auxin created by the carriers generate growth patterns in the tissue that result in the organ formation, as seen in Fig 1.7 [43].

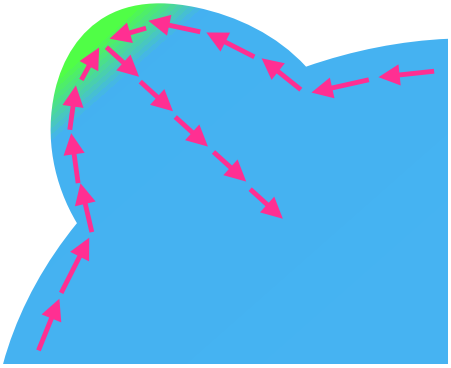

Figure 1.7: PIN is polarised towards the primordium creating the flow of auxin (shown by red arrow) into the primordium from the outer layer of the meristem and later drained into the inner tissue. The gradient of auxin (in green) generated with the maximum at the tip promotes the growth of organ on SAM [43].

1.1.3 Feedback between mechanics, cellular growth and growth hormones

Mechanics itself is thought to be the key organiser of the patterning of auxin and PIN1 on SAM leading to the organ formation. This view is supported by the observation of strong correlation between PIN1 and microtubule patterning and initiation of organ by modification of cell wall properties [15, 46]. Further, the alteration of mechanical properties of the SAM through osmotic treatments and application of external forces displayed significant changes in the density of PIN1 localisation in cells [16]. In hypoosmotic solution, the cells absorb more water and inflate in size causing additional stress on the walls, which causes an increase in PIN1 density in the cells. While in hyperosmotic solution, cells lose water and deflate reducing the stresses, this results in lower density of PIN1. This implies that the mechanics is directly involved in the regulation of PIN1 and hence the auxin flow.

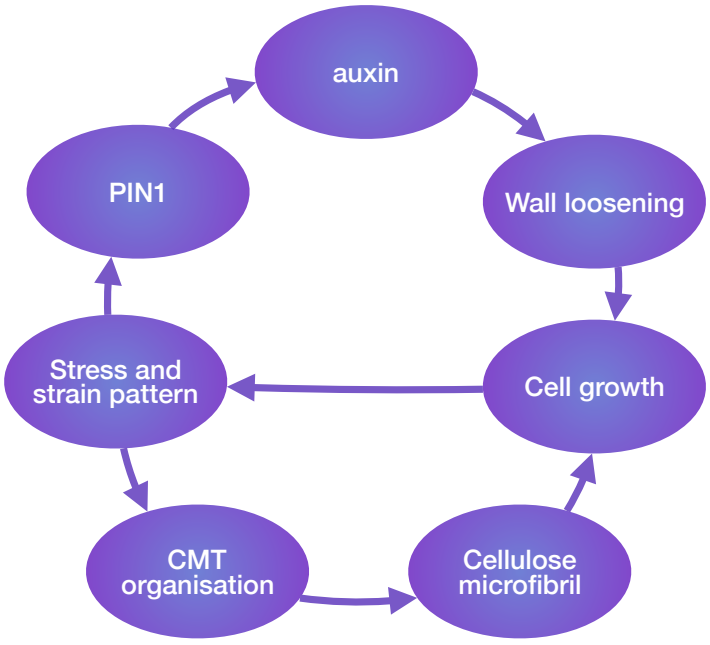

Figure 1.8: Mechanics (stress and strain patterning) of the plant tissue regulates cellular growth by controlling the flow of auxin (upper cycle) and by modulating the cell wall properties (lower cycle).

As auxin promotes growth by modulating the cell wall properties and reducing the stiffness, an interesting prospect of feedback between PIN1 localisation, auxin flow and mechanical properties

comes out of the observations [16, 40]. The polarity of PIN1 have been observed to change with distribution of auxin and further aid the auxin mediated growth [16, 44]. The growth induced by auxin modulates stiffness and stresses on walls that impacts PIN1 polarity and in return influence the auxin flow itself. The complete schematics of involvement of mechanics with biochemical messengers along with organisation of cellular growth as discussed in section 1.1.1 can be summarised as shown in Fig. 1.8.

1.2 Mechanical models for stress dependent growth in plants

The cells in plants are fixed in their location by rigid walls and the tissues are shaped without cell migration and intercalation. The plant cells grow through the slow elongation or *creep* of walls under the turgor pressure. The speed of the *creep* depends on the wall stiffness and stiffer walls *creep* slower than softer ones [7]. This mechanistic growth in plants provides an excellent subject to employ the physical knowledge developed in past centuries with the rigorous study of inanimate materials, and expand similar deep understanding to the self-assembling and morphing animate life. The development of growth models, in the footsteps of the physical laws, have played an invaluable role in this pursuit. They have shed light on the contribution of mechanical forces on otherwise considered biochemical processes, such as cell growth and organ formation, and carry the potential to unify the underlying physical mechanism with biological signalling that could unravel the mystery of morphogenesis.

Several classes of growth models have been developed to simulate the plant growth that vary in scale and type from wall-based, cell-based to continuous models. The study of virtual growth in the plants has implicated mechanics in several growth processes. The stresses on cells and their response has been found to regulate the growth variability in plant cells [26]. With the microtubules-based stress sensing, the cells are able to pick up and respond to the mechanical patterns on the tissue that cause amplification of any growth heterogeneities and results in morphological changes. Similarly, cell division organisation and robust shaping of sepal have also been found to be influenced by stress sensing through the employment of growth models [47, 48].

The tissues in these models are generally described as a cumulation of regions that can be single cells or a patch of cells. The growth of overall tissue is the result of growth in these regions and the adjustments between them (Fig. 1.9). Most of the growth models have focused on the analysis

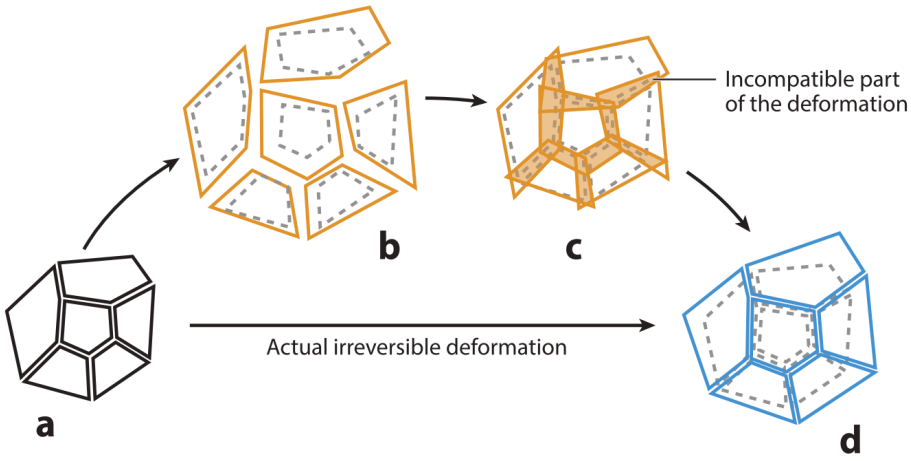

Figure 1.9: The combination of regional growth and adjustment drives plant tissue growth. (a) Individual regions on plant tissue. (b) The shape growth of each region if they were isolated. (c) The conflict due to the regional growth. (d) The regions adjusts to shape the final tissue. *Reprinted from [49].*[5]

of the stress patterns created by differential growth of these regions in two-dimensions. But in the recent times, the development of three-dimensional growth models have demonstrated the importance of capturing both the geometry and the mechanical properties of the tissue in examination of the tissue morphogenesis.

Utilising the stereotypic geometry of meristem, the CMT orientation in cells of shoot apical meristem were faithfully recreated by aligning them with the stress field generated by the differential growth in the meristem [50]. In a recent work, this approach was taken further with inclusion of direct modelling of wall sitffness on a meshed plant tissue [51]. Again with simulation of stress and strain field generated on stereotypic tissue shapes, the authors were able to show complex growth dynamics like longitudinal strains on the shoot and wound healing.

Many other growth models have focused on the generation of morphological and geometrical features on the plant tissues instead of relying on the mould of tissue-like shapes for the study. The morphological changes leading to the organ growth on a three-dimensional meristem was shown to be initiated by changes in tissue properties with a small amount of gene activity [52]. The growth of the primordia like outgrowth was verified to be prompted by the local loosening or the accelerated growth of the cells. Several factors such as directional loosening of walls, stiffening of regions around the primordia or the overall promotion of growth rates in the primordial cells were sug-

[5]Copyright 2014 Annual review of cell and developmental biology by ANNUAL REVIEWS, INC. Reproduced with permission of ANNUAL REVIEWS in the format Thesis/Dissertation via Copyright Clearance Center.

gested to contribute to the primordial growth. The differential growth created by polarity field of genes on the tissue was also found to be behind the complex flower morphology [53]. The conflicts between separately growing regions in a tissue and the consequent resolution were shown to cause the folding and bulging of epithelium to create elaborate shapes of flowers. Similar conflicts and resolution caused by differential growth on tissues can be expected to be the foundation of all kinds of morphology in plants.

1.3 What drives primordial growth?

The organs on shoot apical meristem begin as primordia on the tissue surface. The flow of auxin into the primordial region locally promotes growth in the cells leading to eventual budding of the organs (Fig. 1.7) [15, 16, 42–44]. Nevertheless, it is not clear if the large growth rates on a group of cells is sufficient to have an organ budding on the tissue. The faster growing patch of tissue can either spread on the surface of the tissue or it can instead bulge out (Fig. 1.10). What causes the primordial cells to bulge out instead of spreading on the tissue is not yet known.

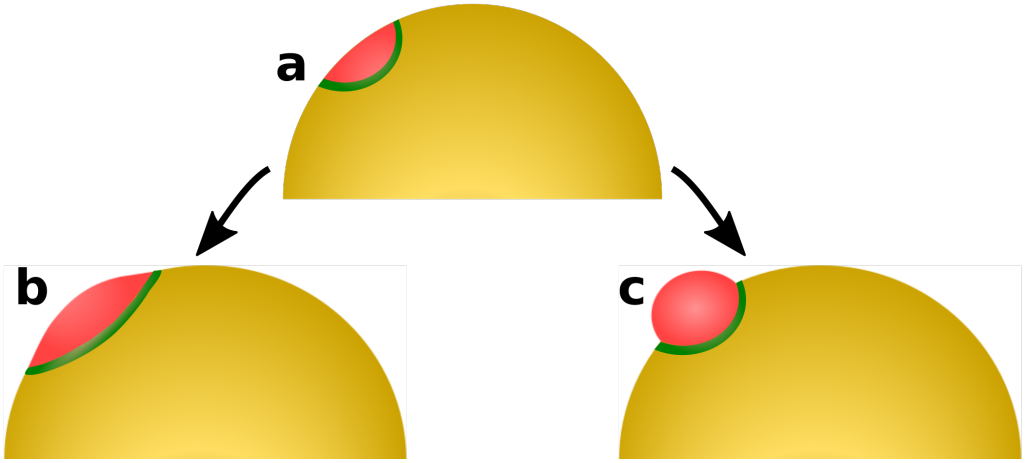

Figure 1.10: The outgrowth of aerial organs in plants starts from primordia on the shoot apical meristem. (a)–(c) show the growth of primordia from a group of faster growing cells on the mertistem. (a) A patch of cells (in red), due to the auxin accumulation, grows faster and leads to the initiation of primordium. The cells in the boundary (in green) between the primordia and meristem also play vital role in the budding of primordium. The higher growth of primordial cells can either lead to a spread out of the region on the surface of SAM, as shown in (b), or bulging of the region out of the SAM, like in (c), laying the foundation for the organogenesis.

The mechanical models have shown that the loosening of cell walls and promotion of growth in a region can lead to some growth of primordia [10, 52, 54]. However, the models required additional stiffening of the cells around the primordia and directed growth on the primordial cells to show significant organ outgrowth [52, 54]. This again points to the question if the elevation of growth in the primordial region is sufficient for plants to create organs from the meristem. The models have also not yet explored the disparate growth patterns that emerge on the meristem during the primordial growth.

With the auxin-led wall loosening, the cells in the primordia grow faster and isotropically, but the cells surrounding the primordia, on the boundary between the primoridal region and the meristem, show slow growth and anisotropic shapes [55–57]. Cell division rate on the boundary cells is also significantly reduced and the boundary grows into a saddle shape with negative curvatures in the radial direction [56, 57]. The elongated shapes of these cells are created by growth in circumferential direction that is accompanied by compression in the direction toward the primordia (radial) [58]. A puzzling observation is that the cells in the boundary show strong orientation of microtubules along the circumferential direction possibly due to the high anisotropic stresses [10, 50]. The cellulose microfibril on the boundary cells also follow the same direction of orientation, reenforcing the walls circumferentially, around the growing primordia [59]. This raises an interesting question: as the boundary cells show higher circumferential growth, how do the cells grow more in the stiffer direction?

Recent works have shown the high stress pattern around the primordia are outcome of the tissue geometry and the expansion of primordial region [10, 50, 51]. But there are still no clear understanding on the cause of strange growth patterns of the boundary cells and other mechanical patternings on the tissue. The cells at the boundary are observed to have different gene expression patterns to that of the meristem or the primordia [57]. Are these genes manifesting the unexpected growth through their regulatory actions or are the growth patterns an outcome of the interaction between the cells and the tissue mechanics? The answer is still not known.

1.4 How does the shoot elongate?

The longevity of plant is dependent on the development of its organs and elongation of the shoot to enlarge the reach of those organs. To initiate and maintain the longitudinal growth of the shoot,

the cellular growth in the meristem needs to be coordinated [51, 52, 60]. Without any organisation, the isotropic tip of the meristem could grow out as a spherical bulb and disrupt the elongation of plant body (Fig. 1.11). There is lack of understanding on how the cellular growth is organised on meristem to transform it from hemispherical shape to an elongated shoot.

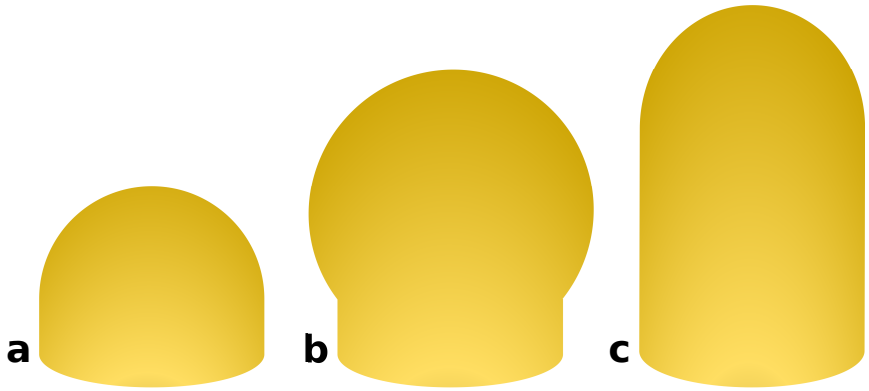

Figure 1.11: The meristem is shaped as a dome sitting on top of a cylindrical shoot. The initial shape of the meristem, as shown in (a), can transform into a spherical bulb as seen in (b), if all the cells in the isotropic tip of the SAM grow uniformly. However, the meristem is seen to grow longitudinally adding to elongation of the shoot as shown in (c).

At the fundamental level, to elongate, the tissue needs to undergo a symmetry breaking in growth. The investigation for mechanism behind such symmetry breaking in biology has been a topic of interest for a long time. The large body of work that examine the generation of cylindrical growth in biological systems cover bacteria, pollen tubes, fungal hyphae, root hairs, shoot growth among others [51, 52, 60–64] . Much of cylindrical or tip-like growth in these systems are thought to be the consequence of regionally constricted growth [60]. The pollen tube or root hair is considered to have a growth gradient from the tip producing the elongation (Fig. 1.12 a) [62]. Bacteria instead exhibit growth on the cylindrical body, adding material to extend the shape (Fig. 1.12 b) [63]. Remarkably, the shoot growth in plants does not fall in either of these categories. The meristem is known to have slower growth at the very tip (in the central zone) and have confined elevated growth on the cells in the region around the center or the periphery zone (Fig. 1.12 c) [55, 56, 65]. The impact of this unique patterning in generation of an elongated shape is still to be studied.
The cellular growth in plants is intrinsically equipped with mechanism for symmetry breaking. The deformation-led growth with mechanical feedback on cells can orient the stiffness and hence

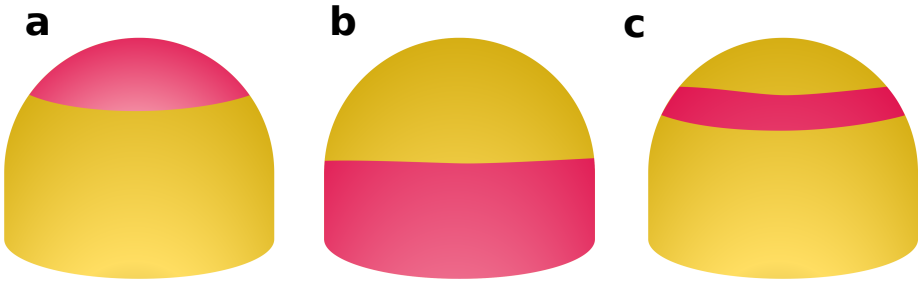

Figure 1.12: Generation of elongated shapes in biological systems relies on locally constricted growths (highlighted in red). (a) Growth at the tip of the shape is found in pollen tubes. (b) Diffusive growths in the cylindrical body is used in bacteria to grow tube-like shapes. (c) Enhanced growth in shoot apical meristem is localised in the off-center region called the periphery zone.

the cellular growth. The strong anisotropic stresses on the flanks of the meristem (Fig. 1.4) that lead to anisotropic stiffness have been suggested to be involved in the shoot elongation [51, 52]. Further, by decreasing the wall stiffness with chemical treatment that lead to homogeneous mechanics on the tissue, the meristem has been shown to inflate like a sphere [66]. Thus, the regulation of stiffness and cell growth in meristem are central in the shaping of the elongated shoot.

The addition of new material by cell division in the tissue can also be suspected to have an influence on the initiation and maintenance of shoot elongation. The cell division adds new walls to the meristem that modify the structure of the tissue. The orientation, number and location of these walls can modify the tissue mechanics significantly. The pattern of divisions on the meristem has been known to exhibit a strong trend: the central cells at the tip divide much less compared to the peripheral cells [8, 55, 56]. These confined divisions along with their orientation and enhanced growth in the peripheral cells could be consequential in the transition of the dome shaped meristem to the cylindrical shoot. An investigation to examine this and understand the influences of the growth, division patterns and the mechanical feedback in shoot elongation and maintenance is yet to be done.

1.5 Understanding the organ growth and shoot elongation with mechanics

In the work presented here, we build upon the works of the community determined to understand the root of robust plant morphology. The three-dimensional model that will be developed in the next chapter is utilised to study the budding of primordia out of the shoot apical meristem and elongation of the shoot. The chapter 3 and 4 will investigate the organogenesis on the meristem and the cylindrical growth of the shoot respectively.

In the investigation of organ growth in plants, we will study the causes for the noted patterns in the tissue during the organ development and study their importance in the outgrowth. Further, we explore the role of stress based feedback on cellular growth and if it interacts with the emerging mechanical patterns on the tissue to organise growth. The patterns around primordia could be vital cues for cells to direct budding of organ. We test this hypothesis by varying the degree of mechanical feedback on the cellular growth and analysing the resulting tissue. We also study the significance of mechanical feedback itself and if the elevated growth on primordial cells is enough for the growth of the plant organs. What leads the primordial growth to bud out (Fig. 1.10 *c*) instead of just spreading of cells on the meristem (Fig. 1.10 *b*)? Our goal is to understand how the mechanical patternings in the tissue arise and what role the mechanics-led feedback plays during the organ development.

In the context of shoot elongation, we want to understand the vital mechanisms behind the directed large scale growth in plant tissue. A näive expectation of the resulting morphology of tissue formed by the dome shaped meristem would be an inflated tissue of the same shape. However, plants elongate themselves to better position to gather resources. What are the main organisers behind this elongation of plant shoot? We will investigate the role of noted patterns of growth and division and if they are behind this asymmetric tissue growth. We will also explore the influence of mechanical feedback to understand mechanism behind the creation of large scale growth patterns that might lead to shoot elongation. We want to understand what are the main factors behind the initiation of elongated shoot from dome-like meristem and how are plants able to maintain their cylindrical morphology.

2

Vertex model for plant tissue

This research aims to uncover the entangled role of mechanics in the shaping of tissues in plants. Our goal is to explore the emergent growth patterns in the shoot apical meristem (SAM) and address the question: is mechanics a significant contributor in the development of SAM? To answer this, we developed a three-dimensional mechanical model of the tissue that we utilised to study the morphing of the SAM with cellular resolution. The built model is a three-dimensional vertex model of the SAM (Fig. 2.1), where individual cells, represented by a collection of vertices, are tiled together to form a tissue.

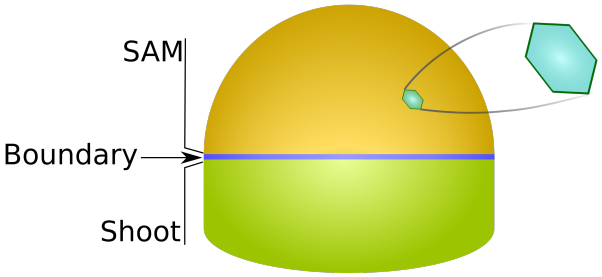

Figure 2.1: The shoot apical meristem is idealised as a hemispherical tissue composed of polygonal cells on top of a hardened shoot. The boundary connecting SAM and the shoot defines the boundary condition for the simulation.

The basic ingredients required to simulate the mechanics of a plant tissue are the cellular structure or the topology of the tissue, a constitute law for the tissue mechanics and a constitutive law for cellular growth [49]. In this chapter, we will describe these main elements of the model and further

additions that helps us to understand the development of the SAM.

2.1 Epidermal morphogenesis in plants

The SAM in eudicot plants is composed of organised layers of cells, with L1 as outer layer, L2 as the next immediate layer and L3 as the inner cells of the tissue [67] (in many monocots, the SAM can also be composed of only 2 layers of cells [68]). The L1 and L2 layers divide predominantly in anticlinal[1] orientation maintaining the layer separation, while cells in L3 layer divide in all directions. The width of the layer is also well maintained in the epidermis, with cells of uniform thickness of $\sim 5\mu m$ [48]. The epidermal cells are known to play central role in the shaping of the shoot as they have been shown to accumulate and organise flow of key biochemical molecules controlling the growth in the tissue and initiating new organs in the SAM [44, 69]. Further, the epidermal layer is considerably stiffer than the inner tissue and acts effectively as a stiff surface under tension from the turgor pressure of homogenous tissue underneath [10, 11].
We build our model with these consideration on the L1 layer and assume the SAM as a stiff shell of cells that is inflated by a turgor pressure exerted from the inner tissue. This general assumption is a feature in many computational models studying the behaviour of plant tissue and has been successful in providing insights on the orientation of cortical microtubules and the growth behaviours in plants [10, 51].

2.2 Three-dimensional vertex model

Vertex models have been used to explore tissue shapes in epithelial morphogenesis in a variety of model systems [3, 70–73]. A vertex model represents cells as a collection of vertices that describe their shape. The cells are here modelled as a two-dimensional polygon (Fig. 2.3). The cells may be in addition given a thickness by adding a height term. In our formalism, we instead use bending stiffness of cells to represent their height. The vertices are shared between the neighbouring cells and this provides a vital advantage in modelling plant cells as they share cell walls and do not slide past each other, unlike animal cells. Each of these vertices represent a junction between cells and is subject to force balance. The movement of vertices, representing deformation of cells, arise

[1] Cell walls perpendicular to the tissue surface

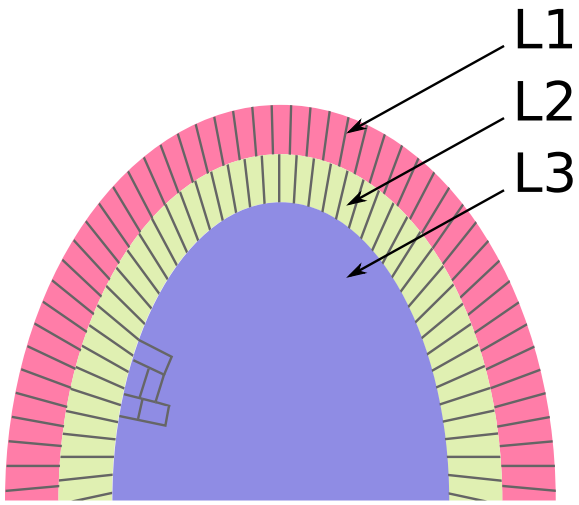

Figure 2.2: The shoot apical meristem has well organised epidermal (L1) and subepidermal (L2) layers of cells. The cells in these two layers divide almost exclusively in anticlinal direction preserving the layer separation (shown by the organised layers of cells). The cells in inner layer (L3) can divide in any direction (also shown) and they push on the epidermal cells with turgor pressure.

from changes in this force balance due to processes like cellular growth and cell division. The cells in our computational model are two-dimensional polygons but are free to move around in three-dimensional space. This allows us to investigate how individual cell growth dynamics can drive plant tissue growth.

2.2.1 Implementation with quad-edge data structure

The vertex model simulation requires the storage of the topological and the positional information of the vertices in the tissue. A convenient solution to this is the quad-edge data structure [74]. It can represent all types of polyhedra through the use of edge, vertex and face information (Fig. 2.4 *a*). The central characteristic of the data structure is the emphasis on the role of the edge in the topology. Quad-edge stores the mesh topology and its dual at the same time by storing a group of four directed edges for each undirected line joining two points in the mesh. The operations **Sym**, **Rot** and **InvRot** allow to jump among the the four edges as shown in Fig. 2.4 *b*. The first two edges stored (**e** and **e**→**Sym**) are the two directed edges between two vertices in the mesh and the other two are the dual of these first two edges. These two dual edges (**e**→**Rot** and **e**→**InvRot**) are directed edges between the two faces on the sides of the original edge (edge **e** in Fig. 2.4 *b*). The

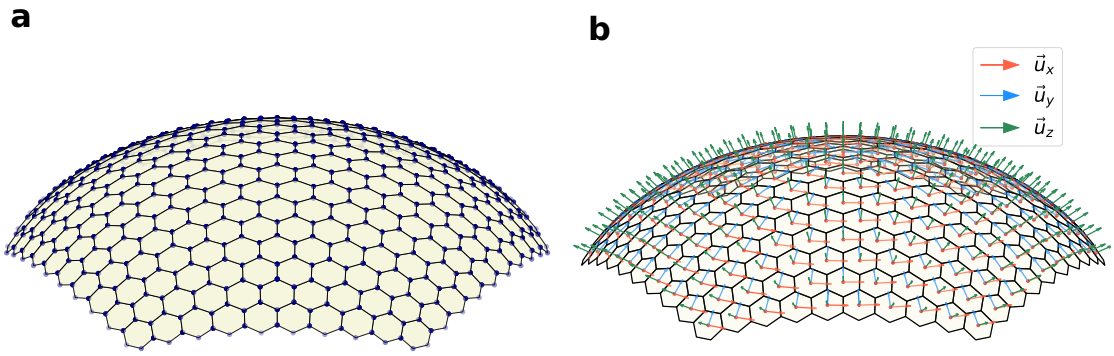

Figure 2.3: (a) The SAM in the three-dimensional vertex model is completely defined by the positional and the topological information of the vertices. The whole mesh is described as the tissue and each face closed by a collection of vertices on the mesh is the cell. These cells share walls or more appropriately, the vertices with adjacent neighbours. (b) An intrinsic coordinate system is defined for each of the cells with origin on the centroid and two orthonormal vectors on the surface of cells as the unit x and y vectors. The unit z vector is taken as the normal to the cell surface. This intrinsic coordinate is used in computation of the mechanical energy. The arrows show the unit vectors in x (red), y (blue) and z (green) directions for each cell.

simplicity in moving around in this group of edges also allows for organised and easy movement around the mesh. In addition, the vertices are shared between the edges and the faces. As a consequence, movement of a vertex is automatically recognised by all of the neighbours.
We use an open implementation of quad-edge data structure in the simulation of plant tissue [75]. The computational simulation described in the following sections is built on top of the quad-edge implementation and utilises the ease of movement in the mesh and organised storage of information.

2.2.2 Shape matrices as cell representation

The representation of cells and the tissue in the vertex model is discreet. To gauge the deformation and other physical quantities from this discrete representation, we define a shape matrix for a cell. The shape matrix is computed as a second moment of area matrix M_c on the vertices with respect to the intrinsic coordinate system (Fig. 2.3 b) for each cell c, written as

$$M = \begin{bmatrix} \iint_S x^2 dxdy & \iint_S xydydx \\ \iint_S xydydx & \iint_S y^2 dxdy \end{bmatrix}, \tag{2.1}$$

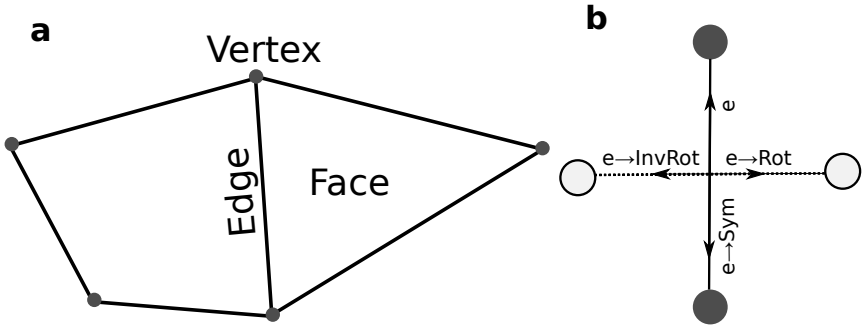

Figure 2.4: Quad-edge data structure can represent a polygonal mesh topology by storing edge, vertex and face information. (a) Edges are the boundary between two faces and the vertices are the end points of edges. (b) In quad-edge, the edges are directed, thus an *origin* and a *destination* for each edge is defined. Simple operations of moving to the adjacent edges are described in quad-edge (**Sym**, **Rot** and **InvRot**) as shown for an edge **e**. The edge **e** and its flipped edge **e**→**Sym** are the two directed edges between the two vertices (black cirlce). The other two (**e**→**Rot** and **e**→**InvRot**) are the two dual edges that connect the two faces (white circle) on the either side of edge **e**.

with the integral over the tissue surface S. The diagonal terms have been flipped from the usual definition of the second moment of area matrix to align the matrix geometrically with the shape of the polygon. This has no bearing on the computation of the energy functional but is an aid for visual representation. The matrix M_c can be discretised on the polygonal cells as,

$$\begin{aligned} M_{xx} &= \frac{1}{12}\sum_i a_i(x_i^2 + x_i x_{i+1} + x_{i+1}^2) \\ M_{xy} = M_{yx} &= \frac{1}{12}\sum_i a_i(x_i y_{i+1} + 2x_i y_i + 2x_{i+1}y_{i+1} + x_{i+1}y_i) \\ M_{yy} &= \frac{1}{12}\sum_i a_i(y_i^2 + y_i y_{i+1} + y_{i+1}^2) \end{aligned} \tag{2.2}$$

where the summation is over the vertices of the cells and $a_i = (x_i y_{i+1} - x_{i+1} y_i)$.
The cells reside in a tissue and are deformed due to the forces on them from the interactions with the neighbouring cells. Like an elastic line under tension, we can write a rest shape and a current (deformed) shape for each cell. The current shape is the shape of the cell c that is observed in the tissue and is described by the shape matrix M_c (Eq. 2.1). The rest shape is the shape that a cell c wants to acquire in order to reach its energy minimum and is denoted by M_c^0. The energy minimum for the whole tissue lies away from the individual minimum of each cells due to the intercellular coupling. This implies that all of the cells can face some deformation of their rest shape in tissue's

equilibrium state.

The rest shape of an individual cell is its form in complete mechanical equilibrium, but it is not possible to observe a plant cell out of the tissue environment. In the simulation, we start with a mesh of homogenously shaped cells and under the application of forces on the tissue, the cells deform away from their initial shape (Fig. 2.5). We take the initial homogenous shape as the rest shape for the cells and the deformed shape as the current shape.

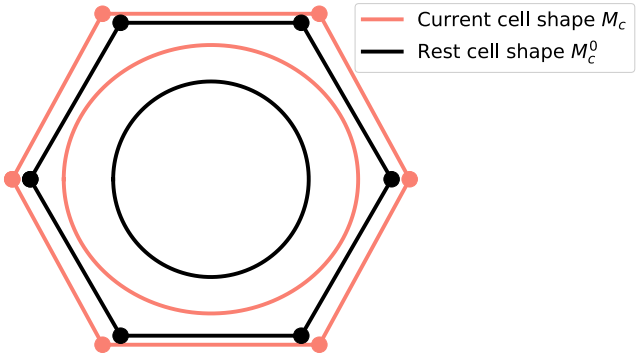

Figure 2.5: The cells are represented by a current cell shape matrix M_c and a rest cell shape matrix M_c^0. The cells in the simulation start initially as a regularly shaped hexagons (black) and due to the stresses on them, they deform to their current shape (red). The shape matrix of initial shape (black ellipse) is taken as the rest cell shape and deformed shape matrix (red ellipse) defines the current shape.

2.3 Mechanical energy of tissue

The morphology of a tissue is a result of the competition between the mechanical equilibration of the system and active biological processes inside that push it out of equilibrium. The mechanical energy for equilibration can be written as a functional with sum of the energy costs for specific deformations. We take the functional for shoot apical meristem as

$$U = U_{\text{elastic}} + U_{\text{bending}} + U_{\text{pressure}}, \tag{2.3}$$

accounting for cell's elastic deformation, bending and the shoot's internal pressure as discussed in detail in the following sections. This functional is minimised to obtain the equilibrium shape of the tissue.

2.3.1 Elastic energy for the cells

The central aspect of tissue growth is the deformation on the cells. The shape and the growth of the cells are product of the deformation on them. We can quantify the strain energy on the cells by assuming isotropic linear elastic properties for the cells.
The generalised Hooke's law for linear materials relating the stress and the strain can be written as

$$\sigma_{ij} = C_{ijkl}\epsilon_{kl}. \tag{2.4}$$

C_{ijkl} is the fourth-order stiffness tensor of the material (elastic moduli). For an isotropic material, taking advantage of the symmetries, the stiffness tensor can be simplified to

$$C_{ijkl} = \mu(\delta_{ik}\delta_{jl} + \delta_{il}\delta_{jk}) + \lambda\delta_{ij}\delta_{kl}. \tag{2.5}$$

The parameters λ and μ are Lamé's first parameter and second parameter, respectively. These parameters are related to the elastic moduli of the material and can be expressed as

$$\lambda = \frac{E\nu}{(1-2\nu)(1+\nu)} \tag{2.6}$$

$$\mu = \frac{E}{2(1+\nu)}. \tag{2.7}$$

E is Young's modulus and ν is the Poisson's ratio of the material. With Eq. 2.4 and 2.5, we can write the stress-strain relation as,

$$\sigma_{ij} = 2\mu\epsilon_{ij} + \lambda\delta_{ij}\sum_k \epsilon_{kk}. \tag{2.8}$$

Using the Eq. 2.8, the strain energy density of an isotropic material, which is a quadratic function in strain, can then be written as[2]

$$\upsilon_{\text{elastic}} = \mu\sum_{ij}\epsilon_{ij}^2 + \frac{1}{2}\lambda\Big(\sum_i \epsilon_{ii}\Big)^2. \tag{2.9}$$

[2] As $\sigma = \frac{\partial U}{\partial \epsilon}$, the energy is of second order in ϵ ($U = \frac{1}{2}C_{ijkl}\epsilon_{ij}\epsilon_{kl}$). To get a second order scalar equation of energy, we need terms in second order of ϵ. This can be written as two invariants for second order tensors, square of sum of diagonal elements $\sum_i \epsilon_{ii}$ and square of sum of all elements $\sum_{ij}\epsilon_{ij}^2$ [76].

We need to define an appropriate strain tensor to compute the strain energy for the cells from Eq. 2.9 in the vertex model. We write the strain tensor as the difference of current cell shape and rest cell shape matrices (Eq. 2.1) as shown in Fig. 2.6 , written as

$$\epsilon = \frac{M_c - M_c^0}{\mathrm{Tr}(M_c^0)}. \tag{2.10}$$

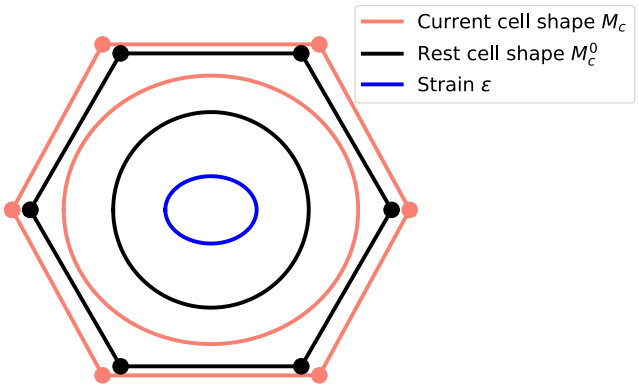

Figure 2.6: The strain ϵ (blue ellipse) on a deformed cell is defined as the difference between the current cell shape (red ellipse) and the rest cell shape (black ellipse).

The stress can then be calculated using Eq. 2.8. With these definitions, a complete expression for the elastic energy can be calculated by integrating Eq 2.9 over the tissue surface to obtain

$$U_{\text{elastic}} = \mu \sum_c A_c \frac{\|M_c - M_c^0\|_2^2}{\mathrm{Tr}^2(M_c^0)} + \frac{1}{2}\lambda \sum_c A_c \frac{\mathrm{Tr}^2(M_c - M_c^0)}{\mathrm{Tr}^2(M_c^0)}. \tag{2.11}$$

$\|\cdot\|_2$ is the Frobenius norm for a matrix defined as

$$\|A\|_2 = \sqrt{\sum_{ij} a_{ij}^2} \quad , \tag{2.12}$$

where A is a matrix with components a_{ij}. The summation is over all the cells in the tissue. We set $\lambda = 0$, which is proportional to the Poisson ratio ν (Eq. 2.6), to further simplify the elastic energy

expression to

$$U_{elastic} = \mu \sum_c A_c \frac{\|M_c - M_c^0\|_2^2}{\mathrm{Tr}^2(M_c^0)}. \tag{2.13}$$

This simplification has no impact on the simulation resultss as the mechanical behavior in developing tissues can be considered stable under varying Poisson ratio [50].

2.3.2 Bending energy of the tissue

Considering cells on a two-dimensional surface free to move in the three-dimensional space allows for twists and bends of cells. For epithelial cells in a tissue, the cells are restricted by, first, the walls that are perpendicular to the surface (anticlinal walls) and, second, by junctions with cells around them. Any significant bend or twist away from the epithelial surface would mean a major deformation on the anticlinal walls and on cells underneath. Thus, we add a bending term to the mechanical energy that penalizes deformations of anticlinal walls. It is based on works of Canham and Helfrich, who considered a three-dimensional soft object with an infinitely thin interface with bending resistance [77–79],

$$U_{bending} = 2\mu_b \int_S (H - H_0)^2 dA + \int_S \mu_K K dA, \tag{2.14}$$

$$H = \frac{1}{2}(k_1 + k2), \tag{2.15}$$

$$K = k_1 k_2, \tag{2.16}$$

where H is the local mean curvature and K is the Gaussian curvature. k_1 and k_2 are the principal curvatures at a point on the tissue surface S. H_0 is the spontaneous curvature of the surface and μ_b and μ_K are the associated bending stiffnesses. H is taken to be positive for the dome shape of the shoot tip. The Gaussian curvature K can be integrated out of the energy equation as it remains constant for a surface with fixed topology, which leaves a single term of mean curvature for bending energy [80, 81].

The tissue in the vertex model is a discrete mesh of vertices, which poses challenges for the computation of H. We adpated the discretization developed by Meyers et al. to compute Eq. 2.14 for the tissue [79, 81].

The local mean curvature arround a point on the surface can be rewritten as

$$H(\vec{x}_i) = \frac{1}{2}(\Delta_S \vec{x}_i) \cdot \vec{n}(\vec{x}_i), \qquad \vec{x} \in S. \tag{2.17}$$

$\vec{n}(\vec{x}_i)$ is the normal vector at point $\vec{x}_i$. The operator Δ_S is the Laplace-Beltrami operator for the surface S, and is expressed as,

$$\Delta_S = \nabla^S \cdot \nabla^S, \tag{2.18}$$

with ∇_S as the gradient of the surface. The mean curvature H can be obtained from the operator Δ_S by rewriting the Eq. 2.17 as

$$H = \frac{1}{2}\|\Delta_S \vec{x}\|. \tag{2.19}$$

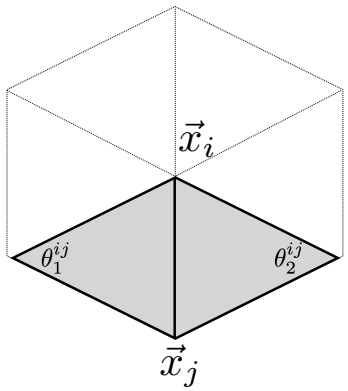

Figure 2.7: For a vertex $\vec{x}_i$, 1-ring neighbours are all the vertices that are joined by an edge to $\vec{x}_i$ in the mesh and θ_1 and θ_2 are opposite angles to the edge joining vertex $\vec{x}_i$ and its neighbour.

We can write a discretisation of Laplace-Beltrami operator on a triangulated mesh by considering directly connected neighbours for each vertex $\vec{x}_i$. We call these connected neighbours as 1-ring neighbours for a vertex. The discretisation of the operator is then obtained by a contour integral around 1-ring neighbouring vertices of a vertex $\vec{x}_i$ (Fig. 2.7) as [81]

$$\Delta_S w(\vec{x}_i) \approx \frac{\sum_{ji}(cot\theta_1^{ij} + cot\theta_2^{ij})(w(\vec{x}_i) - w(\vec{x}_j))}{2A^i_{mixed}}. \tag{2.20}$$

θ_1^{ij} and θ_2^{ij} are the angles opposite to the edge joining vertex $\vec{x}_i$ and $\vec{x}_j$ in the triangular mesh

(Fig. 2.7). w is an arbitrary two-times continuously differentiable function on S, which can be taken as the position $\vec{x}_i$ itself, and the above equation can be expressed as

$$\Delta_S \vec{x}_i \approx \frac{\sum_{ji}(cot\theta_1^{ij} + cot\theta_2^{ij})(\vec{x}_i - \vec{x}_j)}{2A^i_{mixed}}. \tag{2.21}$$

The summation is over all 1-ring neighbouring vertices of vertex $\vec{x}_i$. A^i_{mixed} is the mixed area for the vertex $\vec{x}_i$. It is calculated as described in Algorithm 1 to insure the A_{mixed} for all vertex will tile the surface [81]. Either voronoi area of a vertex or a fraction of triangular area ($area(T)$) from the neighbourhood of the vertex is summed depending on the condition defined in Algorithm 1 to calculate the mixed area. The voronoi area for a vertex $\vec{x}_i$ can be calculated as

$$A_{voronoi} = \frac{1}{8}\sum_j (cot\theta_1^{ij} + cot\theta_2^{ij})\|\vec{x}_i - \vec{x}_j\|^2, \tag{2.22}$$

where the sum is again around the 1-ring neighbours of the vertex.

Algorithm 1: Algorithm to calculate A_{mixed} on an arbitrary mesh [81]

```
A_mixed = 0
for each triangle T from the 1-ring neighborhood of x⃗ do
    if T is non-obtuse then // Voronoi safe
        // Add Voronoi formula
        A_mixed+ = Voronoi region of x⃗ in T
    else // Voronoi inappropriate
        // Add either area(T)/4 or area(T)/2
        if the angle of T at x⃗ is obtuse then
            A_mixed+ = area(T)/2
        else
            A_Mixed+ = area(T)/4
```

Since the tissue surface is tiled with hexagonal cells (Fig. 2.3 a), we triangulate the hexagonal lattice for the calculation of mean curvature by using the centroid of the cells as shown in Fig. 2.8 a. The complete discretised form of Eq. 2.14 on the triangulated tissue can then be expressed as

$$U_{bending} = 2\mu_b \sum_{\vec{v}_T}(H(\vec{v}_T) - H_0(\vec{v}_T))^2, \tag{2.23}$$

where $\vec{v}_T$ includes all the nodes of triangulated mesh, *i.e.* all the vertices and the centroid of the cells.

Similarly, a discretised expression for Gaussian curvature K at a vertex on the triangulated mesh can be written as

$$K(\vec{x}_i) = \frac{1}{A_{mixed}} \left(2\pi - \sum_f \theta_f \right). \tag{2.24}$$

The summation is over 1-ring neighbouring triangulated faces f of vertex $\vec{x}_i$ (Fig. 2.7 and 2.8 a) and θ_f is angle at vertex $\vec{x}_i$ in triangle f.

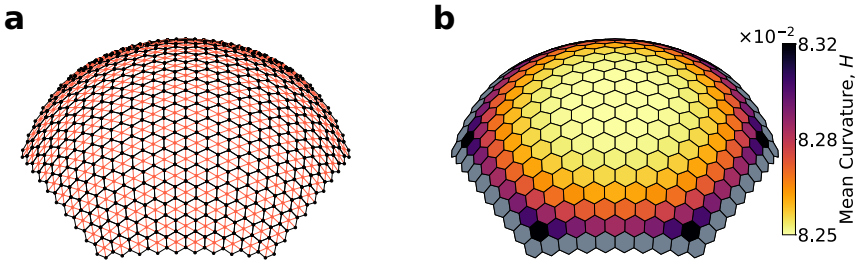

Figure 2.8: (a) The hexagonal cells of the tissue (in black) is further discretised using the centroids (red points) of the cells. (b) Mean curvature of the initial dome like tissue. For each cell, the mean curvature is calculated as an average of the curvature at its vertices and centroid. The boundary cells (in grey) are excluded in the plot as the boundary vertices have significantly high curvature. This artifact can be ignored since the boundary is fixed in its position. The slight variation in the mean curvature on the dome cells is the result of the hexagonal discretisation of hemispherical surface.

2.3.3 Pressure inside the tissue

The cells below the surface epithelial layer of the shoot apex push outwards on the surface layer. The net force acting on the cells in the surface layer promotes the outward growth. Following previous approaches we represent this outward pressure by an additive pressure term in the energy [10, 48, 52] ,

$$U_{pressure} = -PV_T, \tag{2.25}$$

where P is the pressure from underneath and V_T is the volume of the total shoot apex.

The volume is computed with a general algorithm for all polyhedron with polyhedral surface as boundary [82]. An important requirement of this computation is the cyclic ordering of vertices in the faces (cells) of polyhedron (tissue) as shown in Fig. 2.9. With quad-edge, the iteration of edges

around a face is always in strict anti-clockwise ordering, ensuring this combinatorial procedure. The triangulated mesh is then used for computation of the tissue volume. For each triangulated face T of polyhedron, containing vertices (A, B, C) in the strict orientation, the determinant of the position vectors of vertices is defined as

$$d(T) = \det(A, B, C). \tag{2.26}$$

The volume of the tissue can then be computed by

$$vol(P) = \frac{1}{6}\left|\sum_{T} d(T)\right|. \tag{2.27}$$

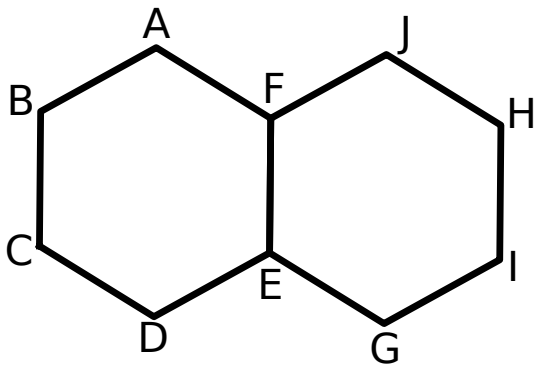

Figure 2.9: The orientation of vertices ensures that when the same edge is summed over, it orients in the opposite directions for adjacent cells. For example, for two cells that share one edge FE between them, the edge should appear as EF for cell $ABCDEF$ and as FE for $EFJHIG$. This can be achieved by ordering all the vertices in the cell by same cyclic ordering, clock-wise or anti-clockwise.

2.4 Rotation of rest cell shape

The SAM is free to move in three dimensions meaning the cells in SAM bend, twist or rotate. As the cellular deformation is quantified as difference between shape matrices (Eq. 2.10), the alignments

of the two matrices must be maintained. Under pure rotation, the cell themselves should not face any strain as the shape is unchanged. However, if the alignment of current cell shape matrix M_c, which is function of the vertices of the cell, and rest cell shape matrix M_c^0, which is an intrinsic property of the cell, is not corrected, the rotation of the cells can invoke artificial strain on the cells (Fig 2.10 a and b).

To prevent this, we consider the rotation of the cell for each deformation, by checking the alignment of current cell shape M_c under old and updated intrinsic axes of the cell (the intrinsic axes change when cells deform as they are defined on the cellular surface). We can write M_c in terms of both old $\vec{v}_i$ and updated $\vec{v}_i'$ axes as

$$M_c = \sum_i \lambda_i \vec{v}_i \vec{v}_i^T = \sum_i \lambda_i' \vec{v}_i' \vec{v}_i'^T. \tag{2.28}$$

We then calculate the rotation of M_c under the two axes by considering the primary directions, $\vec{v}_1$ and $\vec{v}_1'$. The rotation angle is calculated as the angle ϕ between the two vectors,

$$\phi = angle(\vec{v}_1, \vec{v}_1'). \tag{2.29}$$

The rest cell shape matrix M_c^0 is then rotated by ϕ to compensate for the cellular rotation and rotation of the intrinsic axes (as shown in Fig 2.10 c),

$$M_c^{0\prime} = R(\phi) M_c^0 R(\phi)^T. \tag{2.30}$$

$R(\phi)$ is the rotation matrix and $M_c^{0\prime}$ is the rest cell shape for updated reference frame.

2.5 Cellular growth: *Lockhart* and *exponential* growths

The plant cell growth results from a controlled *creep* of cross-linking polymers in cell wall under turgor pressure from inside the cell [83, 84]. The cellular growth can be modelled concentrating on this process of wall creep and is generally described by a viscoplastic theory that was initially developed by Lockhart [13, 85, 86]. We adapt a similar approach in considering the cell growth as extension of a Bingham material under stress in our vertex model.

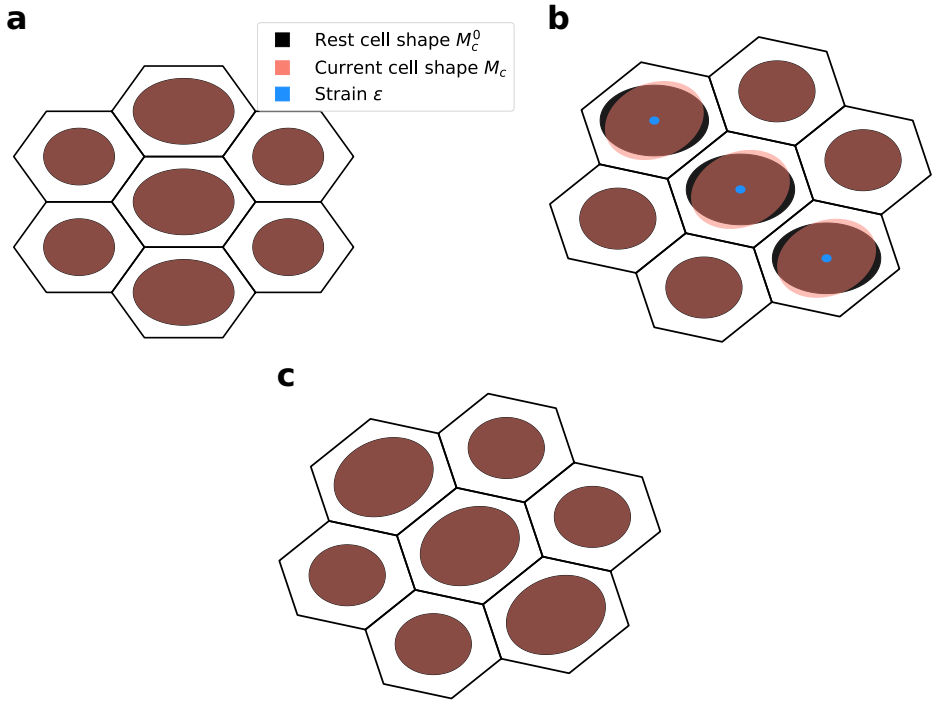

Figure 2.10: The rotation arising due to the deformation of tissue surface in 3D can cause artificial strain on the system if the rest cell shape is not corrected. (a) The initial tissue with middle three cells elongated horizontally. The current cell shapes and rest cell shapes are taken equal for all cells, shown by complete overlap of two ellipses and the absence of the strain ellipse. (b) The same tissue is rotated while adding no other deformation on the cells. The elongated cells acquire strain even though their shape is intact, as their rest cell shape is directional (elongated horizontally) and is not corrected with the rotation of the tissue. Other cells are regular hexagons, thus their rest cell shape is invariant under rotation. (c) The mentioned correction is made to the rest cell shape and the strain artifact is not present.

The rest cell shape grows proportionally to the deformation put on it. With the shape matrix definition, this can be expressed as

$$\frac{dM_c^0}{dt} = \kappa(1+\gamma)(M_c - M_c^0)_+, \tag{2.31}$$

where κ is the growth rate of cells, fluctuating with amplitude γ. The difference of the current shape, M_c, and the rest shape, M_c^0 (*i.e.* the deformation on the cells), drives the growth. The operation $(.)_+$ ensures Bingham plastic-like growth by applying a threshold on growth. For simplicity, we choose the threshold for growth to be zero, ensuring that the cells do not shrink if faced with

compressive stresses. The operation $(.)_+$ on a symmetric second order tensor T with rank decomposition given in Eq. 2.32, with λ_n and t_n as eigenvalues and eigenvectors, can be written as Eq. 2.33.

$$T = \sum_{n=1}^{d} \lambda_n t_n \otimes t_n \tag{2.32}$$

$$(T)_+ = \sum_{n=1}^{d} max(\lambda_n, 0) t_n \otimes t_n \tag{2.33}$$

An alternative growth equation can also be written from the observation that the plant cells have exponential like growth during the majority of their lifetime [87]. A shape dependent growth equation,

$$\frac{dM_c^0}{dt} = \kappa(1+\gamma)M_c^0, \tag{2.34}$$

can describe this type of growth. We use this *exponential* growth equation as a comparative tool for the more mechanistic or the *Lockhart* growth equation (Eq. 2.31).

2.6 CMT-led mechanical feedback on cell wall

The anisotropic cellular expansion and growth patterning in plants depend on the anisotropic cell wall stiffness as the forces generating growth are isotropic. The complex relation of CMT orientation led by tissue derived stresses and subsequent cellulose microfibril formation can be subsumed into dynamics of the desired cell shape without specifically modelling CMT's [26, 88]. Given the observation that CMT orient according to the highest stress and thus reduce growth in the direction of highest stress, we model this effect by coupling the growth rate to the cell's distorting stress component, the deviatoric stress D,

$$D = \sigma - \pi I, \tag{2.35}$$

where π is the mean stress,

$$\pi = \frac{1}{N} \sum_{i}^{N} \sigma_{ii}. \tag{2.36}$$

This extends the growth equation Eq. 2.31 to

$$\frac{dM_c^0}{dt} = \kappa(1+\gamma)(M_c - M_c^0) - \frac{\eta}{2}\Big(D(M_c - M_c^0) + (M_c - M_c^0)D\Big) \tag{2.37}$$

and similarly, Eq. 2.34 extends to

$$\frac{dM_c^0}{dt} = \kappa(1+\gamma)M_c^0 - \frac{\eta}{2}(DM_c^0 + M_c^0 D). \tag{2.38}$$

The feedback parameter η represents the cell wall's ability to respond to the stress and with higher η, the efficiency of reorganizing of the cell walls is higher. Increasing mechanical feedback results in growth that is more and more orthogonal to the higher stress direction (Fig. 1.6), as expected from the wall strengthening in that direction (Fig. 2.11 a and b).

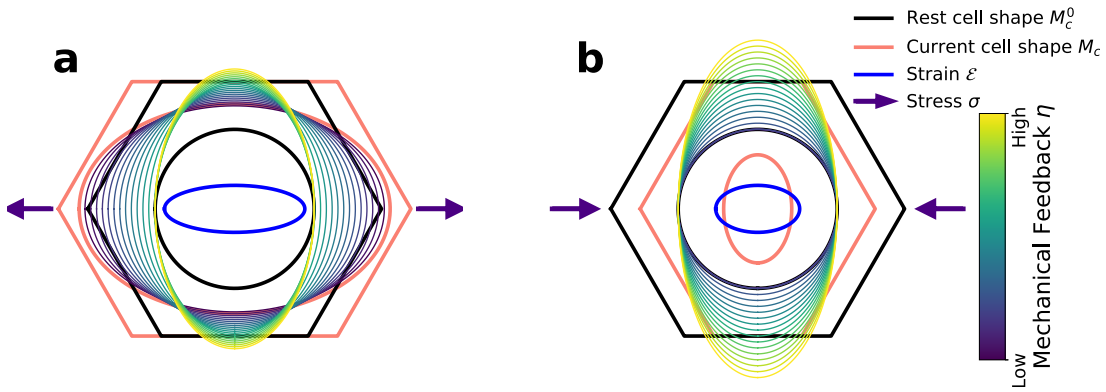

Figure 2.11: Increasing feedback by tuning the parameter η leads to stronger reaction from the cells. The stress applied on the cells is shown by the *purple* arrow and the resulting strain is show by the *blue* ellipse. The *black* and *red* ellipse show the rest shape and the current shape of the cell respectively. The ellipses with the varying color represent the result after the growth with varying strength of feedback η. (a) The stretched cells grow orthogonal to stress direction with increasing feedback. (b) The cells do not shrink in their rest cell shape under compressive stress and also show similar response of orthogonal growth to stress direction.

2.7 Localized enhanced growth with auxin

An important group of hormones that plays significant role in the cellular growth, by loosening up the cell wall, is auxin [16, 38, 40]. It is responsible for reduction in cell wall hemicellulose

polysaccharides, increase in pectin polymerization and viscosity, among other things in the plant biology [38–41]. Auxin initiates organ formation on the SAM by increasing the growth rate of primordial cells through loosening of the cell walls [10, 16, 42]. Yet, the faster growing cells in primordial region are still tightly connected to the slower growing cells in the meristem tissue through the shared cell walls [10, 52, 53]. Thus, it is unclear how fast both primordial and meristem cells can effectively grow and how both kinds of cells deform due to the localized enhanced growth rate. To study the morphological changes in the tissue during primordial growth, we define a prepatterned localization of auxin in the SAM (Fig. 2.12) with an enhanced growth rate κ_f relative to the surrounding meristem tissue, with κ_s as initial condition (Fig. 2.12).

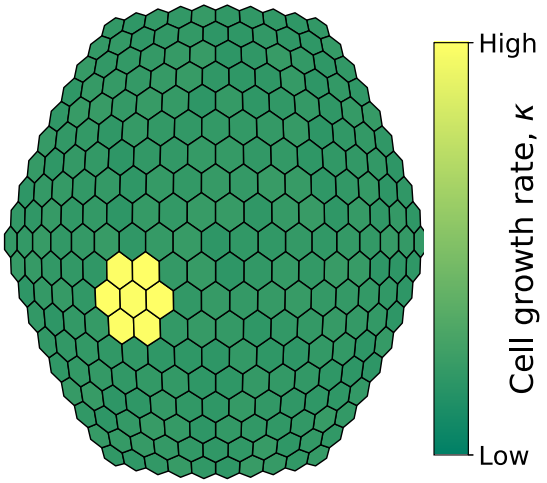

Figure 2.12: The localized accumulation of auxin causes an increased growth rate in primordium cells (yellow), top-down view on shoot tip. This is modelled by assigning higher growth rate to cells of designated primordial region.

2.8 Tissue simulation and boundary conditions

The growth of the SAM involves the minimisation of tissue mechanical energy (Eq. 2.3) and the cellular growth (Eq. 2.31 and 2.34). One time step in the simulation is the single minimisation run followed by the cell growth in response to changed morphology after energy optimisation.

We use the SubPlex algorithm implemented in the open-source non-linear optimization library

NLOPT to minimize the mechanical energy Eq. 2.3 and find the equilibrium shape of the tissue [89, 90]. The vertices at the boundary of the tissue, which represents the connection of the SAM to the mature and hardened shoot (as shown in Fig. 2.1), are fixed in their position (Fig. 2.13). Except this restriction on the boundary vertices, the rest of the tissue is free to move in all three-dimensions.

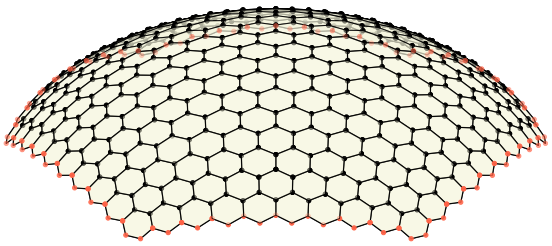

Figure 2.13: The boundary vertices (red) of the SAM dome in vertex model are fixed in their position, while the rest of the vertices (black) are free to move in all three-dimensions.

3

Mechanical examination of primordial growth

We idealised the shoot apical meristem (SAM) as a hemispherical dome composed of hexagonal cells (Fig. 2.3) and utilised our developed three-dimensional vertex model to understand the intricate role of mechanics in the shaping of plant tissue. The simulation of the growth of the shoot apical meristem at the cellular scale allowed us to study the emerging growth patterns in the tissue and the outgrowth of the primordia from homogeneously shaped cells. In the following chapter, the investigation on the initiation of primordia and examination of the role of mechanical sensing in organ outgrowth from the SAM is presented.

3.1 Growth of the shoot apical meristem

We took the initial SAM for the simulation as a hemispherical surface composed of homogeneous hexagonal cells that has been relaxed under the chosen simulation parameters (see Table A1). The growth of the SAM is driven by the deformation of the surface cells due to the volume pressure from the tissue underneath (Eq. 2.3) and addition of material onto walls by the cells as response to the deformation (Eq. 2.31) . With a uniform cellular growth rate κ for all the cells, we observed that the tissue expanded without significant morphological changes on the surface (Fig. 3.1). The growth of the simulated tissue is quantified by measuring the total surface area A_T,

$$A_T = \sum_c A_c \,, \tag{3.1}$$

where A_c is the area of the cell c.

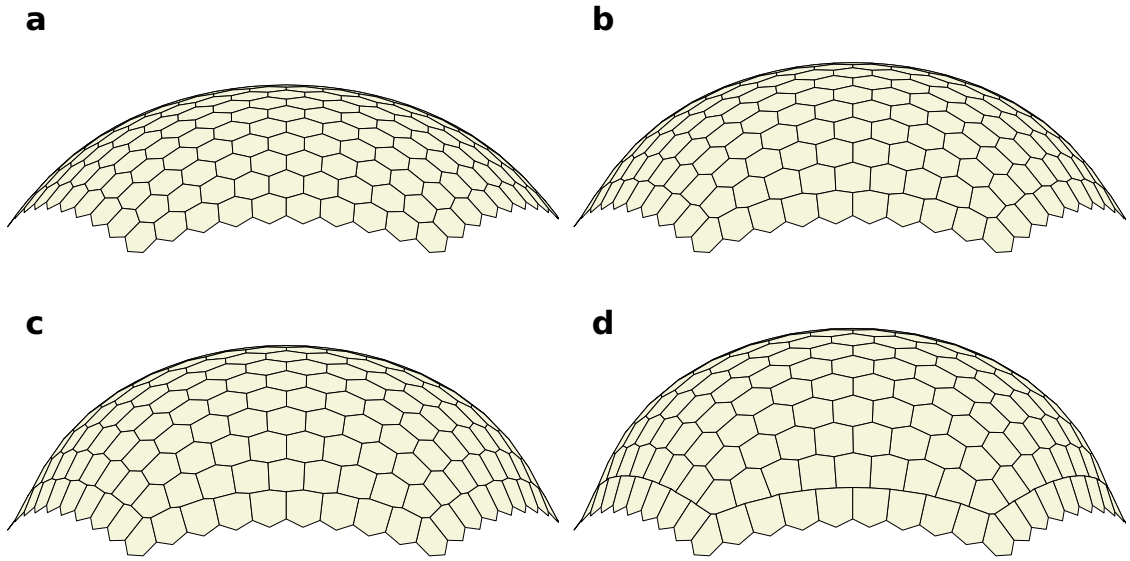

Figure 3.1: The SAM expanded uniformly outwards with homogenous growth rates on the dome. The figures $a - d$ show the tissue at various steps of the simulation with growth rate $\kappa = 0.5$, no feedback ($\eta = 0$) and cellular growth defined by Eq. 2.37. (a) The initial tissue with surface area of $A_T = 665$. (b) Simulated tissue at $A_T = 727$. (c) $A_T = 792$. (d) $A_T = 852$.

3.2 Introducing locally enhanced growth on the SAM

Aerial organs in plants start out as a bulge initiated by differential growth of cells in SAM, called the primordia. During the emergence of primordia, cells in primordial region are observed to grow faster and isotropically whereas the cells in boundary regions between the primordia and the rest of the meristem have arrested growth and are highly anisotropic [55–57]. To understand the cause of these growth patterns, the overall role of mechanics-led growth feedback and their effect on primordium outgrowth, we simulated the growth process with the vertex model.

Plant organ growth on the SAM was observed to be initiated by prepatterning the tissue with a localised higher growth rate corresponding to auxin accumulation in primordial cells, as discussed in section 2.7. The faster growing cells bulged out from the SAM and created the primordia on the tissue surface (Fig. 3.2).

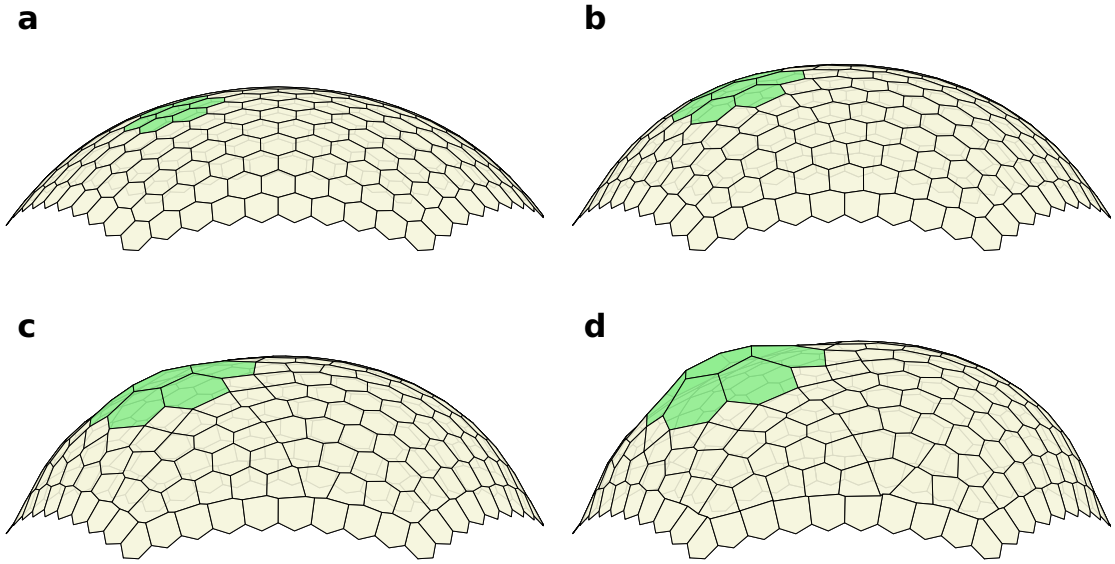

Figure 3.2: The growth of primordia from the primordial cells (shown in green) on SAM with no feedback ($\eta = 0$) and growth rates $k_f = 0.5$ and $k_s = 0.05$. The primordia bulged out of SAM as shown in the four snapshots of the tissue growth. (a) Initial tissue with $A_T = 665$. (b) Tissue at $A_T = 727$. (c) $A_T = 789$. (d) $A_T = 850$.

We quantified the outgrowth of the primordia by measuring the height of the bulge as

$$h = \|\vec{v}_{\text{top}} - \vec{v}_{\text{boundary}}\|, \tag{3.2}$$

where $\vec{v}_{\text{boundary}}$ is the average position of the vertices at the boundary of the primordial region and $\vec{v}_{\text{top}}$ is the position vector to the centroid of the cell at the top of the primordium, as shown in Fig. 3.3. A simple look into the height measured on the primordial and non-primordial region of the SAM showed the significant bulging arising in the primordia (Fig. 3.4).

We analysed the outgrowth height as a function of tissue surface area A_T (Eq. 3.1). This facilitated a comparison independent of the chosen intrinsic cell growth rates. The total simulation time and cellular growth over one time step can differ significantly depending on the choice of growth rates. However, as all of the dynamics in biology occur concurrently and lead to a robust timescale for the growth of tissue, we were able to safely compare the simulated tissues under different sets of parameters using the tissue surface area.

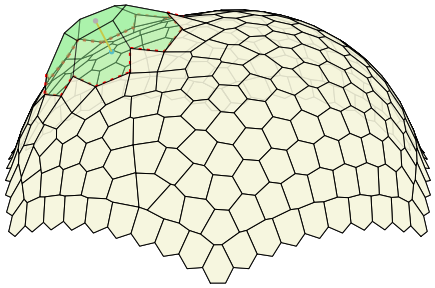

Figure 3.3: The height of the primordium (green) above the shoot apical meristem is shown in orange. The red dotted line shows the primordium boundary.

In the following sections, we examined the simulation results of organ outgrowth to investigate the role of tissue mechanics during primordial growth.

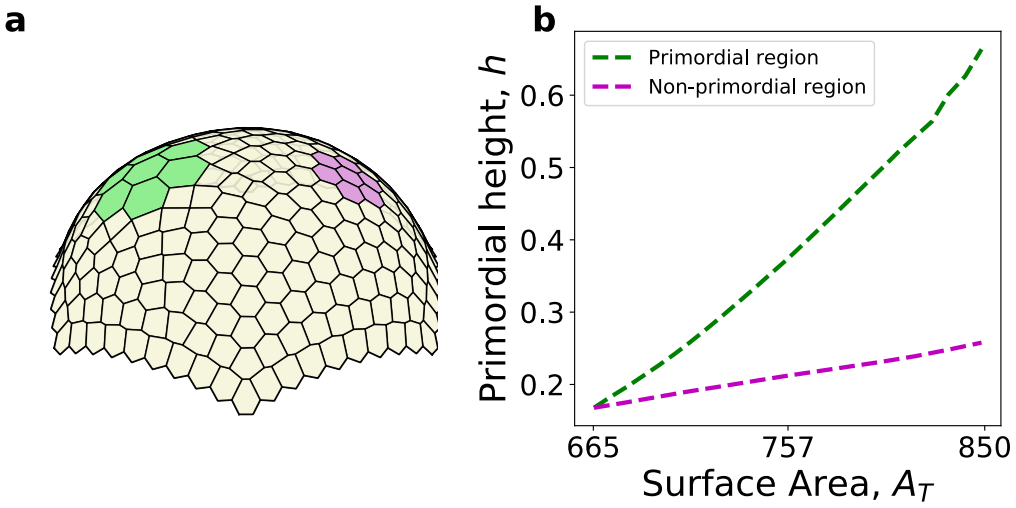

Figure 3.4: Comparison of height in primordial and non-primordial region quantified the presences of significant outgrowth in the primordial region. The growth rates used for this simulation were $k_f = 0.5$ and $k_s = 0.1$. (a) Regions of primordia (green) and non-primordia (magenta) shown on the tissue. (b) Increase in height of primordial and non-primordial region.

3.2.1 Growth ratio between primordia and meristem cells

Due to the cell-cell junctions and tissue mechanics constraining the cells, the actual growth rates of cells, κ^*, differed from the input growth rate κ in Eq. 2.31 or Eq. 2.34. The input growth rate of cells

(κ in Eq. 2.31) defined the growth of the rest cell shape. However, the actual cell shape on the tissue is not only dependent on the rest cell shape but also on the shapes of surrounding cells, curvature and the volume of the tissue. Thus, the actual rates of growth for primordial κ_f^* and meristematic κ_s^* cells were measured by fitting an exponential growth curve ($A = A_0 e^{\kappa^* t}$) to the areal growth (Fig. 3.5 and Fig. A1).

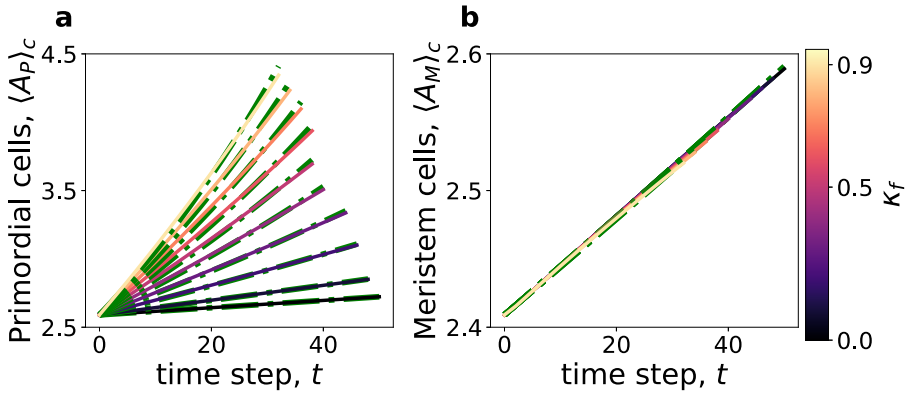

Figure 3.5: The areal growth obtained from the simulation are fitted with exponential growth curve (dotted green line) to get the actual growth rate of cells (κ^*). In these simulations, the meristem growth rates were kept constant ($\kappa_s = 0.05$), while the primordial growth rates (κ_f) were varied as shown by the color map. $\langle . \rangle_c$ is average over the two kids of cells (either meristem or primordial cells). (a) Increasing κ_f led to larger area for primordial cells. (b) The growth of meristematic cells was unchanged with constant κ_s.

Ultimately, we found that the ratio

$$r_g = \kappa_f^* / \kappa_s^* \tag{3.3}$$

of these two growth rates was the governing parameter for the growth dynamics of the entire tissue. The change in the primordial and meristematic growth rates while keeping the growth ratio constant had no effect on the primordial outgrowth (Fig. 3.6).

3.2.2 Primordial growth is initiated by the growth ratio

The faster growing primordial cells, with differential growth rates defined by the growth ratio r_g (Eq. 3.3), pushed outwards from the SAM surface leading to the organ bulging out of the tissue. With the simulation of varying growth ratios, we found that for $r_g \approx 1$ the growth rates were homogeneous throughout the tissue and the SAM just expanded outwards without any bulging (Fig. 3.8

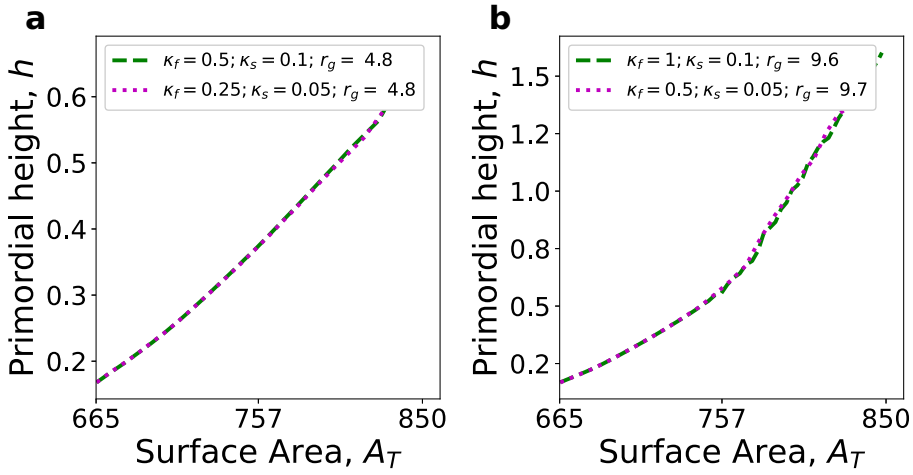

Figure 3.6: The same growth ratio described same primordial outgrowth dynamics with respect to overall tissue growth. The comparison between two different sets of growth rates keeping the growth ratio fixed showed that the outgrowth dynamics is dictated by the growth ratio. (a) Simulation with growth ratio $r_g = 4.8$. (b) Simulation with growth ratio $r_g = 9.6$

a). With increasing r_g, we started observing the outgrowth of primordium from the SAM and the height of primordia increased monotonically with r_g, see Fig. 3.7 b. The resulting primordial bulge on the surface of the tissue was clearly visible for large r_g (Fig. 3.8 $c - d$). This was driven by the stronger growth of primordial cells and the formation of bigger bulge (Fig. 3.7 a and Fig. 3.8 $a - d$).

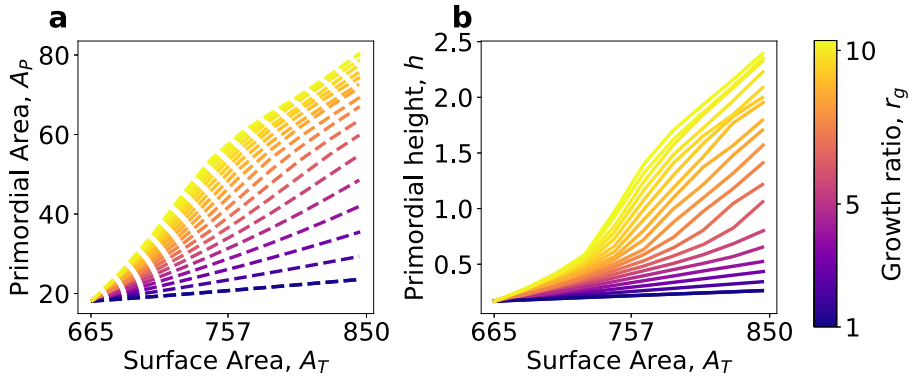

Figure 3.7: Higher growth ratio led to higher primordial growth. The growth rate for meristem (κ_s) was kept constant while the primordial growth rate (κ_f) was increased for larger growth ratio r_g. (a) The primordium grew larger with the growth ratio. (b) The primordium bulged out further due to the increase in its size as seen with higher primordial height on greater growth ratio.

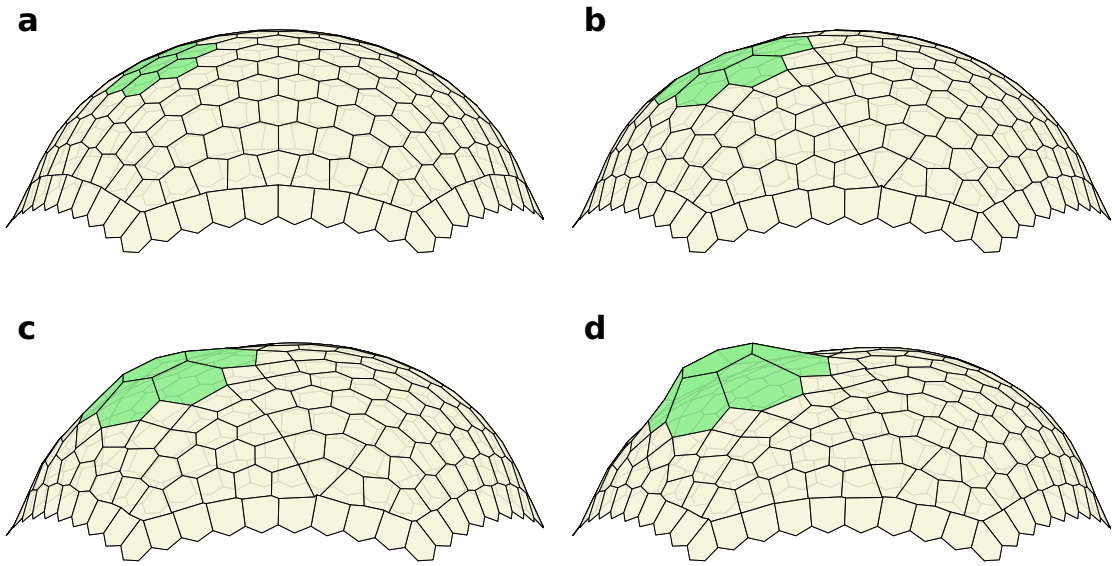

Figure 3.8: Tissues with different growth ratios but at the same stage of growth ($A_T = 850$) are shown. The patch of primordial cells are highlighted in green. (a) $r_g = 1.1$. (b) $r_g = 4.8$. (c) $r_g = 7.0$. (d) $r_g = 9.6$.

3.3 Active mechanical response from cells drives outgrowth

To further explore the emergence of primordia, we took the simulation of $r_g = 4.8$ and introduced mechanical feedback on the cellular growth. The growth ratio of 4.8 was chosen so as to stay close to the biological observations of cell growth rates in primordia and meristem [91].

Mechanical stresses in tissue are propagated among cells through the shared cell walls. The walls themselves are actively remodelled by cells as a response to the stresses acting on them. This restructuring, led by microtubules, organises cellular growth and is crucial in tissue morphogenesis [10, 16, 17, 26]. We modelled the mechanical feedback on cellular growth by implementing a stress dependent term in the growth equation that accounts for active strengthening of walls in higher stress direction (Eq 2.37). See section 2.6 for further details on the equations.

We found that the ability of cells to sense stresses and react accordingly is vital for organ outgrowth on the meristem. By modulating the mechanical feedback of a tissue, we observed that the outgrowth is higher when cellular response to mechanics is enhanced (Fig. 3.10 *b*).

Note that contrary to the dynamics for an increasing growth ratio, increasing mechanical feedback only promoted the outgrowth height while leaving the primordial tissue area almost unchanged (Fig. 3.7 a and Fig. 3.10 a). This indicated that mechanical feedback promoted organ outgrowth by a different mechanism than increase in primordial cell size. Notably, growth rates in cells of primordial and meristematic regions were unaffected by the mechanical feedback (Fig. 3.10 a), keeping the growth ratio stable. Thus, it is all the more puzzling that the reorganisation of growth led by mechanical feedback was able to bulge out the primordium more efficiently with increasing feedback. A little bit of insight was found with the simulation snapshots in Fig. 3.9 $a - b$, where the tissue of the same overall area with and without feedback were compared. The growth was directed outwards for the primordium with mechanical feedback, leading to a clear bulging (Fig. 3.9 a), while the primordial cells without feedback grew predominantly within the meristem surface and were not able to bulge outwards (Fig. 3.9 b). For similar analysis on impact of mechanical feedback on tissue with growth ratio $r_g = 9.6$, see section A.5.

Mechanical feedback was able to grow the same height with low growth rates for cells resulting in efficient primordial growth. The primordia of the tissue with growth ratio $r_g = 4.8$ and mechanical feedback of $\eta = 8$ (Fig. 3.10 b) grew to the height of $h = 1.6$ at $A_T = 850$) which was same as the tissue with twice the growth ratio $r_g = 9.6$ without feedback (Fig. A3 b).

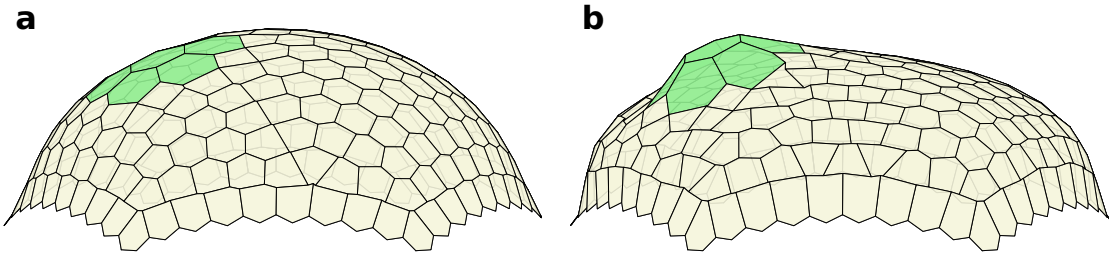

Figure 3.9: The tissues shown have growth ratio $r_g = 4.8$ and have grown to $A_T = 850$. (a) Without feedback ($\eta = 0$), the primordial growth is not yet pronounced at this stage. (b) With high feedback of $\eta = 8$, for the same growth ratio $r_g = 4.8$, clear development of primordia can be observed.

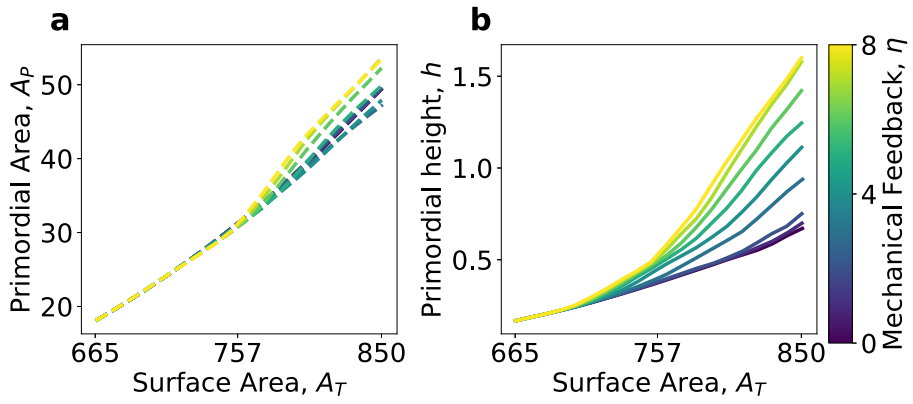

Figure 3.10: Increasing mechanical feedback of cells to the tissue wide mechanical stresses resulted in efficient primordial growth. Here, a tissue with growth ratio $r_g = 4.8$ was simulated for varying mechanical feedback. (a) The overall areal growth of the primordium was relatively unchanged with changing mechanical feedback. (b) The height of primordium increased significantly with higher mechanical feedback.

3.3.1 Diverging stresses reorganize growth in boundary cells

We next investigated how growth is reorganised within the tissue by the mechanical feedback and how it can lead to greater height growth in primordia. The differential growth rates between primordium and meristem reshaped the stress patterns on the SAM, which were used by cells, through mechanical feedback, to reorganise their growth.

We mapped the stresses on the cells surrounding the primordium, called the boundary cells (Fig. 3.11), to shed light on the mechanism behind the stronger primordial growth with feedback. The stresses acting on the cells were read from the strains using Eq. 2.8. We expressed the stresses in terms of their radial and orthoradial component with respect to primordia to help understand the repatterning of mechanics with bulge formation. The radial direction for a cell was given by unit vector ($\hat{u}_r$) pointing directly towards the tip of the primordia and the orthoradial direction was the orthogonal unit vector ($\hat{u}_o$) to radial vector on the cell surface (Fig. 3.11) and section A.3).

The stress on a cell were written in its radial/orthoradial component as

$$\sigma_{r,o} = \hat{u}_{r,o}^T \sigma \hat{u}_{r,o}. \tag{3.4}$$

Mapping out the stresses on the cells at the boundary of the primordia, we found that the stress distribution in the boundary cells became increasingly anisotropic during primordia development

with mechanical feedback (Fig. 3.12 a). The orthoradial stress σ_o in the boundary cells remained high throughout the outgrowth, whereas the radial stress σ_r declined.

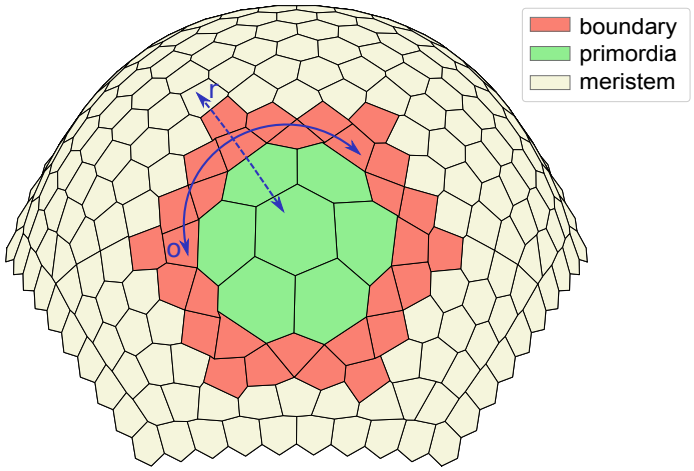

Figure 3.11: The meristematic, boundary and primordial cells labelled on the shoot tissue. The solid and dotted arrow show the orthoradial and radial direction respectively.

As with stresses, we also mapped out the growth of cells in their radial and orthoradial direction and found that the growth of the boundary cells exhibited distinct anisotropic patterns (Fig. 3.12 b). This was caused by the strong anisotropic stresses on the cells and the mechanical feedback reorganising the cellular growth. In the absence of feedback, both orthoradial and radial growth remained stable and strong, with the orthoradial growth being about twice as large as the radial growth. Mechanical feedback reduced both orthoradial and radial growth on the boundary cells over time, eventually ceasing the growth entirely at high mechanical feedback. The cessation of growth of the boundary cells was clearly visible when plotting the total area of boundary cells over the period of tissue development, see in Fig. 3.12 c. We found that the increase in mechanical feedback not only led to the slower growth of the boundary region but also to its compression due to the increasing stresses from the neighbouring cells (note negative stresses arising in Fig. 3.12 a). We inferred from these observations that the cessation of growth in primordium boundary cells, due to mechanical feedback to the arising stresses, was the vital mechanism behind the efficient outgrowth of primordium.

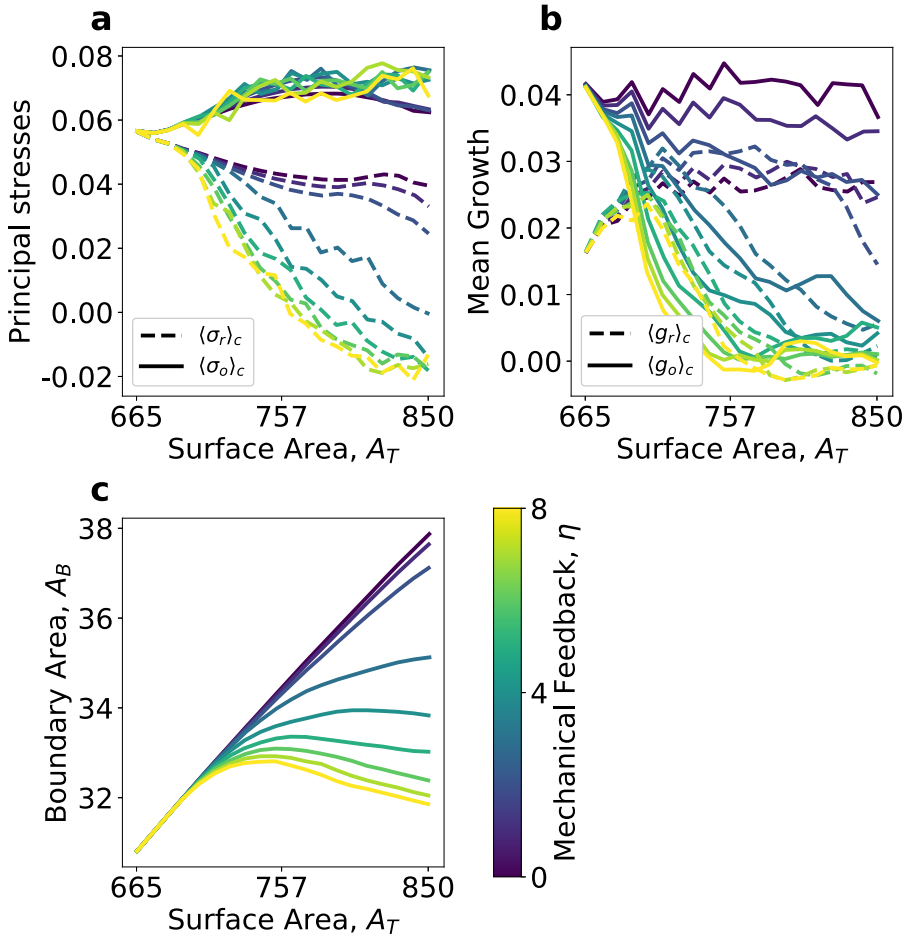

Figure 3.12: Pattern of stresses and growth in boundary cells undergo significant modification by mechanical feedback. Here, $\langle\cdot\rangle_c$ represents an average over the cells in boundary of primordium. (a) Stresses in radial (σ_r) and orthoradial (σ_o) directions diverged during growth more and more with increasing feedback. (b) Growth rates of boundary cells decayed with feedback. (c) The boundary cells not only ceased in growth but were also compressed by primordium and meristem cells.

3.3.2 Mechanical feedback modulates the height growth rate

To link the relation of generated stress pattern and growth reorganisation caused by mechanical feedback, we examined the rate of height growth in primordium with respect to the growth of tissue surface as a function of anisotropy in stresses on boundary cells (Fig. 3.13). The stress anisotropy was defined as the difference between the two principal stresses acting on the cells. We observed

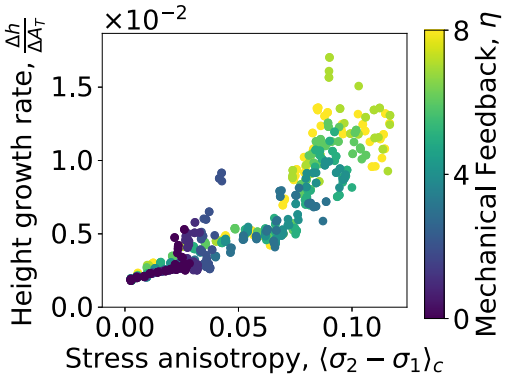

Figure 3.13: Rate of primordial height growth was boosted significantly by mechanical feedback. With higher mechanical feedback, both the rate of height growth and the stress anisotropy of cells on the primordial boundary increased. By this two-way reinforcement, mechanics was able to guide efficient primordium outgrowth on the SAM.

that along with the boost in the height growth rate, which results directly from cellular growth reorganisation, mechanical feedback generated greater stress anisotropy in the boundary cells. The averaged difference in principal stresses increased with higher mechanical feedback. This amplified the growth heterogeneity in the tissue and established the large scale stress pattern that promoted the efficient organ outgrowth. Without the mechanical feedback, both height growth rate and stress anisotropy were low, see Fig. 3.13. Only the stress anisotropy in boundary cells arising from mechanical feedback, also seen by diverging stress in Fig. 3.12 *a*, allowed the growth reorganisation in cells that resulted in a strong growth in primordium height. The schematic of the two-way reinforcement in primordial growth by mechanical feedback is summarised in Fig. 3.14.

3.3.3 Negative curvatures arise on the boundary

The cells at the boundary of primordia and meristem are under considerable anisotropic stress (Fig. 3.12 *a*). With the initiation of bulging on the SAM, the efficient protrusion of primordia relies on bending of boundary region. To examine the bending boundary, we plotted the Gaussian curvature (Eq. 2.24) on the tissue surface and looked at the bending on the cells surrounding the primordia (Fig. 3.15). We found that under mechanical feedback the boundary cells showed significantly low Gaussian curvature (Fig. 3.15 *b*) as compared to the tissue with no mechanical feedback (Fig. 3.15 *a*).

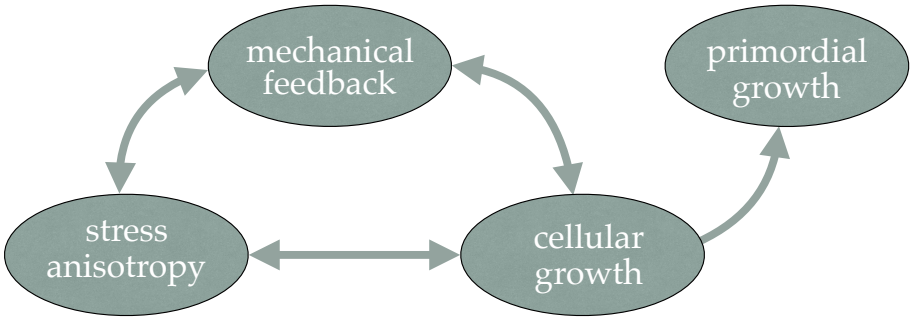

Figure 3.14: Mechanical feedback directs the strong primordial outgrowth with two distinct mechanisms. Firstly, it organises cellular growth on the boundary aiding the primordial growth and secondly, it repatterns the stresses on the cells, which further strengthens the effectivity of feedback in creating outgrowth.

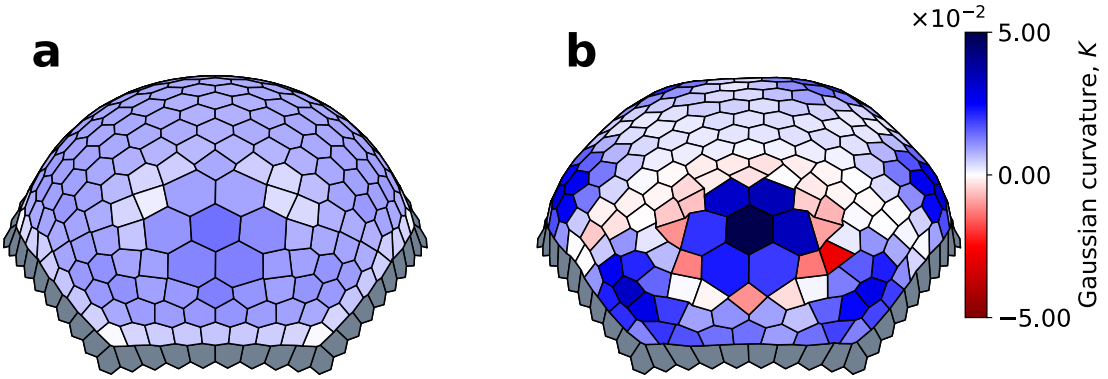

Figure 3.15: The tissue with $r_g = 4.8$ at $A_T = 850$ and with (a) no mechanical feedback and (b) feedback of $\eta = 8$. The figure shows the direct top view of primordia on the tissue. Gaussian curvature at the boundary was found to be significantly lower for high feedback, as seen in (b).

Further, the Gaussian curvature on the boundary region decreased gradually with increasing mechanical feedback, as seen in Fig. 3.16, and reached negative values for high feedback strengths. This demonstrated that with high mechanical feedback on cellular growth, the boundary region folds to a saddle shape allowing for swift outgrowth of primordia on the SAM.

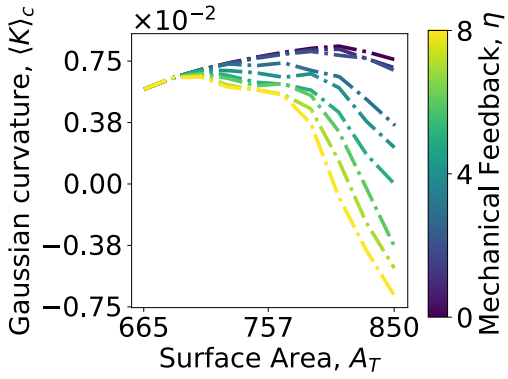

Figure 3.16: The average Gaussian curvature in the boundary cells declined with mechanical feedback; for high feedback, the curvature was negative.

3.4 Modulating the bending stiffness impacts the primordial outgrowth

We showed the formation of primordia on the SAM occurs through the auxin-led loosening of wall stiffness and is guided by the stress based mechanical feedback on cellular growth. We can imagine a similar action of auxin on the anticlinal walls of the cells on the tissue. The bending stiffness of the tissue surface in the vertex model (Eq. 2.23) represents the resistance to deformation of the anticlinal walls and sub-epidermal cells. The loosening of walls by auxin would therefore lower the bending stiffness of the tissue.

We found that such loosening of the bending stiffness is also effective in the expansion of primordia. With lower μ_b, the primordia is able to attain much higher height in comparison to tissue with higher stiffness (Fig. 3.17 b). This was again directly related to the overall growth of primordia to larger size with lower bending stiffness (Fig. 3.17 a). The mechanism was much like the one behind the bigger primordial height observed with stronger growth ratio r_g (see section 3.2.2 and Fig. 3.7).

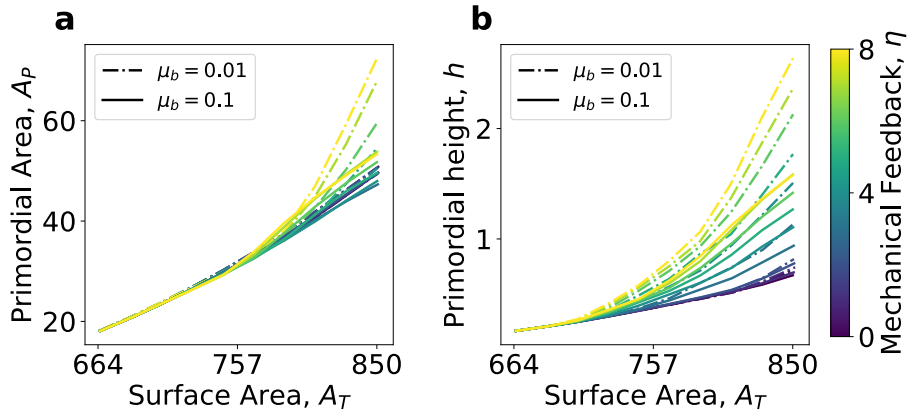

Figure 3.17: The growth of primordia with bending stiffness of $\mu_b = 0.01$ and $\mu_b = 0.1$, and same growth ratio $r_g = 4.8$. (a) The primordia grew to a larger size with lower bending stiffness μ_b. (b) The primordia grew to greater heights with low stiffness as compared to high bending stiffness.

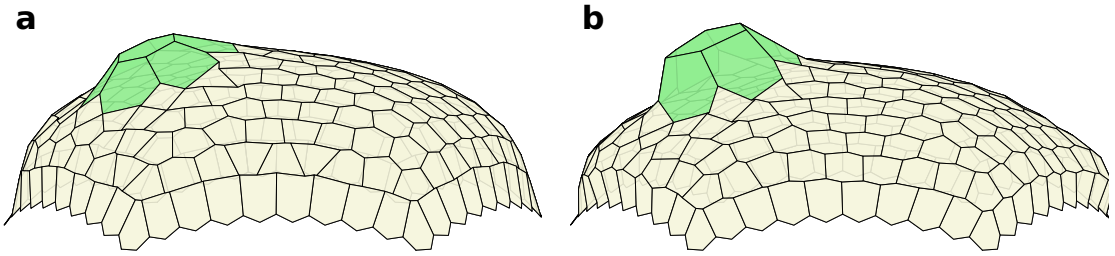

Figure 3.18: Lowering the bending stiffness μ_b resulted in larger primordia. The figures (a) and (b) show the tissue with $r_g = 4.8$ at $A_T = 850$ and with $\mu_b = 0.1$ and $\mu_b = 0.01$, respectively. With lower bending stiffness, the primordia was significantly larger with greater height as seen in (b) compared to (a).

3.5 Growth under exponential growth law

We examined the growth of the plant cells as a mechanical process driven by deformations (Eq. 2.31). The growth law, initially proposed by Lockhart, was able to capture the morphological changes occurring in a plant tissue during primordial development. To test if the dynamics of outgrowth is robust under differing growth equations, we studied the primordial formation with another growth equation. The shape dependent growth equation (Eq. 2.34) used for this analysis described

the growth of a cell as an exponentially growing shape. This was a direct interpretation of the experimental observations which showed that cells grow at exponential rate for a majority of their lifetime [87]. [1]

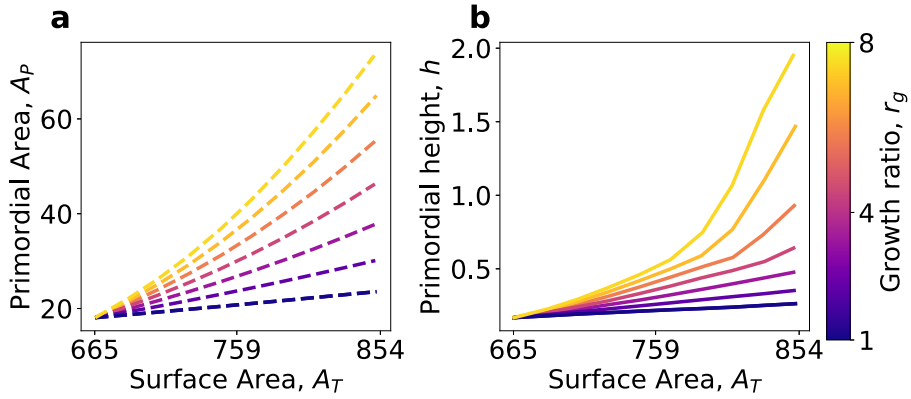

Figure 3.19: Using *exponential* growth for the cellular growth to simulate the primordial outgrowth. (a) The primordia grew to be larger with higher growth ratio r_g. (b) The resulting primordial height was also larger with higher r_g.

We employed the *exponential* growth (Eq. 2.34) and ran similar simulations as we have done with previous deformation driven or the *Lockhart* growth (Eq. 2.31). We allowed the primordial cells to grow faster than the rest of the meristem (see section. 2.7) and measured the formation of bulge on the SAM. We found again that the growth ratio (Eq. 3.3) was vital in the generation of primordia from the shoot apical meristem. The bulge grew outwards with greater height as the growth ratio was increased (Fig. 3.19 *b*). This was again caused by the growth of primordia to a larger size (Fig. 3.19 *a*).

We then probed the impact of stress based feedback on the primordia growth. The height growth of the primordia, as it was with *Lockhart* growth, was significantly promoted by the feedback (Fig. 3.20). The change in the morphology of the tissue was visible on the direct snapshots of the tissue with and without feedback (Fig. 3.21). The primordial cells grew bigger but spread out on the surface without feedback (Fig. 3.21 *a*), while with feedback, the primordial cells grew outwards (Fig. 3.21 *b*). A remarkable observation with the *exponential* growth was the completely identical areal growth of primordia with varying mechanical feedback (Fig. 3.20 *a*). The growth with *expo-*

[1] A thing to note is that deformation driven growth is also able to exhibit exponential growth (check section A.6 and [13]).

nential or shape dependent growth law (Eq. 2.38) led to a growth independent of cues from neighbourhood of the cell or strain on the cell. Cellular deformations and mechanical interactions with rest of the tissue had little impact on the overall size growth of the rest cell shape, consequently, with *exponential* growth, the area of faster growing primordial cells remained unchanged.

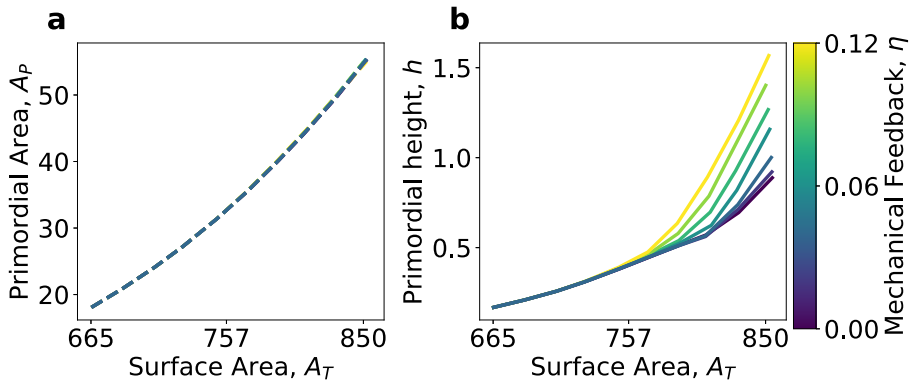

Figure 3.20: The simulation with growth ratio $r_g = 6.2$ and with varying mechanical feedback. (a) The overall areal growth of the primordia was remarkably stable with the changing mechanical feedback. All the growth curves completely overlapped. (b) Even with stable primordial growth, the growth reorganisation by mechanical feedback acted to produce taller priomordia. The impact of feedback on the growth of primordial height was similar as it was with *Lockhart growth*. Increasing the feedback led to higher growth of the primordia.

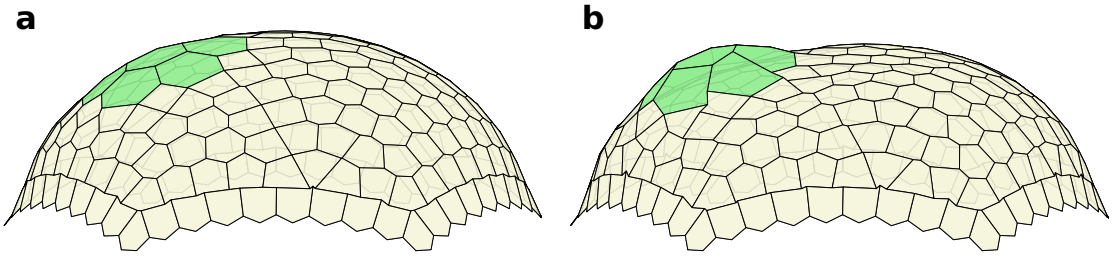

Figure 3.21: The snapshot of tissues with $r_g = 6.2$ shown with different feedbacks at $A_T = 850$. (a) Without feedback ($\eta = 0$), the primordial growth is not yet pronounced at this stage. (b) With high feedback of $\eta = 0.12$, for the same growth ratio, better development of primordia can be observed.

For a direct comparison of the two growth laws, we plotted the growth curves with similar growth ratios for the *Lockhart* and *exponential* growth (Fig. 3.22). We saw that for lower growth ratio, the growth dynamics are quite similar, while for larger growth ratio, the curves diverged. The differ-

ing long term dynamics of cells for the two growth laws were behind this. In the case of *exponential* growth, the size of the cells in primordia and meristem diverges as the rates of growth are different and the cellular growth is exponential. While in the case of *Lockhart* growth, the cellular growth is dependent on the deformation on the cells. With constant pressure from underneath the tissue driving the deformation, the deformation on the cells slowly decays as the tissue reaches an equilibrium between the strain on the cells and the volume pressure of the tissue. This stabilises the gap between the primordial and meristem cells in a long run. The growth ratio controls the speed of this diverging size of the primordial and meristematic cells. So, for lower growth ratio, where the cell sizes do not diverge significantly for both growth laws, we observed the dynamics of primordial growth was similar.

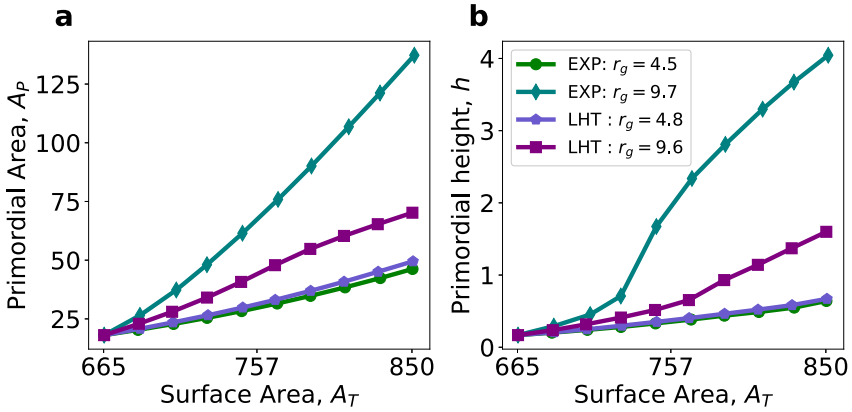

Figure 3.22: The areal and height growth of primordia with *exponential* (EXP) and *Lockhart* (LHT) growth. (a) The areal growth for the low growth ratios overlapped for the two growth laws and was found to diverge for higher r_g. (b) The dynamics was similar for the primordial height with complete overlap for lower growth rates. Primordial height for the larger ratio again diverged due to the large growth of the primordial cells with exponential growth and higher rates.

3.6 Discussion on the primordial growth

We developed a three-dimensional vertex model for plant development to understand how a primordium, as precursor of aerial organs, can grow out on the shoot apical meristem given the tight connections of plant cells via their cell walls. Primordium is initiated on the meristem by biochemically triggered local wall softening that results in higher growth rate in the primordial region.

Following the initiation in the simulation, we quantified the outgrowth dynamics by measuring the organ height above the tissue level. Taking into account the mechanical feedback mediated by cortical microtubules and cellulose deposition, which reinforces cell walls in the direction of higher mechanical stress and promotes growth in the orthogonal direction, we observed higher and more efficient primordium outgrowth.

Higher growth rates in the primordial region with respect to the surrounding meristematic tissue were found sufficient to trigger organ outgrowth (Fig. 3.7 *b*). We saw that the absolute values of primordial and meristematic growth rates were irrelevant since the dynamics of primordium formation was dictated by the *ratio* of growth rates between the faster growing primordial cells to the slower growing meristematic cells (Fig. 3.6). However, with mechanical feedback on cell growth from tissue-wide mechanical stresses, organ shaping was more efficient. While mechanical feedback did not strongly impact the overall growth of a primordium in area, it directly controlled the height of the primordium (Fig. 3.10). Mechanical feedback could account for the same height with half the growth ratio as seen in the following example: the primordia of tissue with growth ratio $r_g = 4.8$ and mechanical feedback of $\eta = 8$ was able to grow to the same height ($h = 1.6$ at $A_T = 850$) as the tissue with twice the growth ratio $r_g = 9.6$ without feedback. This enhancement in efficiency of organogenesis with stress-based feedback in the SAM was established to be robust under varying cellular growth law (Fig. 3.20). Thus, we found that plants are able to push out the organs from SAM in faster and efficient manner utilising the CMT-mediated mechanical feedback.

We saw that the surprising increase in organ height was due to the reorganization of growth and stress on the cells at the boundary of primordium (Fig. 3.12 *a-c*). Boundary cells are under considerable anisotropic stress and this stress anisotropy was further enhanced by mechanical feedback (Fig. 3.12 *a*). The feedback slowed down the boundary cell growth and even ceased the growth for high feedback (Fig. 3.12 *b*). Since primordial tissue area was unaffected by mechanical feedback (Fig. 3.10 *a*), the key role of the slower growing boundary cells was to act as a stiff ring on the tissue surface which pushes out the primordium. The boundary region was even compressed due to the strong stresses from the meristem and primordium in the high feedback regime (Fig. 3.12 *c*). The emergence of saddle like curvature (Fig. 3.15 and 3.16) was also seen in the boundary with mechanical feedback that is corroborated by the experimental observations [56, 57]. We, thus, identified an entirely different mechanism that effectively acts analogous to contractile-ring like dynamics, known to cause shape transformations in animal epithelial tissue [71].

While a decrease in circumferential strain along with the promotion of radial strains in primordium boundary cells has been suggested to promote primordium outgrowth [51], we here showed how such growth dynamics could self-organise due to mechanical feedback. We could therefore finally explain the experimental observations of very low or no growth and even compression of cells in the boundary region [48, 55–57]. The formation of distinct boundary region between the primordia and meristem has been suspected to be caused by different gene expressions found in the boundary cells [57]. Here, we propose that the emerging mechanical patterning can also be the cause of separation of meristem and primordium, as it establishes a mechanically distinct boundary region on the SAM.

Correlating primordial height growth rate and stress anisotropy of boundary cells for different values of mechanical feedback (Fig. 3.13), we observed a clear correlation substantiating that the increase in boundary cell stress anisotropy, proportional to the mechanical feedback, was behind the driving of primordium outgrowth. Interestingly, for high mechanical feedback, stress anisotropy and height growth rate saturated. This suggested that the gain in primordial growth could flatten out in the high feedback regime and there could be an optimal level of mechanical feedback for efficient growth in plants clarifying previous model observations [26, 88].

Taken together, our key insight was that mechanical feedback reorganised cell growth by two distinct mechanisms. First, feedback directly influenced the cell growth by modulation of wall properties. Second, feedback changed the stress patterns on cells, thereby self-amplifying and propagating the growth anisotropies that then indirectly influenced the cell growth again. This twofold mechanism was found to allow plant tissue in initiating the organ outgrowth efficiently by modifying their growth pattern through stress feedback, rather than amplifying further the growth rates at the expense of cell material.

In the next steps, the investigation can be directed to understand the control imposed by the modulation of hormonal transport by the primordial outgrowth. The lateral organ growth is known to modify the flow of auxin on the meristem regulating the growth of the tissue [92]. The mechanical model augmented with hormonal flow can help elucidate the complete mechanism behind the SAM development. In addition to it, the inclusion of cell division in the investigation of organ growth on the meristem can also be imagined. The cells on the boundary region exhibit stereotypic division guided by mechanical stresses [48]. The emergence or the role of such division patterns on the formation of organ can be studied.

4 Tip growth of plant shoot

The body of the plant is elongated to place the aerial organs in a better position to gather resources. This polarised growth in plants relies on the organised growth of the shoot apical meristem (SAM) sitting on top of the shoot [51, 52, 60]. As the cells in the SAM grow and get incorporated into the shoot, the stereotypic patterns of growth and divisions observed on the meristem (Fig. 4.1) may have an indispensable influence on the lengthening of the shoot . The cells at the center of the meristem are known to grow slow and divide less while the cells at the peripheral region have faster growth and a larger number of divisions (detailed in section 1.4) [8, 55, 56, 65]. In this chapter, we examined the elongation of the shoot using vertex model (see chapter 2) and investigated the role of the growth and division patterns in guiding the meristem development and the shoot elongation.

4.1 Zonal patterns of cellular growth in meristem

The elongation of the shoot in plants is driven by the coordination of growth in cells on the shoot apical meristem. To understand the ramification of the growth patterns that are exhibited on the meristem, we started with the vertex model representation of the tissue (Fig. 2.3). We partitioned the hexagonal cells on the dome-shaped SAM into three zones and applied enhanced growth in these zones individually (Fig. 4.2 and top view shown in Fig. A6). We then analysed the morphological differences arising from the varied spatial arrangements of growth to shed light on the development of elongated shoot from the hemispherical meristem.

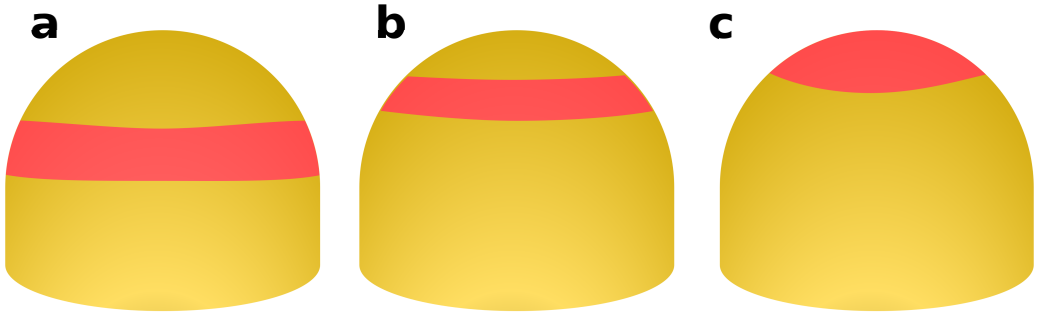

Figure 4.1: The shoot apical meristem is dome shaped and is seated at the top of the cylindrical shoot. The growth and divisions in the meristem is known to have stereotypic patterns. (a) The boundary of meristem near the hardened shoot grows slow. (b) The growth in the meristem in concentrated at the peripheral region with cells here growing and dividing at faster pace. (c) The central zone of the meristem has cells that grow slow and have lower rate of division.

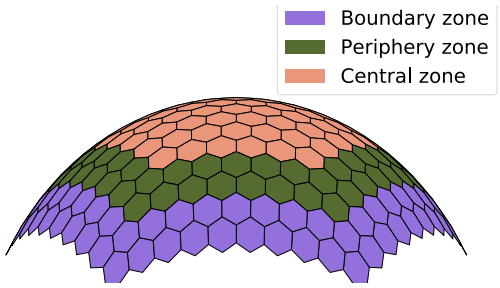

Figure 4.2: The initial SAM used for simulation is shown with the division of cells on the tissue into zones. The zonal division has been chosen to keep the area of all three zones near equal.

4.2 Varying morphology of the shoot with zonal growth

In order to study the impact of growth patterns on the elongation, we simulated the tissue with various zonal growths. The rate of growth on the cells in the SAM were taken to be homogeneous with $\kappa = 0.1$ and for each case of enhanced growth in one of the zones (Fig. 4.2), the growth rate in the chosen zone was elevated to twice the value ($\kappa = 0.2$). The cellular growth was taken to follow the deformation-led growth (*Lockhart* growth) as defined in Eq. 2.37.

Confining the enhanced growth in different zones on the meristem resulted in tissue morphologies that were very distinct from each other (Fig. 4.3 $a - c$). When the cellular growth was elevated in the boundary or the periphery zone, the meristem grew to have more cylindrical and elongated shape (Fig. 4.3 a and b). Whereas, locating the enhanced growth in the central zone resulted in a

tissue that resembled an inflated sphere more than an elongated shoot (Fig. 4.3 c).

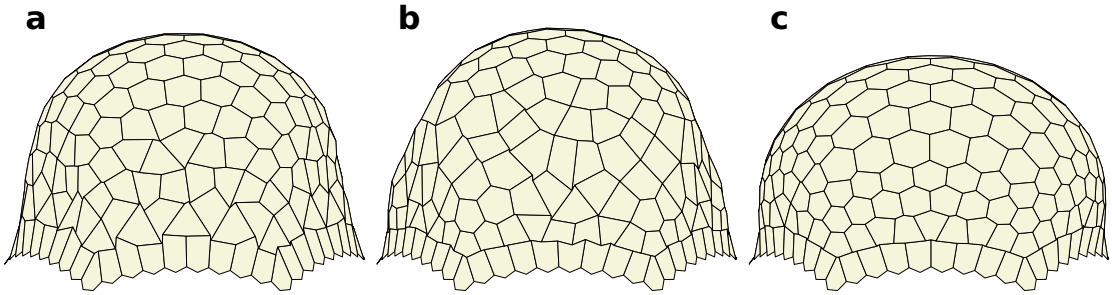

Figure 4.3: The dissimilarity of the meristem simulated with enhanced growth in different parts of the tissue. All of the tissues have grown to surface area of $A_T = 1400$. The mechanical feedback is not included in the cellular growth at this moment ($\eta = 0$). The location of enhanced growth is at: (a) the boundary zone, (b) the periphery zone and (c) the central zone.

To quantify the elongation, we measured the height of the simulated tissue H_T as

$$H_T = max(\{z_i - z_0\}), \tag{4.1}$$

where, z_i is the $z-$coordinate of a vertex i and z_0 is the $z-$coordinate at the base of the tissue. We analysed the growth of tissue height H_T as a function of tissue surface area A_T (Eq. 3.1) to compare the efficiency of varied growth patterns in elongating the shoot.

4.2.1 Effectiveness of zonal growth in shoot elongation

In this section, we quantified the shoot elongation with plain cellular growth without any mechanical feedback ($\eta = 0$ on Eq. 2.37). As stated previously, the morphologies of the tissues with different zonal growth enhancement differed significantly from each other (Fig. 4.3). Remarkably, the overall growth of the volume and the surface area of the tissues remained unchanged for all zonal growths (Fig. 4.4 a). The comparison of tissue height growth to that of surface area, however, yielded clear differences in the effectiveness of each zone (Fig. 4.4 b). The elongation of the tissue with boundary and periphery zone was observed to be nearly the same, while with enhanced growth in the central zone, the elongation was noticeably slower. This indicated that for the effective lengthening of the shoot the elevated growth might need to be located on the cells in the outer

parts of the meristem.

The source of better performance in growing elongated tissues for the boundary and periphery zone cases might lie in the constraints imposed on the cells at the outer regions by the shoot boundary and the cells at the tip. The cells in the outer zones of the meristem are squeezed between the strong boundary at the bottom and the rest of the tissue at the top. For any expansion of these cells to occur, the tissue sitting on top of them need to be pushed outwards. Instead, the cells at the top of the tissue or the central zone do not face such restrictions, thus can expand isotropically and uniformly (as also seen in Fig. 4.3 c). This results in better efficiency for the outer zones to convert the cell expansion into the tissue elongation.

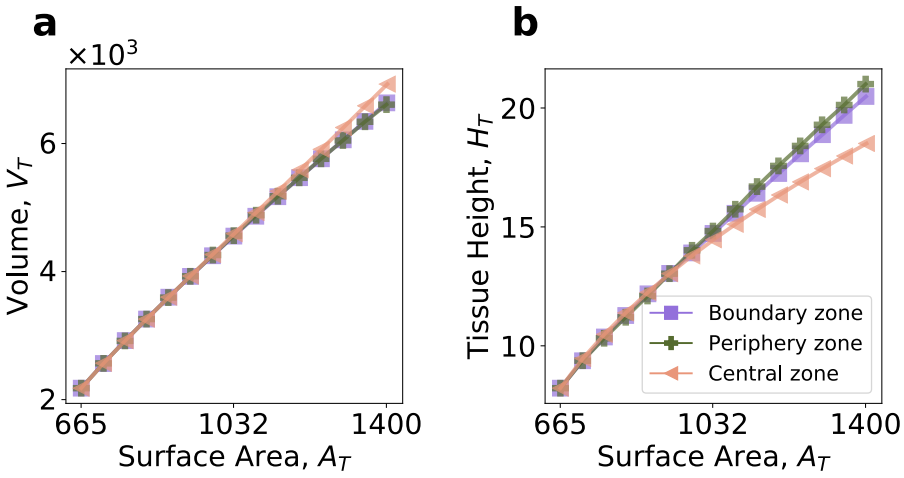

Figure 4.4: The volume and height growth of tissue for different zonal growths without mechanical feedback on cellular growth ($\eta = 0$). (a) Volume of the tissue grew proportionally to surface area for all three growth types. (b) The tissue height growth was stronger for the boundary and the periphery zones as compared to the central zone.

4.3 Mechanical feedback on shoot growth

The cellular growths in plants are known to be organised by the stresses acting on the walls [10, 26]. As the stresses in meristem are higher in the periphery as compared to the tip (Fig. 1.4), the mechanics-led response from the cells might have an impact on the overall morphology of the tissue. We examined this by introducing the mechanical feedback on the cellular growth and placing

enhanced growth in different zones as in previous section.

We found that increasing mechanical feedback on the cellular growth acted negatively on the elongation of the tissue. For all three zonal growths, the growth of tissue height lessened with increase in feedback (Fig. 4.5). The periphery and boundary zones performed marginally better than the central zone till the lower feedback regime. However, when we looked at the high feedback, the central zone outperformed the two outer zones in elongating the tissue (Fig. 4.5) and Fig. A7 b). The volume and surface areal growth of tissue were still steady with different zonal growth and high feedback (Fig. A7 a).

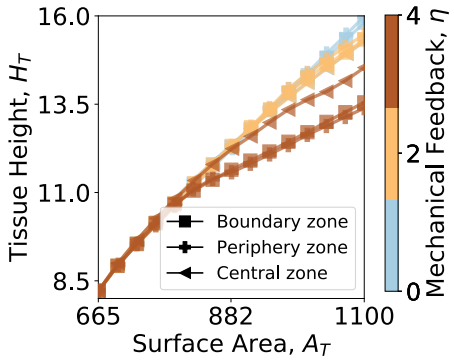

Figure 4.5: The height growth as function of tissue surface area with varying mechanical feedback. With feedback, overall height growth was found to be lower for the same type of zonal growth. For high mechanical feedback, the effectivity of tissue elongation reversed for the zones. As seen with $\eta = 4$ (in brown), The central zone displayed larger growth of tissue height as compared to the boundary and peripheral zones.

The morphology of the tissue with various zonal growths and mechanical feedback displayed noticeable differences (Fig. 4.6). The cases without feedback for all three zones exhibited a curved and outwards growing tip of the meristem (Fig. 4.6 $a - c$), while with mechanical feedback the tip was flattened for the boundary and periphery zone cases (Fig. 4.6 $d - e$). The tissue morphology remained similar for central zone growth (Fig. 4.6 c and f), but the tissue height was clearly reduced as quantified in Fig. 4.5 b.

The reduced impact of mechanical feedback in the case of central zone on the tissue elongation and morphology could be attributed to the homogenous stress field at the tip of the tissue (Fig. 1.4). As the stresses are isotropic at the top of the dome and mechanical feedback relies on anisotropic stresses (section 1.1.1), the feedback was unable to act on the cellular growth and cause major changes to the overall shape of the tissue. In boundary and periphery zones, the stresses are

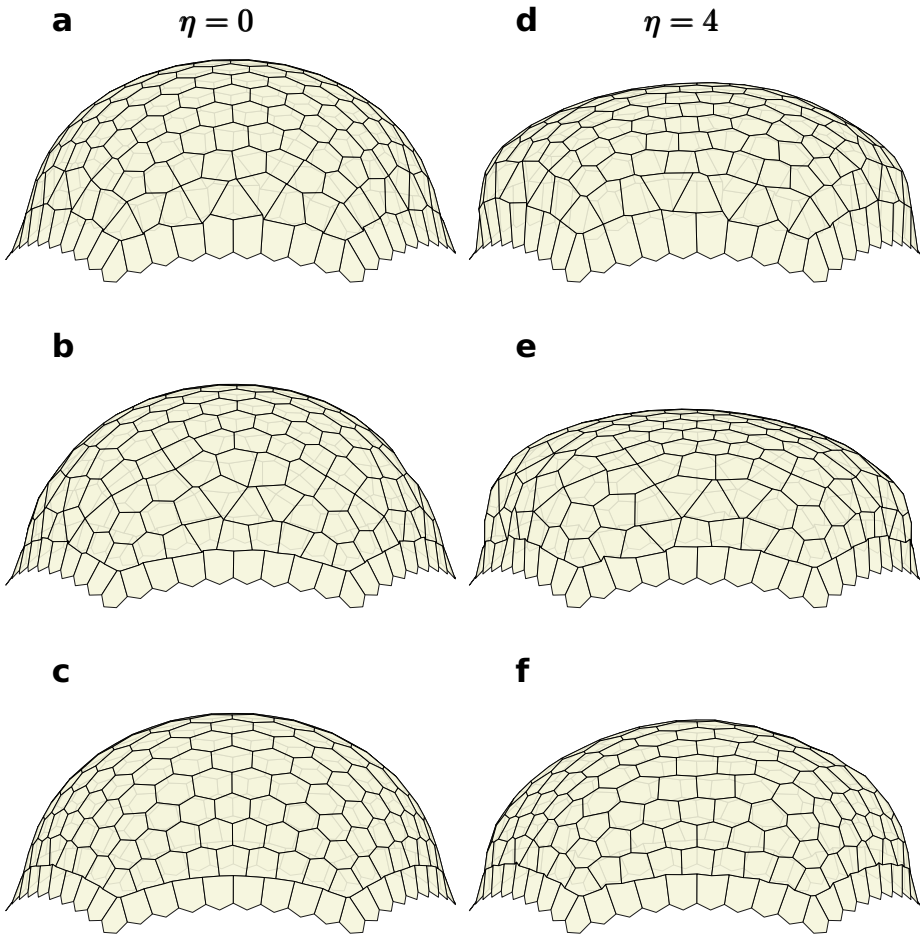

Figure 4.6: The snapshots of tissue after reaching surface area of $A_T = 1000$ with and without mechanical feedback. (a)-(c) show the tissue without feedback for enhanced growth in boundary, periphery and central zone respectively. (d)-(f) show the tissue with mechanical feedback of $\eta = 4$ for enhanced growth in boundary, periphery and central zone respectively.

anisotropic and thus, inclusion of mechanical feedback caused significant changes to the cellular growth resulting in the observed changes in the tissue morphology.

The explanation behind the decay in the tissue height by introduction of mechanical feedback, however, is not still apparent. The growth reorganisation was able to support outwards growth in the primordia formation (as found in chapter 3), thus, it was puzzling to see negative impact from feedback on the tissue elongation. The boundary effect on the outer cells of the meristem

constrain the growth of the cells in the boundary and periphery zones. The impact of this strong boundary could be seen in the tissue growth by the formation of four-walls junctions or inwards bending walls on the tissue surface (Fig. 4.6). These conflicts between the cellular growth and strong restraints could become more prominent with mechanical feedback, as the feedback elevates anisotropic growth in cells.

To eliminate the effects of boundary, we next incorporated cell division on the cells of the meristem. The division adds more degrees of freedom on the tissue by adding new vertices and walls. In the following section, we investigated if this dilution of boundary effect by inclusion of cell division changed the dynamics of tissue elongation.

4.4 Cell division on meristem

The cellular division in the shoot apical meristem is another vital organiser of the morphology in the meristem [48, 55, 88, 93] . The added walls and junctions after cell division provide greater support to the integrity of the tissue. Although it is vital in the growth and shaping of the whole organism, the exact rule by which the cells decide to divide is still not known [48, 94, 95]. For our examination of the shoot elongation, we incorporated a collection of division rules in our vertex model. This allowed us to check if the cell division is essential in the tissue elongation and if a particular division rule is preferable to achieve larger tissue lengthening.

When a cell divides, two new daughter cells are created with a wall between them. In the context of the vertex model, it translate into the division of the polygonal cell into two smaller polygon with an edge going through the center of the mother cell. A challenge in introducing the cell division in the model is to not add large perturbations on the system and keep tissue wide mechanics unchanged after the division. For that, we passed the growth rates and stresses of the mother cell to the newly created daughter cells [48]. This meant

$$\kappa_m = \kappa_d \,, \tag{4.2}$$

where κ_m is the growth rate of mother cell and κ_d is the growth rate of daughter cell. In addition, we took

$$\epsilon_m = \epsilon_d \,, \tag{4.3}$$

where ϵ_m is the strain on the mother cell and ϵ_d is the strain on the daughter cell. From Eq. 4.3 and Eq. 2.10, we determined the rest cell shape for the daughter cells as

$$M_d^0 = M_d + \frac{\mathrm{Tr}(M_d)}{\mathrm{Tr}(M_m)}(M_m^0 - M_m). \tag{4.4}$$

This ensured that tissue mechanics is unchanged with cell division and the division of one cell did not have large influence on the shapes of the neighbouring cells.
The five division rules that we explored in this context are listed in the following subsections. The first three of the rules used were cellular based and the other two relied on the tissue wide information or cues external to the mother cell. In cellular based rules, the direction of the division in mother cells was chosen based on cues from the cell shape and the mechanics of the mother cell. While in the tissue based division rules, the division orientation was decided with some reference point on the tissue away from the mother cell. The tissue wide division rules were used as a reference to understand the impact of having larger division patterns on the plant tissue.

4.4.1 Cell based division

A variety of cell division rules for plant cells that rely on cell geometry or mechanics have been proposed [48, 88, 95]. Among them, we investigated the tissue elongation with one geometry-based and one mechanics-based division rule (Fig. 4.7). The first rule, which is based on the cellular geometry, adds a new wall in the shortest direction through the center of the mother cell (Fig. 4.7 b) [96]. The next rule we used was the division of a cell in the direction of maximal stress (Fig. 4.7 c) [48]. Finally, we also investigated the tissue growth under randomised division (Fig. 4.7 d) to compare the influences of other division rules to that of simply choosing a division direction randomly.

4.4.2 Tissue based division

We also introduced two different types of divisions that read from a tissue wide cue. We took these two division rules to be always following either the radial or the orthoradial direction from a reference point in the tissue (Fig. 4.8). The reference point was taken to be the very tip of the meristem. Thus, the radial division followed the radial direction and orthoradial division followed

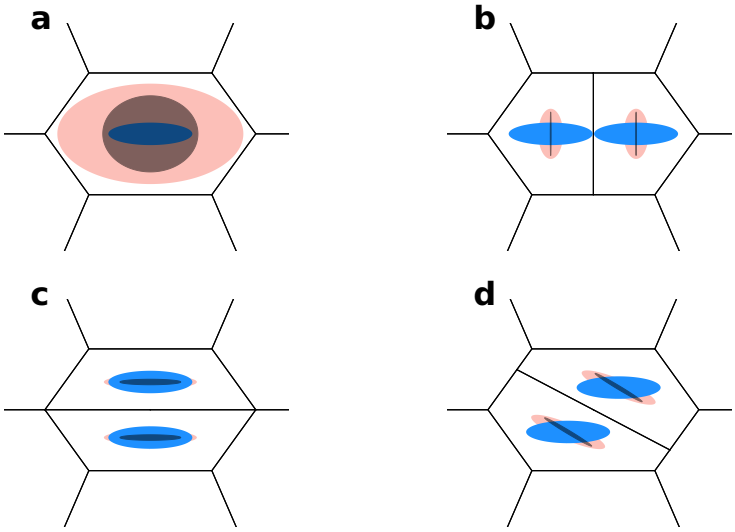

Figure 4.7: The three cellular-based approaches for the selection of the new wall through the centroid of the cell. (a) Initial cell with strain (stress) in the horizontal direction. The current cell shape (red ellipse) is stretched compared to rest cell shape (black) resulting in a strain (blue). (b) Short-axis: shortest line through the centroid of the cell is chosen as division line. (c) Maximal-stress: the direction of maximal stress is chosen. (d) Random: a random direction for division plane is chosen.

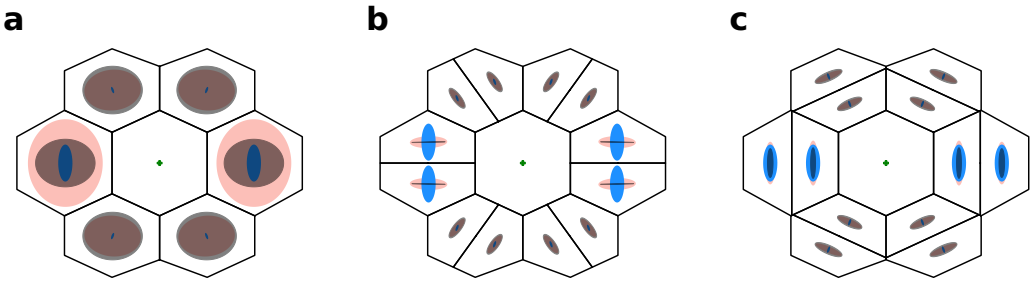

Figure 4.8: The two cell division rules that take tissue wide cues are the radial division and orthoradial division. (a) The initial tissue (with six cells in the outer ring with a cell in the center) is shown to demonstrate the two rules of division. Rest cell shape is shown with black ellipse, while the current cell shape is given in red. The blue ellipse shows the strain in the cells. Here, the reference point of radial and orthoradial direction is taken to be the centroid of the central cell (green cross). (b) Radial division: the cells divide by adding new walls in the radial direction pointing towards the centroid of the central cell. (c) Orthoradial division: the cells divide by adding new walls orthogonal to the direction pointing towards the centroid of the central cell.

the circumferential direction around the tissue.

4.4.3 Role of cell division on the shoot growth

Equipped with the various rules of cell division, we again simulated the elongation of the tissue by applying enhanced zonal growth on the meristem (as discussed in section 4.2). We allowed the cells in the chosen zone to divide once they reach a target size. For simplicity, the target size was taken as the initial size of the cells at the start of the simulation. This allowed the cells to divide immediately from the first step of the simulation. We also allowed only one division per time-step to refrain from adding large perturbation to the system at once. The cells in the meristem are known to have mitotic index[1] of $1\% - 4\%$ depending on the region of the tissue [8]. The central zone of meristem exhibits lower mitotic index, while the outer zones have larger mitotic index. Each of the partitioned zones on the simulated tissue contained around hundred cells Fig. A6), therefore, the simulation of one division per step were close to the biological observations.

The influence of the feedback on the general lengthening of the shoot was still observed to be negative (Fig. A8 with feedback for short-axis division). Albeit, it was not as much pronounced for the boundary and periphery zones as was previously without cell division (Fig. 4.5). In the case of the central zone, the shoot elongation was slowed down for low feedback with the inclusion of cell division, while for higher feedback, the elongation surprisingly again shot up. To investigate further, we plotted the generated tissue height for different division rules without and with mechanical feedback ($\eta = 0$ or 4) as a function of surface area (Fig. 4.9 and 4.10). We found that the growth of the tissue height slowed down considerably for the central zone both with or without mechanical feedback (Fig. 4.9 c and 4.10 c). In both with and without feedback, the short-axis division performed better than all the others for the central zone growth.

For the boundary and the periphery zone, the tissue height showed strong growth in all cases with cell division. Surprising, we saw little impact on the height growth by the choice of division rule in the boundary zone. While for the periphery zone, the radial division faired the best while the orthoradial and the short-axis were the slowest. In contrast to the case without cell division (Fig. 4.5), the enhanced growth in the periphery and boundary zone performed better in all cases than the central zone (direct comparison of short-axis division is shown in Fig. 4.9 d and 4.10 d). Overall, the growth in periphery zone with cell division outperformed the boundary or the central zone to elongate the meristem.

[1] Mitotic index is the percentage of cells under going mitosis (cell division) in a population.

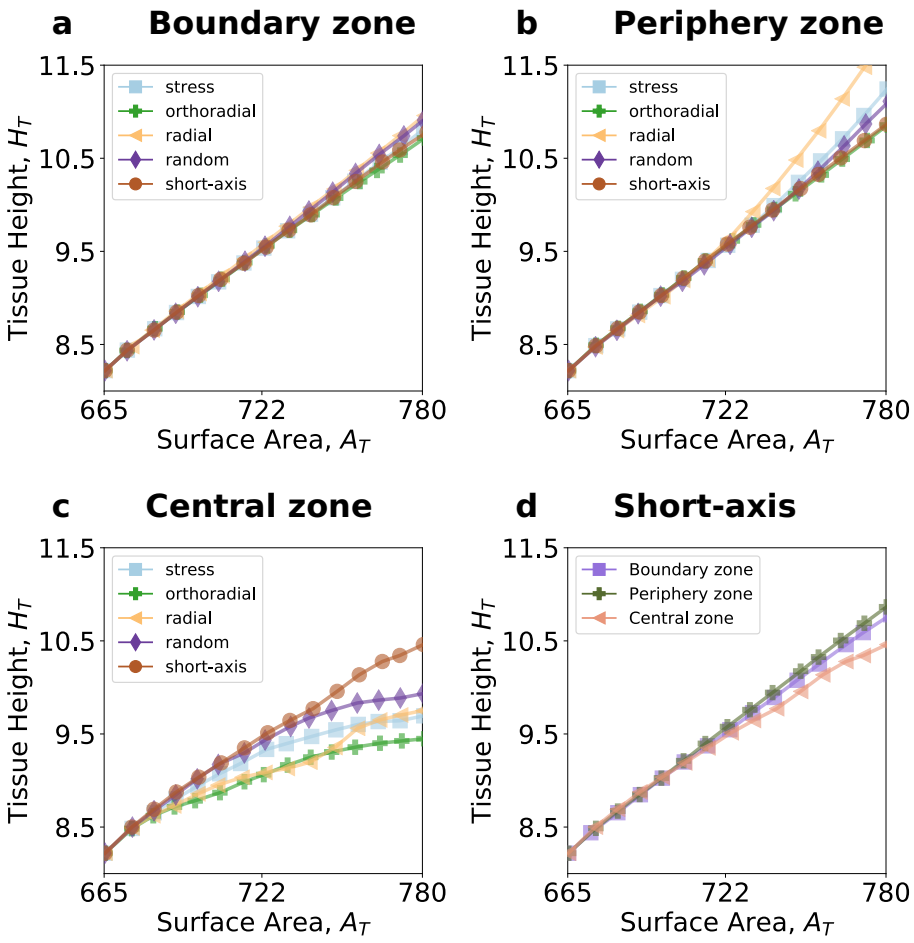

Figure 4.9: The growth of tissue height with surface area of meristem with different rules for division and zonal growth. The analysis shown here is of tissue with no feedback on cellular growth ($\eta = 0$) and with enhanced growth in (a) boundary zone, (b) periphery zone and (c) central zone. For boundary and periphery zone, the cell division rules had little impact on the overall growth of tissue to the growth of the tissue height, while for central zone, the addition of the cell division changed the tissue growth significantly.

Comparing the direct morphology of the simulated tissue for short-axis division with and without feedback (Fig. 4.11), we observed that the cells in the boundary zone case were noticeably deformed into unnatural shapes (Fig. 4.11 a and d). Such misshapen cells were not as pronounced in the periphery or the central zone growth (Fig. 4.11 $b - c$ and $e - f$). This again suggested that it is better for the meristem to localise its growth on the periphery zone for the optimal shoot elongation and for the healthy growth of the cells.

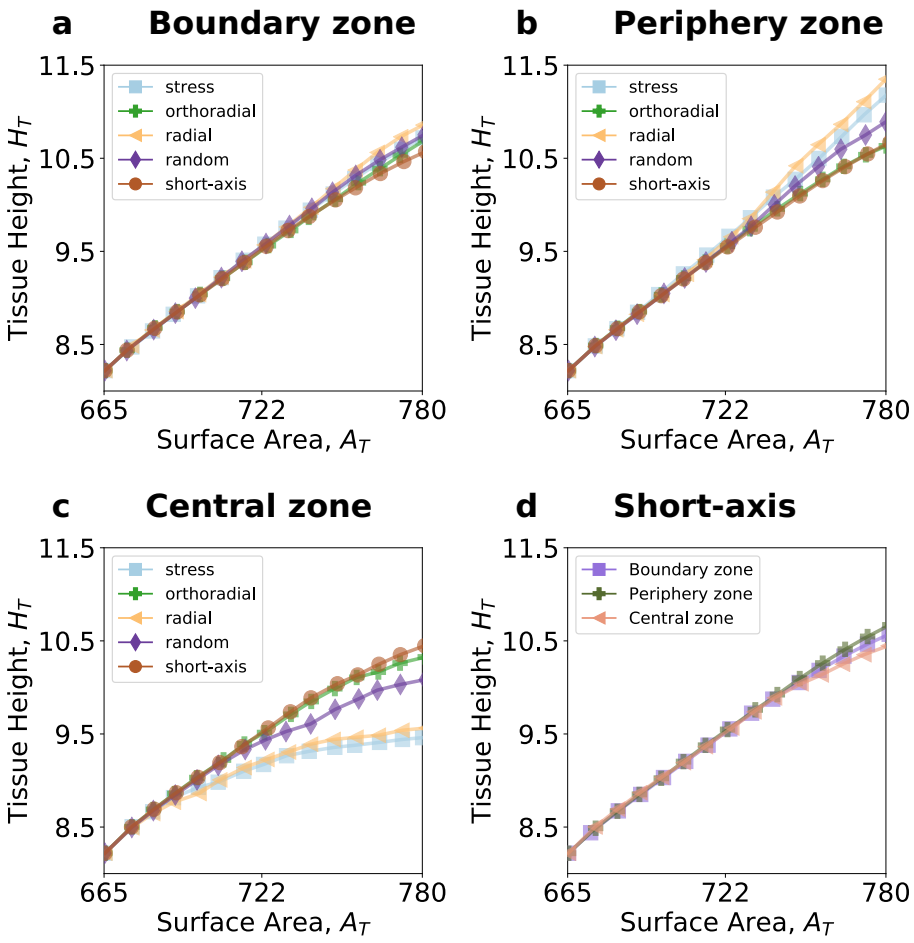

Figure 4.10: The growth of tissue height with surface area of meristem with different rules for division and zonal growth added with mechanical feedback of $\eta = 4$ on cellular growth. The plots show enhanced growth in different zones: (a) boundary zone, (b) periphery zone and (c) central zone. For boundary and periphery zone, the cell division rules again did not show significant change to the height growth. The curves overlapped for all the division rules as seen in (a) and (b). While for central zone, the addition of the cell division had notable impact on the tissue morphology.

4.5 Discussion on the tip growth

The elongation of plant body is maintained by the growth of the shoot apical meristem. It balances the preservation of its dome like apical surface with the polarised growth of the cells to lengthen the shoot [51, 52, 60]. With the aim to understand the evolution of shoot-like cylindrical morphol-

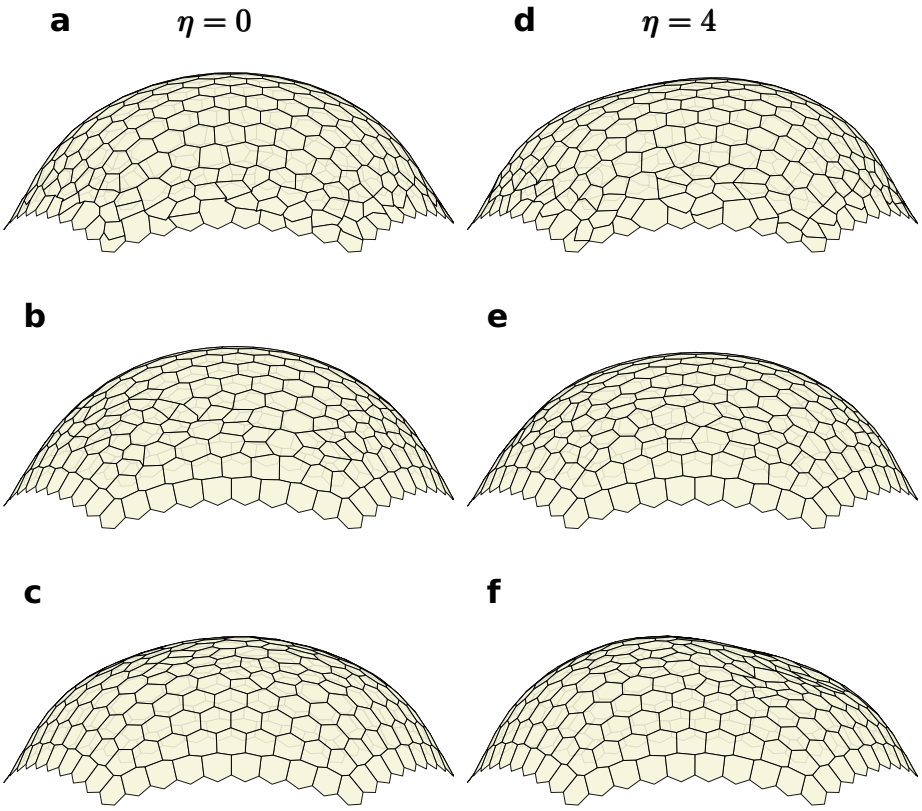

Figure 4.11: The resulting tissue simulated with cell division following short-axis rule. (a)-(c) show the tissue without feedback for enhanced growth in boundary, periphery and central zone respectively. (d)-(f) show the tissue with mechanical feedback of $\eta = 4$ for enhanced growth in boundary, periphery and central zone respectively. (a), (b), (d), (e) show tissue at surface area of $A_T = 800$, while (c) and (f) shows tissue with surface area of $A_T = 780$.

ogy from the hemispherical meristem, we simulated the growth of meristem tip with the use of our three-dimensional vertex-model. We investigated the efficiency of generating asymmetric growth on the tissue by enhancing the cellular growth in confined regions of the meristem.

Considering the patterns of growth and division observed in the SAM [55, 56, 65], we divided the meristem into three zones (boundary, periphery and central as shown in Fig. 4.2). We examined the relevance of locating enhanced growth on these zones in generate elongated shapes. The morphology of the meristem resulting from confined growth in these zones were visibly distinct from each other (Fig. 4.3). The outer zones (boundary and periphery) produced cylindrical shapes for

the tissue, while tissue with growth in central zone resembled an inflated spherical structure. With the plots of tissue height as a function of surface area of the SAM (Fig. 4.4), we found that the localisation of growth on the outer regions of the meristem was superior in comparison to the very tip (central zone) for elongating the tissue.

The cellular growth in the cells is organised by the mechanical feedback that reads the stresses acting on the cells to restructure the cell walls [10, 26]. In chapter 3, we found that mechanical feedback is able to aid outwards growth of primordia from the meristem surface by strengthening the stress patterns and organising cellular growths. Peculiarly, in the case of shoot elongation, we found that mechanical feedback acted negatively, with or without cell division in the overall lengthening of the tissue (Fig 4.5 and A8). The slowing down of elongation with feedback, however, was noticeably lower with the inclusion of cell division in the boundary and the periphery zones (Fig. 4.9 $a-b$, 4.10 $a-b$ and A8 $a-b$). Also, the addition of cell division reestablished the better performance of the boundary and periphery zones in comparison to the central zone (Fig. 4.9 d and 4.10 d). In all, the enhanced growth in the periphery zone was found optimal for elongation of the meristem (Fig. 4.9 and 4.10). The growth in shoot apical meristem in plants are known to be confined on the periphery of the tissue [8, 55, 56, 65]. Thus, our results show that the arrangement of growth in plant tissue is optimised to generate efficient elongation of the shoot.

In regards to the preferred division rule, the benefit of using one over the other was still not clearly identified. The cell shape integrity should also be consider in the further investigation of the prominent cell division rule. With the visual examination of the simulated meristem (Fig. 4.11), we observed that the tissues with enhanced growth in the periphery or center zone exhibited greater likelihood of cells to keep their natural shapes. An investigation to understand the influence of division rules on the cell shapes and the tissue development should be conducted to explore the prevalence of one of the division rules.

The results presented and discussed in this chapter are preliminary and extra refining and investigation are needed to draw further conclusions. The boundary of the tissue was noticed to have strong influence in the shoot growth. The cell division did tame much of the boundary effect but a more thorough investigation can be conducted to study the further impact of the boundary on the shoot elongation. Another direction to probe could be the underlying methods used for cell division in the simulation. We found the rest shapes of cells by equating the strains to make sure the tissue wide mechanical patterns are not disturbed. However, other methods can also be imagined

and have been employed [88]. A test on the robustness of zonal growth with cell division on varying methods of division could also be imagined to elucidate the generation of polarised growth in plants.

5

Conclusion and outlook

Our motivation for undertaking this project was to decipher the mechanism underneath the creation of robust and recognisable shapes in plants. To investigate the dynamical formation of plant tissue, we developed a three-dimensional vertex model and formulated a mechanical description for the tissue and cellular growth. We employed the model in examination of two particularly significant events in plant morphogenesis: the formation of organs in shoot apical meristem (SAM) and the elongation of the shoot.

In the investigation of organogenesis, we found that the initiation of the early organs, or the primordia, is caused by the locally enhanced growth on the cells triggered by a biochemical signal. The growth hormone auxin is accumulated in the primordial cells and causes the loosening of cell walls and the faster expansion of cells in the primordial region [38–41]. Additionally, microtubules in the plant cells are known to reorient along high stresses, guiding the directional deposition of cellulose fibers and leading to the anisotropic stiffening of the cell walls. We mimicked the action of auxin by locally augmenting growth, and the stiffness remodelling via microtubules by adding a stress-led feedback term to the cellular growth. With the inclusion of the mechanical stress response on the cellular growth, we were able to show that the plants rely on the mechanical feedback to drive the growth of the primordia. Instead of depending on modulation of growth rates and increase in cell size at the expense of more materials, plants organise their cellular growth by reading cues from the stresses on the tissue and efficiently squeeze the primordia outwards for the healthy growth of new organs. We found that the mechanical feedback strongly acts on the boundary cells, surrounding the primordia, and slows their growth. This creates a stiff ring of cells with little or

no growth around the faster growing primordial cells which pushes them out of the tissue surface. This slow growth of the boundary region has been observed experimentally ([48, 55–57]) but an explanation for their formation and role in the organogenesis has been lacking. Here, we showed that the mechanical feedback is behind the emergence of this boundary region around the primordia and that the cells in this boundary are vital in driving organogenesis. We identified a twofold mechanism with which mechanical feedback was able to organise the tissue growth. First, feedback was able to organise the cellular growth by modulation of the wall properties and second, the mechanical feedback could modulate the stress patterns on the cells effectively self-amplifying its influence on the cellular growth. With this mechanisms, we found that the mechanical feedback could organise cell growth in the SAM and efficiently generate the plant organs.

On the second part of the research, we investigated the role of growth and division patterns on the shoot apical meristem, addressing in particular the preservation of its hemispherical surface and development of the elongated shoot. We found that changing the patterns of growth on the meristem resulted in very different morphologies of tissues. For the plants to preserve their three dimensional forms and generate polarised growth of their shoot, a spatially arranged growth of the cells on the meristem was required. We saw that for the most efficient lengthening of the shoot, the growth in meristem needs to be confined on the periphery region of the tissue. Similar growth patterns on the SAM have been widely noted in the literature [55, 56, 65], and with this investigation, we showed that such growth patterns fine tunes the elongated development of plant tissue maintaining their cylindrical shape and with minimal waste of the cellular materials. We also aimed to identify the preferred rule of cell division on the meristem with this examination. However, we were not yet able to isolate the significance of employing one over the other. A close inspection of growth and division patterns on the shoot [55–57, 65], along with additional emphasis on the shape integrity of the cells could help us shed light on this issue.

On the extension of this investigation, we could examine the influence of cell divisions in the study of organ formation from the shoot apical meristem. The cell divisions on the boundary region around the primordia are known to orient circumferentially following the higher stress direction [48, 57]. The mechanism behind the appearance of such stereotypic pattern is not yet clear. A hypothesis can be formulated that this could be advantageous for the cells as the addition of new walls in the direction of larger stress would lead to higher resistance to the cellular deformation. Such hypothesis can be tested by studying the emerging mechanical properties or the changing

morphology of the tissue and the new organs with the introduction of cell division on the boundary cells.

We investigated the development of shoot apical meristem with the mechanical model from the onset of stiffness modulation by biochemical action. To investigate further the cause of such modulation, the mechanical model can be directly augmented with the flow of biochemicals. The polarised flow of the auxin has been strongly suggested to be driven by tissue mechanics ([16]) and the inclusion of these flow along with their modulation of mechanics can shed further light on the generation and positioning of the organs on the meristem. It might also be desirable to expand the model beyond the epidermis to the sub-surface cells. The growth of lateral organs has been suggested to control the development of meristem by disrupting the flow of auxin in the cells underneath the tissue surface [54]. A complete three-dimensional model following similar principle of mechanical and biochemical interactions might be able to elucidate these larger patterns of growth on the plant tissue.

The key insight found here was of mechanical feedback generating robust growth with twofold promotion of growth heterogeneities; by directly organising growth and by patterning stresses. This mechanism can also be expected to be behind morphogenesis in other systems in plants. The lateral growth in roots, shaping of sepal, leaves or flowers, phyllotaxis (arrangement of leaves or flowers around a stem) and many other developmental processes can be studied by employing the principle of stress-led feedback on the plant cellular growth [47, 53, 97, 98].

Ultimately, the questions in developmental biology are never ending, the mystery of robust morphogenesis of all life forms can only be hoped to be demystified one system at a time. We presented our contribution to the understanding of origin of forms in plants; new steps can be taken in any direction to add to the vast knowledge of morphogenesis that we can hope, one day, will accumulate into the complete understanding behind the formation of life.

Appendices

A.1 Rewriting the mean curvature relation

Eq. 2.17 for $H = 0$ is the Euler-Lagrange equation for surface area minimisation [81]. This leads to the direct relation between surface area minimisation and mean curvature flow as

$$2H\vec{n} = \lim_{diam(A)\to 0} \frac{\nabla_S A}{A} \quad , \tag{A1}$$

where ∇_S is the gradient at a point P on the surface. A and $diam(A)$ are the infinitesimal area around a point P and diameter of this area. $H\vec{n}$ is the mean curvature normal. With this, we can define operator Δ_S that maps a point x_i to the mean curvature normal as

$$\Delta_S(x_i) = 2H\vec{n}(x_i) \quad . \tag{A2}$$

This operator is also known as the Laplace-Beltrami operator for a surface, and is expressed as

$$\Delta_S = \nabla_S \cdot \nabla_S \quad . \tag{A3}$$

From this relation we can also derive the previous mentioned relation of H as,

$$\begin{aligned} \Delta_S(x_i) &= 2H\vec{n}(x_i) \\ 2H\vec{n}(x_i) \cdot \vec{n}(x_i) &= \Delta_S(x_i) \cdot \vec{n}(x_i) \\ H(x_i) &= \frac{1}{2}(\Delta_S x_i) \cdot \vec{n}(x_i) \end{aligned} \tag{A4}$$

Also to get the mean curvature H from the Laplace-Beltrami Operator $\Delta_S(x_i)$, we can just take the half of the magnitude of the $\Delta_S(x_i)$.

$$\begin{aligned} \Delta_S(x_i) &= 2H\vec{n}(x_i) \\ \|\Delta_S(x_i)\| &= \|2H\vec{n}(x_i)\| \\ \|\Delta_S(x_i)\| &= 2H\|\vec{n}(x_i)\| \\ H &= \frac{1}{2}\|\Delta_S(x_i)\| \end{aligned} \tag{A5}$$

A.2 Simulation parameters

The parameters used for the simulation of growth of SAM and primordia are given in Table A1. The Lamé's first parameter μ, bending stiffness μ_b and pressure P were kept constant through all the simulations in both investigations (of primordial growth and of shoot elongation). The noise in the growth, given by γ, was defined as a uniform noise in the range $[-0.1, 0.1]$, thus simulating 10% deviation of growth rates from their initial values. The analysis for feedback were based on the analysis of simulations with a growth ratio $r_g = 4.8$, and the same results holds true for varying growth rate, checked by increasing the growth ratio to $r_g = 9.4$.

μ	μ_b	P	γ
1.0	0.1	0.0126	$\mathcal{U}(-0.1, 0.1)$

Lockhart growth

$r_g = 9.4$		$r_g = 4.8$	
κ_f	κ_s	κ_f	κ_s
0.5	0.05	0.5	0.1

Exponential growth

$r_g = 9.6$		$r_g = 4.5$	
κ_f	κ_s	κ_f	κ_s
0.09	0.005	0.02	0.005

$r_g = 6.2$	
κ_f	κ_s
0.05	0.01

Table A1: Parameter values used for simulation of primordial growth and shoot elongation using three-dimensional vertex model. $\mathcal{U}(-0.1, 0.1)$ is an uniform random number taken in the interval of $[-0.1, 0.1]$. The growth rates for different growth ratios with *Lockhart* and *Exponential* growth is also given.

A.3 Radial/Orthoradial vectors

For a cell c, the radial ($\hat{u}_r$) unit vector is defined as

$$\hat{u}_r = \frac{(\vec{p} - \vec{v}_c)}{\|(\vec{p} - \vec{v}_c)\|}, \tag{A6}$$

where, $\vec{p}$ is the position vector to the tip of the primordia and $\vec{v}_c$ is the vector to the centroid of the cell c. The orthoradial ($\hat{u}_o$) unit vector can then be written as,

$$\hat{u}_o = \hat{u}_r \times \hat{n}_c, \tag{A7}$$

where, $\hat{n}_c$ is the normal vector to the cell c. Fig. 3.11 shows the directions of radial and orthoradial unit vectors.

A.4 Growth curve fitting with *exponential* growth law

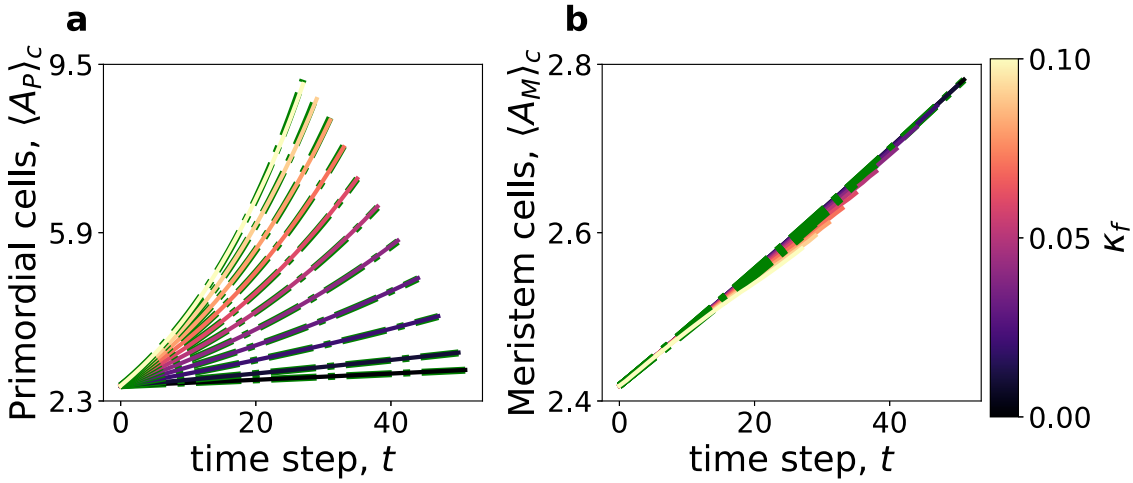

Figure A1: Fitting exponential growth curves (dotted green line) on the areal growth of primordial and meristematic cells under *exponential* growth. The meristematic growth rates are kept constant while the primordial growth rates are varied.

A.5 Growth of primordia with growth ratio $= 9.6$

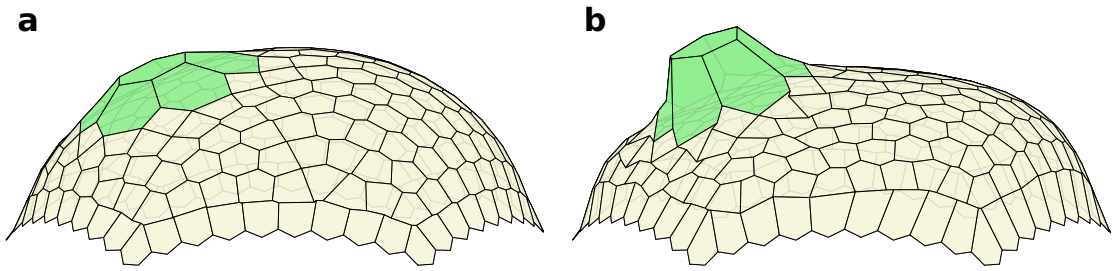

Figure A2: The tissues shown have growth ratio $r_g = 9.6$ and have grown to $A_T = 850$. (a) Without feedback ($\eta = 0$), there is little outgrowth of primordia. (b) With high feedback of $\eta = 8$, for the same growth ratio $r_g = 9.6$, the primordia push significantly outwards with clear development.

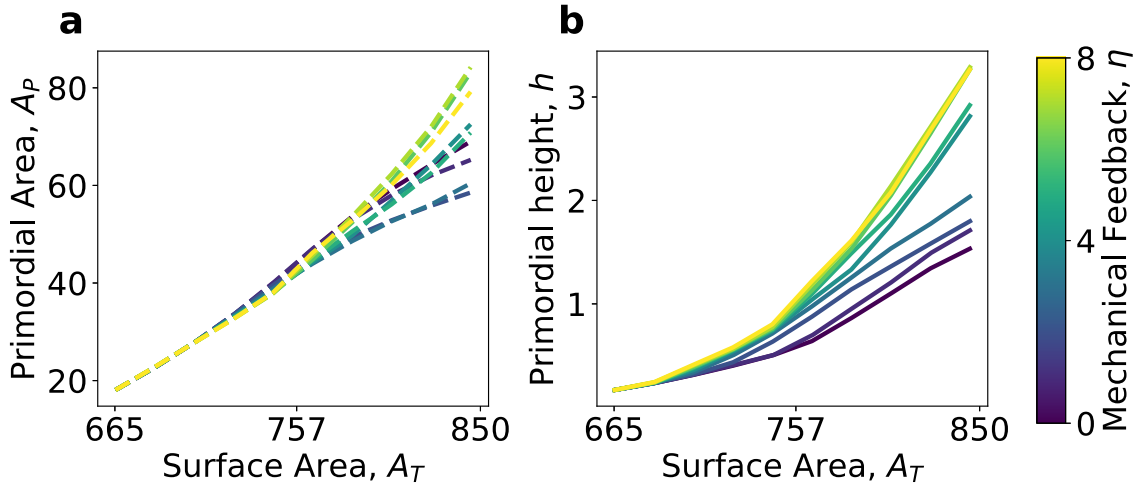

Figure A3: Increasing mechanical feedback of cells to tissue wide mechanical stresses results in efficient primordial growth. Here, a tissue with growth ratio $r_g = 9.6$ is grown for varying mechanical feedback. (a) The overall areal growth of the primordium is relatively stable with changing mechanical feedback. (b) The height of primordium increases significantly with higher mechanical feedback.

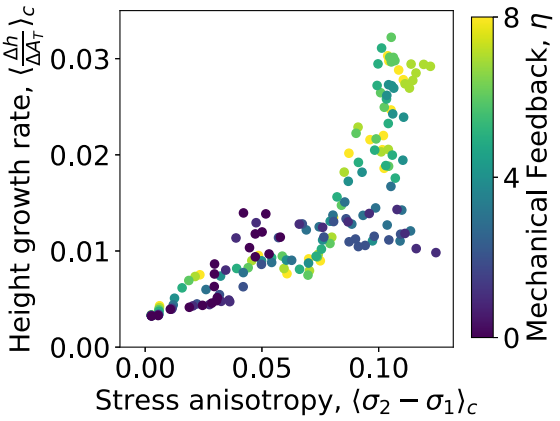

Figure A4: The anisotropy of stress along with height growth rate under varying mechanical feedback for tissue with $r_g = 9.6$. With higher mechanical feedback, both the rate of height growth and the stress anisotropy of cells on the primordial boundary increase.

A.6 Exponential growth with mechanical growth law for one-dimensional cell

We can show that for a one-dimensional cell with similar elastic energy and pressure to expand the growth is exponential. We start by writing the energy for a single cell as,

$$E = \alpha l \left(\frac{l - l_0}{l_0} \right)^2 - Pl, \tag{A8}$$

From the energy equation, the minimisation condition becomes,

$$\frac{dE}{dl} = -P + \frac{d}{dl} \left(\alpha l \left(\frac{l - l_0}{l_0} \right)^2 \right) = 0. \tag{A9}$$

We can then find expression for length of the cell, l,

$$l = \frac{1}{3} l_0 \left(2 \pm \sqrt{4 + 3(P/\alpha - 1)} \right) = \frac{1}{3} l_0 \left(2 \pm \sqrt{3P/\alpha + 1} \right) \tag{A10}$$

The two solutions we have is for the maximum and the minimum of the energy and we can neglect the maximum. We then are left with one solution,

$$l = \frac{1}{3} l_0 \left(2 + \sqrt{3P/\alpha + 1} \right) \tag{A11}$$

The deformation of the length then triggers the growth as

$$\frac{dl_0}{dt} = \kappa(l - l_0). \tag{A12}$$

which is real for the condition, $P/\alpha >$ -1/3, and as P > 0, there is always a real solution that exist. We can rewriting the above equation as,

$$l = \gamma l_0 \qquad \text{where, } \gamma = \frac{1}{3} \left(2 + \sqrt{3P/\alpha + 1} \right) \tag{A13}$$

Solving equation for l_0, we can write

$$l_0 = Le^{kt(\gamma - 1)} \tag{A14}$$

with relation of $l = \gamma l_0$, we now have

$$l = Ce^{kt(\gamma - 1)} \tag{A15}$$

with $\gamma > 1$ for P/α>0, we will always have an exponential growth and the system is always unstable.

A.7 Unstable cell shapes with *exponential* growth

The cells with *exponential* grow proportional to their shape and are not effected by the tissue mechanics or the restriction by the topology. That results in an exponentially growing cells and an unstable tissue morphology for the tissue. The cells at the boundary of the tissue in the simulation start getting crooked and wall angles bend in unnatural angles as seen in Fig. A5 *b*.

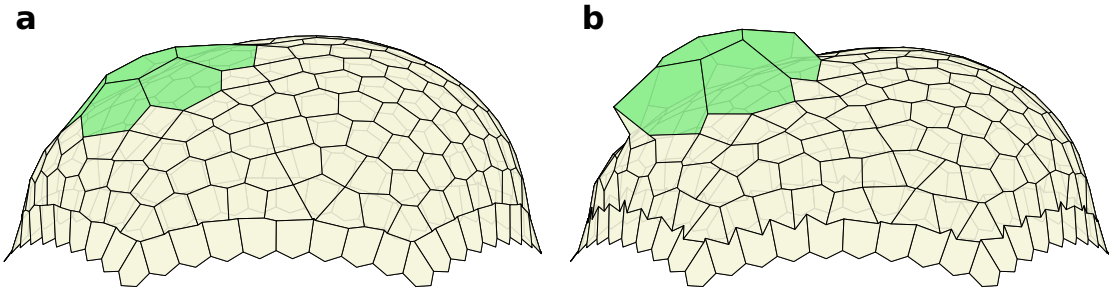

Figure A5: The snapshots of tissue at surface area $A_T = 1000$ and no feedback for *Lockhart* (a) and *exponential* (b) growth. The cell shapes with *exponential* growth is unstable and unnatural as seen by the crooked angles between the walls of cells at the bottom of the tissue.

A.8 Zonal division of cells in tip of shoot

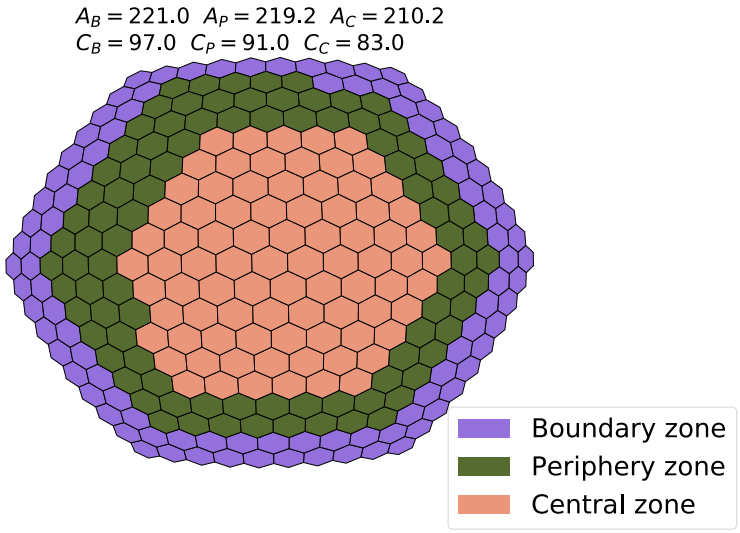

Figure A6: The division of meristem in three zones shown by top view. The areal of zones are kept near equal while dividing the regions on the tissue. The area of each zone is shown by the numbers A_B, A_P and A_C on the figure for boundary, periphery and central zone respectively. The cell number likewise is given by C_B, C_P and C_C.

A.9 Elongation of shoot apical meristem with the feedback on three zones

A.9.1 Comparison of zones without mechanical feedback

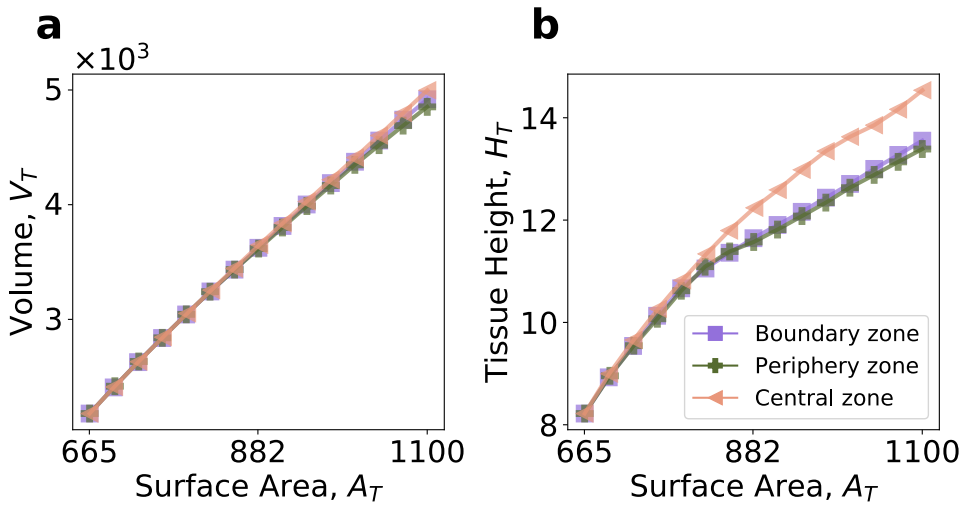

Figure A7: The volume and height growth of tissue for different zonal growths with feedback of $\eta = 4$ and no cell division. (a) Volume of the tissue still grows proportionally to surface area with feedback for all three growth types. (b) The height of the tissue growth is now reversed with higher elongation for enhanced growth in central zone compared to the outer boundary and periphery zones.

A.9.2 Influence of mechanical feedback on tissue elongation with cell division

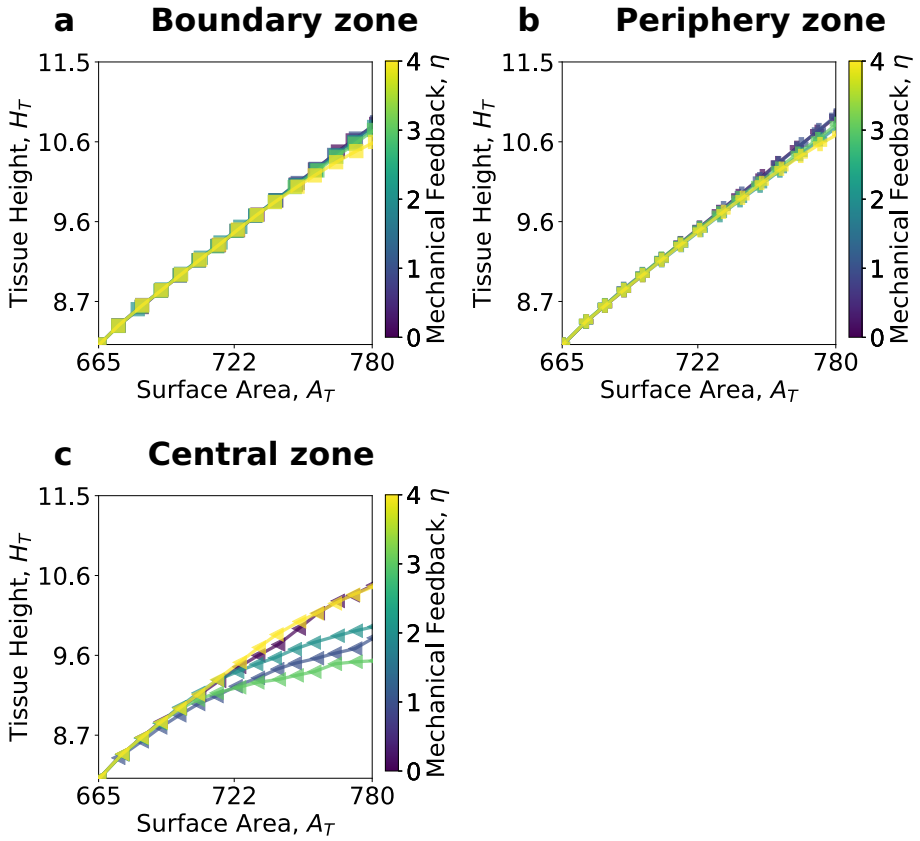

Figure A8: The impact of mechanical feedback on the tissue elongation with cell division shown for short-axis division rule. The feedback still exhibited negative effects on the overall elongation of shoot on all three zones. While for central zone, remarkably, the feedback overshot to recover the elongation for $\eta = 4$. Further investigation is needed to understand the overall impact of the feedback in the elongation of shoot.

Bibliography

[1] D'Arcy Wentworth Thompson. *On growth and form*. Cambridge University Press, 1917. URL: https://archive.org/details/ongrowthform1917thom/.

[2] Alan Mathison Turing. "The chemical basis of morphogenesis". In: *Bulletin of mathematical biology* 52.1-2 (1990), pp. 153–197.

[3] Reza Farhadifar, Jens-Christian Röper, Benoit Aigouy, Suzanne Eaton, and Frank Jülicher. "The influence of cell mechanics, cell-cell interactions, and proliferation on epithelial packing". In: *Curr. Biol.* 17.24 (2007), pp. 2095–2104.

[4] Miriam Osterfield, Celeste A Berg, and Stanislav Y Shvartsman. "Epithelial patterning, morphogenesis, and evolution: *Drosophila* eggshell as a model". In: *Dev. Cell.* 41.4 (2017), pp. 337–348.

[5] Francesco Boselli, Jonathan B. Freund, and Julien Vermot. "Blood flow mechanics in cardiovascular development". In: *Cellular and Molecular Life Sciences* 72.13 (July 2015), pp. 2545–2559.

[6] Karen Alim, Gabriel Amselem, François Peaudecerf, Michael P Brenner, and Anne Pringle. "Random network peristalsis in *Physarum polycephalum* organizes fluid flows across an individual". In: *Proceedings of the National Academy of Sciences* 110.33 (2013), pp. 13306–13311.

[7] Vincent Mirabet, Pradeep Das, Arezki Boudaoud, and Olivier Hamant. "The role of mechanical forces in plant morphogenesis". In: *Annu. Rev. Plant Biol.* 62 (2011), pp. 365–385.

[8] Patrick Laufs, Olivier Grandjean, Claudia Jonak, Kiên Kiêu, and Jan Traas. "Cellular parameters of the shoot apical meristem in *Arabidopsis*". In: *The Plant Cell* 10.8 (1998), pp. 1375–1389.

[9] Cristel C Carles and Jennifer C Fletcher. "Shoot apical meristem maintenance: the art of a dynamic balance". In: *Trends in plant science* 8.8 (2003), pp. 394–401.

[10] Olivier Hamant, Marcus G Heisler, Henrik Jönsson, Pawel Krupinski, Magalie Uyttewaal, Plamen Bokov, Francis Corson, Patrik Sahlin, Arezki Boudaoud, Elliot M Meyerowitz, Yves Couder, and Jan Traas. "Developmental patterning by mechanical signals in *Arabidopsis*". In: *Science* 322.5908 (2008), pp. 1650–1655.

[11] Léna Beauzamy, Marion Louveaux, Olivier Hamant, and Arezki Boudaoud. "Mechanically, the shoot apical meristem of *Arabidopsis* behaves like a shell inflated by a pressure of about 1 MPa". In: *Frontiers in plant science* 6 (2015), p. 1038.

[12] Wilhelm Flügge. *Stresses in shells*. 2nd ed. New York: Springer-Verlag, 1973.

[13] James A Lockhart. "An analysis of irreversible plant cell elongation". In: *J. Theor. Biol.* 8.2 (1965), pp. 264–275.

[14] Peter M Ray, Paul B Green, and Robert Cleland. "Role of turgor in plant cell growth". In: *Nature* 239.5368 (1972), p. 163.

[15] Marcus G Heisler, Olivier Hamant, Pawel Krupinski, Magalie Uyttewaal, Carolyn Ohno, Henrik Jönsson, Jan Traas, and Elliot M Meyerowitz. "Alignment between PIN1 polarity and microtubule orientation in the shoot apical meristem reveals a tight coupling between morphogenesis and auxin transport". In: *PLoS Biol.* 8.10 (2010), e1000516.

[16] Naomi Nakayama, Richard S Smith, Therese Mandel, Sarah Robinson, Seisuke Kimura, Arezki Boudaoud, and Cris Kuhlemeier. "Mechanical regulation of auxin-mediated growth". In: *Curr. Biol.* 22.16 (2012), pp. 1468–1476.

[17] Yuchen Long and Arezki Boudaoud. "Emergence of robust patterns from local rules during plant development". In: *Curr. Opin. Plant Biol.* 47 (2019), pp. 127–137.

[18] Paul B Green. "Mechanism for plant cellular morphogenesis". In: *Science* 138.3548 (1962), pp. 1404–1405.

[19] Sven Kerstens, Willem F Decraemer, and Jean-Pierre Verbelen. "Cell walls at the plant surface behave mechanically like fiber-reinforced composite materials". In: *Plant Physiol.* 127.2 (2001), pp. 381–385.

[20] MC Ledbetter and KR Porter. "A "microtubule" in plant cell fine structure". In: *J. Cell. Biol.* 19.1 (1963), pp. 239–250.

[21] I Brent Heath. "A unified hypothesis for the role of membrane bound enzyme complexes and microtubules in plant cell wall synthesis". In: *J. Theor. Biol.* 48.2 (1974), pp. 445–449.

[22] Alexander R Paredez, Christopher R Somerville, and David W Ehrhardt. "Visualization of cellulose synthase demonstrates functional association with microtubules". In: *Science* 312.5779 (2006), pp. 1491–1495.

[23] Chris Somerville. "Cellulose synthesis in higher plants". In: *Annu. Rev. Cell Dev. Biol.* 22 (2006), pp. 53–78.

[24] Carol L Wymer, Scott A Wymer, Daniel J Cosgrove, and Richard J Cyr. "Plant cell growth responds to external forces and the response requires intact microtubules". In: *Plant Physiol.* 110.2 (1996), pp. 425–430.

[25] Ann L Cleary and Adrienne R Hardham. "Pressure induced reorientation of cortical microtubules in epidermal cells of *Lolium rigidum* leaves". In: *Plant Cell. Physiol.* 34.7 (1993), pp. 1003–1008.

[26] Magalie Uyttewaal, Agata Burian, Karen Alim, Benoît Landrein, Dorota Borowska-Wykręt, Annick Dedieu, Alexis Peaucelle, Michał Ludynia, Jan Traas, Arezki Boudaoud, Dorota Kwiatkowska, and Olivier Hamant. "Mechanical stress acts via katanin to amplify differences in growth rate between adjacent cells in *Arabidopsis*". In: *Cell* 149.2 (2012), pp. 439–451.

[27] Benoît Landrein and Olivier Hamant. "How mechanical stress controls microtubule behavior and morphogenesis in plants: history, experiments and revisited theories". In: *Plant J.* 75.2 (2013), pp. 324–338.

[28] Daniel J Cosgrove. "Plant cell wall extensibility: connecting plant cell growth with cell wall structure, mechanics, and the action of wall-modifying enzymes". In: *J. Exp. Bot.* 67.2 (2015), pp. 463–476.

[29] Theophil Ciesielski. “Untersuchungen über die Abwärtskrümmung der Wurzel”. PhD thesis. 1871.

[30] Charles Darwin and Sir Darwin Francis. “The power of movement in plants”. In: New York: D. Appleton and Company, 1881, pp. 523–545.

[31] Arpád Paál. “Uber phototropische reizleitung”. In: *Jahrbücher für wissenschaftliche Botanik* 58 (1919), pp. 406–458.

[32] Frits Warmolt Went. *Phytohormones*. The Macmillan Company; New York, 1937.

[33] Aldo Carl Leopold. *Auxins and plant growth*. Univ of California Press, 1955.

[34] Von F. Kögl and A. J. Haagen-Smit. “Über die Chemie des Wuchsstoffs”. In: *Proceedings of the royal Netherlands academy of arts and science* 10 (1931), pp. 1411–1416.

[35] Craig W Whippo and Roger P Hangarter. “Phototropism: bending towards enlightenment”. In: *The Plant Cell* 18.5 (2006), pp. 1110–1119.

[36] AJ Haagen-Smit, WB Dandliker, SH Wittwer, and AE Murneek. “Isolation of 3-indoleacetic acid from immature corn kernels”. In: *Am. J. Bot.* (1946), pp. 118–120.

[37] Frits Warmolt Went. “Wuchsstoff und Wachstu”. In: *Recueil des travaux botaniques néerlandais* 25 (1928).

[38] Peter M Ray. “Cell wall synthesis and cell elongation in oat coleoptile tissue”. In: *Am. J. Bot.* 49.9 (1962), pp. 928–939.

[39] Kazuhiko Nishitani and Yoshio Masuda. “Auxin-induced changes in the cell wall structure: Changes in the sugar compositions, intrinsic viscosity and molecular weight distributions of matrix polysaccharides of the epicotyl cell wall of *Vigna angularis*”. In: *Physiol. Plant* 52.4 (1981), pp. 482–494.

[40] Mateusz Majda and Stéphanie Robert. “The role of auxin in cell wall expansion”. In: *Int. J. Mol. Sci.* 19.4 (2018), p. 951.

[41] Catherine Perrot-Rechenmann. “Cellular responses to auxin: division versus expansion”. In: *Cold Spring Harb. Perspect. Biol.* (2010), a001446.

[42] Didier Reinhardt, Eva-Rachele Pesce, Pia Stieger, Therese Mandel, Kurt Baltensperger, Malcolm Bennett, Jan Traas, Jiří Friml, and Cris Kuhlemeier. “Regulation of phyllotaxis by polar auxin transport”. In: *Nature* 426.6964 (2003), p. 255.

[43] Eva Benková, Marta Michniewicz, Michael Sauer, Thomas Teichmann, Daniela Seifertová, Gerd Jürgens, and Jiří Friml. "Local, efflux-dependent auxin gradients as a common module for plant organ formation". In: *Cell* 115.5 (2003), pp. 591–602.

[44] Marcus G Heisler, Carolyn Ohno, Pradeep Das, Patrick Sieber, Gonehal V Reddy, Jeff A Long, and Elliot M Meyerowitz. "Patterns of auxin transport and gene expression during primordium development revealed by live imaging of the *Arabidopsis* inflorescence meristem". In: *Curr. Biol.* 15.21 (2005), pp. 1899–1911.

[45] Jiří Friml. "Auxin transport — shaping the plant". In: *Current opinion in plant biology* 6.1 (2003), pp. 7–12.

[46] Alexis Peaucelle, Siobhan A Braybrook, Laurent Le Guillou, Emeric Bron, Cris Kuhlemeier, and Herman Höfte. "Pectin-induced changes in cell wall mechanics underlie organ initiation in *Arabidopsis*". In: *Curr. Biol.* 21.20 (2011), pp. 1720–1726.

[47] Nathan Hervieux, Mathilde Dumond, Aleksandra Sapala, Anne-Lise Routier-Kierzkowska, Daniel Kierzkowski, Adrienne HK Roeder, Richard S Smith, Arezki Boudaoud, and Olivier Hamant. "A mechanical feedback restricts sepal growth and shape in *Arabidopsis*". In: *Current Biology* 26.8 (2016), pp. 1019–1028.

[48] Marion Louveaux, Jean-Daniel Julien, Vincent Mirabet, Arezki Boudaoud, and Olivier Hamant. "Cell division plane orientation based on tensile stress in *Arabidopsis thaliana*". In: *Proc. Natl. Acad. Sci. USA* 113.30 (2016), E4294–E4303.

[49] Olivier Ali, Vincent Mirabet, Christophe Godin, and Jan Traas. "Physical models of plant development". In: *Annual review of cell and developmental biology* 30 (2014), pp. 59–78.

[50] Behruz Bozorg, Pawel Krupinski, and Henrik Jönsson. "Stress and strain provide positional and directional cues in development". In: *PLoS Comput. Biol.* 10.1 (2014), e1003410.

[51] Hadrien Oliveri, Jan Traas, Christophe Godin, and Olivier Ali. "Regulation of plant cell wall stiffness by mechanical stress: a mesoscale physical model". In: *J. Math Biol.* (Sept. 2018).

[52] Frédéric Boudon, Jérôme Chopard, Olivier Ali, Benjamin Gilles, Olivier Hamant, Arezki Boudaoud, Jan Traas, and Christophe Godin. "A computational framework for 3D mechanical modeling of plant morphogenesis with cellular resolution". In: *PLoS Comput. Biol.* 11.1 (2015), e1003950.

[53] Alexandra B Rebocho, Paul Southam, J Richard Kennaway, J Andrew Bangham, and Enrico Coen. "Generation of shape complexity through tissue conflict resolution". In: *Elife* 6 (2017), e20156.

[54] Massimiliano Sassi, Olivier Ali, Frédéric Boudon, Gladys Cloarec, Ursula Abad, Coralie Cellier, Xu Chen, Benjamin Gilles, Pascale Milani, Jiří Friml, et al. "An auxin-mediated shift toward growth isotropy promotes organ formation at the shoot meristem in *Arabidopsis*". In: *Current biology* 24.19 (2014), pp. 2335–2342.

[55] G Venugopala Reddy, Marcus G Heisler, David W Ehrhardt, and Elliot M Meyerowitz. "Real-time lineage analysis reveals oriented cell divisions associated with morphogenesis at the shoot apex of *Arabidopsis thaliana*". In: *Development* 131.17 (2004), pp. 4225–4237.

[56] Dorota Kwiatkowska and Jacques Dumais. "Growth and morphogenesis at the vegetative shoot apex of *Anagallis arvensis* L." In: *J. Exp. Bot.* 54.387 (2003), pp. 1585–1595.

[57] Mitsuhiro Aida and Masao Tasaka. "Morphogenesis and patterning at the organ boundaries in the higher plant shoot apex". In: *Plant. Mol. Biol.* 60.6 (2006), pp. 915–928.

[58] Dorota Kwiatkowska. "Flowering and apical meristem growth dynamics". In: *J. Exp. Bot.* 59.2 (2008), pp. 187–201.

[59] Paul B. Green and Jeanne M. Lang. "Toward a biophysical theory of organogenesis: Birefringence observations on regenerating leaves in the succulent, *Graptopetalum paraguayense* E. Walther". In: *Planta* 151.5 (May 1981), pp. 413–426.

[60] Jean-Daniel Julien and Arezki Boudaoud. "Elongation and shape changes in organisms with cell walls: A dialogue between experiments and models". In: *The Cell Surface* 1 (2018), pp. 34–42.

[61] Jacques Dumais, Sidney L Shaw, Charles R Steele, Sharon R Long, and Peter M Ray. "An anisotropic-viscoplastic model of plant cell morphogenesis by tip growth". In: *International Journal of Developmental Biology* 50 (2-3 2006), pp. 209–222.

[62] Amir Bidhendi and Anja Geitmann. "Finite element modeling of shape changes in plant cells". In: *Plant physiology* (2017), pp–01684.

[63] Felipe Cava, Erkin Kuru, Yves V Brun, and Miguel A de Pedro. "Modes of cell wall growth differentiation in rod-shaped bacteria". In: *Current opinion in microbiology* 16.6 (2013), pp. 731–737.

[64] Otger Campas and L Mahadevan. "Shape and dynamics of tip-growing cells". In: *Current Biology* 19.24 (2009), pp. 2102–2107.

[65] Daniel Kierzkowski, Naomi Nakayama, Anne-Lise Routier-Kierzkowska, Alain Weber, Emmanuelle Bayer, Martine Schorderet, Didier Reinhardt, Cris Kuhlemeier, and Richard S Smith. "Elastic domains regulate growth and organogenesis in the plant shoot apical meristem". In: *Science* 335.6072 (2012), pp. 1096–1099.

[66] Francis Corson, Olivier Hamant, Steffen Bohn, Jan Traas, Arezki Boudaoud, and Yves Couder. "Turning a plant tissue into a living cell froth through isotropic growth". In: *Proceedings of the National Academy of Sciences* 106.21 (2009), pp. 8453–8458.

[67] Sigal Savaldi-Goldstein and Joanne Chory. "Growth coordination and the shoot epidermis". In: *Current opinion in plant biology* 11.1 (2008), pp. 42–48.

[68] John L Bowman and Yuval Eshed. "Formation and maintenance of the shoot apical meristem". In: *Trends in plant science* 5.3 (2000), pp. 110–115.

[69] Sigal Savaldi-Goldstein, Charles Peto, and Joanne Chory. "The epidermis both drives and restricts plant shoot growth". In: *Nature* 446.7132 (2007), p. 199.

[70] Miriam Osterfield, XinXin Du, Trudi Schüpbach, Eric Wieschaus, and Stanislav Y Shvartsman. "Three-dimensional epithelial morphogenesis in the developing *Drosophila* egg". In: *Dev. Cell.* 24.4 (2013), pp. 400–410.

[71] Mahim Misra, Basile Audoly, Ioannis G Kevrekidis, and Stanislav Y Shvartsman. "Shape transformations of epithelial shells". In: *Biophys. J.* 110.7 (2016), pp. 1670–1678.

[72] Silvanus Alt, Poulami Ganguly, and Guillaume Salbreux. "Vertex models: from cell mechanics to tissue morphogenesis". In: *Phil. Trans. R. Soc. B* 372.1720 (2017), p. 20150520.

[73] John Andrew Fozard, Mikaël Lucas, John R King, and Oliver E Jensen. "Vertex-element models for anisotropic growth of elongated plant organs". In: *Front. Plant Sci.* 4 (2013), p. 233.

[74] Leonidas Guibas and Jorge Stolfi. “Primitives for the manipulation of general subdivisions and the computation of Voronoi”. In: *ACM transactions on graphics (TOG)* 4.2 (1985), pp. 74–123.

[75] Paul Heckbert. *Quad-Edge Data Structure and Library*, 2001. URL: http://web.archive.org/web/20080207010024/http://www.808multimedia.com/winnt/kernel.htm (visited on 11/01/2015).

[76] Lev Davidovich Landau and Eugin M Lifshitz. “Course of Theoretical Physics Vol 7: Theory and Elasticity”. In: Pergamon press, 1959. Chap. 1, p. 10.

[77] Peter B Canham. “The minimum energy of bending as a possible explanation of the biconcave shape of the human red blood cell”. In: *J. Theor. Biol.* 26.1 (1970), pp. 61–81.

[78] Wolfgang Helfrich. “Elastic properties of lipid bilayers: theory and possible experiments”. In: *Zeitschrift für Naturforschung C* 28.11-12 (1973), pp. 693–703.

[79] Achim Guckenberger, Marcel P Schraml, Paul G Chen, Marc Leonetti, and Stephan Gekle. “On the bending algorithms for soft objects in flows”. In: *Computer Physics Communications* 207 (2016), pp. 1–23.

[80] G Gompper and DM Kroll. “Random surface discretizations and the renormalization of the bending rigidity”. In: *Journal de Physique I* 6.10 (1996), pp. 1305–1320.

[81] Mark Meyer, Mathieu Desbrun, Peter Schröder, and Alan H Barr. “Discrete differential-geometry operators for triangulated 2-manifolds”. In: *Visualization and mathematics III*. Springer, 2003, pp. 35–57.

[82] Eugene L Allgower and Phillip H Schmidt. “Computing volumes of polyhedra”. In: *mathematics of computation* 46.173 (1986), pp. 171–174.

[83] Daniel J Cosgrove. “Growth of the plant cell wall”. In: *Nat. Rev. Mol. Cell. Biol.* 6.11 (2005), p. 850.

[84] Francoise Marga, Michel Grandbois, Daniel J Cosgrove, and Tobias I Baskin. “Cell wall extension results in the coordinate separation of parallel microfibrils: evidence from scanning electron microscopy and atomic force microscopy”. In: *Plant J.* 43.2 (2005), pp. 181–190.

[85] Joseph KE Ortega. “Governing equations for plant cell growth”. In: *Physiologia Plantarum* 79.1 (1990), pp. 116–121.

[86] Paul B Green. "Cell walls and the geometry of plant growth." In: *Meristems and Differentiation*. Vol. 16. Brookhaven Symposia in Biology, 1964, pp. 203–217.

[87] Lisa Willis, Yassin Refahi, Raymond Wightman, Benoit Landrein, José Teles, Kerwyn Casey Huang, Elliot M Meyerowitz, and Henrik Jönsson. "Cell size and growth regulation in the *Arabidopsis thaliana* apical stem cell niche". In: *Proc. Natl. Acad. Sci. USA* 113.51 (2016), E8238–E8246.

[88] Karen Alim, Olivier Hamant, and Arezki Boudaoud. "Regulatory role of cell division rules on tissue growth heterogeneity". In: *Front. Plant Sci.* 3 (2012), p. 174.

[89] Thomas Harvey Rowan. "Functional stability analysis of numerical algorithms". In: (1990).

[90] Steven G. Johnson. *The NLopt nonlinear-optimization package*. URL: `http://ab-initio.mit.edu/nlopt`.

[91] Dorota Kwiatkowska. "Flower primordium formation at the *Arabidopsis* shoot apex: quantitative analysis of surface geometry and growth". In: *Journal of Experimental Botany* 57.3 (Dec. 2006), pp. 571–580.

[92] Bihai Shi, Xiaolu Guo, Ying Wang, Yuanyuan Xiong, Jin Wang, Ken-ichiro Hayashi, Jinzhi Lei, Lei Zhang, and Yuling Jiao. "Feedback from lateral organs controls shoot apical meristem growth by modulating auxin transport". In: *Developmental cell* 44.2 (2018), pp. 204–216.

[93] Olivier Grandjean, Teva Vernoux, Patrick Laufs, Katia Belcram, Yuki Mizukami, and Jan Traas. "In vivo analysis of cell division, cell growth, and differentiation at the shoot apical meristem in *Arabidopsis*". In: *The Plant Cell* 16.1 (2004), pp. 74–87.

[94] Bruce E. Shapiro, Cory Tobin, Eric Mjolsness, and Elliot M. Meyerowitz. "Analysis of cell division patterns in the *Arabidopsis* shoot apical meristem". In: *Proceedings of the National Academy of Sciences* 112.15 (2015), pp. 4815–4820.

[95] Sébastien Besson and Jacques Dumais. "Universal rule for the symmetric division of plant cells". In: *Proceedings of the National Academy of Sciences* 108.15 (2011), pp. 6294–6299.

[96] Leo Errera. "Über Zellformen und Seifenblasen". In: *Botanische Centralblatt* 34 (1888), pp. 395–398.

[97] Franck Anicet Ditengou, William D Teale, Philip Kochersperger, Karl Andreas Flittner, Irina Kneuper, Eric van der Graaff, Hugues Nziengui, Francesco Pinosa, Xugang Li, Roland Nitschke, et al. "Mechanical induction of lateral root initiation in *Arabidopsis thaliana*". In: *Proceedings of the National Academy of Sciences* 105.48 (2008), pp. 18818–18823.

[98] Paul B Green, CS Steele, and SC Rennich. "Phyllotactic patterns: a biophysical mechanism for their origin". In: *Annals of Botany* 77.5 (1996), pp. 515–528.

List of Figures

Licenses for figures

Figure	License detail
1.1	License date: 09/04/2019; PLSclear Ref No: 12496
1.2	Permission to reprint granted freely for educational use. https://aspb.org/publications/aspb-journals/permission-to-reprint
1.3	License date: 09/04/2019; License Number: 4553340244307
1.9	License date: 03/13/2019; License Number: 4554780594584

Acknowledgements

Past three and half years working on my Ph.D have been a truly transformative experience for me. It would not have been possible for me to sit here and write these words, on the back of my doctoral thesis, without the support I received from many people. I would like to pay back some of these debt of love and support I gathered, with few words of acknowledgement.

My first words of gratitude go to my supervisor Dr. Karen Alim. The perfect balance of guidance and independence provided by her has been invaluable to me in not just building my research, but also in developing myself personally and professionally. Her endless motivation, patiences and support have guided me in every step of my Ph.D. She taught me how to build a scientific question and how to systematically approach the problem. I will remain eternally thankful to her for always being available and eager to discuss, for all the scientific inputs and for the encouragement in pursing new ideas. She has been a complete mentor that one could ask for.

I would also like to express my special thanks to Dr. Jean-Daniel Julien for being ever present on the other side of my table to discuss science and answer any of my questions. I have immense gratitude for his help with his expertise, scientific scrutiny and patient explanations. I also want to thank him for sharing all the delicious cheese and wine from France.

My special thanks also goes to Prof. Stefan Klumpp and Dr. Florian Rehfeldt. First of all, I want to thank them for agreeing to be part of my thesis advisory committee all those years ago and also for always attending and being active part of my committee meetings, for scrutinising the research, for asking the tough questions, for checking on the credit progress and for all the helpful and supportive comments.

I also want to thank all the present and past members of my group Biological Physics and Morphogenesis. For past three and half years, everyday of my work has been amazingly enjoyable

due to you all. To name a few from my group and others in Göttingen: Nico Schramma, Mirna Elizabetha Kramar, João Ramos, Franz Kaiser, Komal Bhattacharyaa, Dr. Galina Kudryasheva, Estefania Vidal, Rodrigo Galilea Kleinsteuber, Felix Bäuerle, Noah Ziethen, Felix Meigel, Dr. Phlipp Fleig, thank you all for the wonderful moments. Nico, Mirna, J-D, João and Komal, you are my best ends[1].

My friends all around Germany, Anuraag Raj Shakya, Bidhesh Thapaliya, Prabesh Raj Joshi, Joshan Chaudhary, Sophiya Shrestha, Prabal Poudel, Kristina Alushi, Pritam Dhoj Shah, Bishesh Tiwaree, Samit Vaidya and others, you have been a family to me, thank you all for always being there.

I am also specially thankful to Dr. Jean-Daniel Julien and Dr. Agnese Codutti for proofreading my thesis and correcting the text.

My thanks to SFB 937 and DFG-FOR 2581 for funding my research.

I am also grateful to GGNB and IMPRS-PBCS for all their incredible support during my Ph.D.

I would like to also express my gratitude to my mom Radha Shrestha Khadka, my dad Rajesh Khadka and my sister Jenisha Khadka for all the love, belief and encouragement.

My final words of thanks is rightfully reserved to my loving wife Ashna Theeng. The gratitude I feel for all the love, support and care I receive from you is indescribable. You make everything better!

[1] friends